Modeling of magnetic and optical properties of nanoparticles in medical interest

Katarzyna Brymora

l'université nantes angers le mans
PÔLE DE RECHERCHE ET D'ENSEIGNEMENT SUPÉRIEUR

Université du Maine

Thèse de Doctorat

Katarzyna BRYMORA

Mémoire présenté en vue de l'obtention du
grade de Docteur de l'Université du Maine
sous le label de l'Université de Nantes Angers Le Mans

Discipline : Physique des Matériaux
Laboratoire : Institut des Molcules et des Matriaux du Mans (IMMM)

Soutenue le 30 Septembre 2013

École doctorale : 3MPL (ED 500)
Thèse n° :

Modélisation des propriétés magnétiques et optiques de nanoparticules d'intérêt médical

JURY

Rapporteurs :	**Mme Nathalie VAST**, Ingénieur CEA, École Polytechnique
	M. Everett E. CARPENTER, Professeur, Virginia Commonwealth University
Examinateurs :	**Mme Phuong Mai DINH**, MCF-HDR, Université Paul Sabatier, IUF
	Mme Souad AMMAR, Professeur, Université Paris Diderot
	M. Jean-Marc GRENECHE, Directeur de recherche CNRS, Université du Maine
Directeur de thèse :	**M. Florent CALVAYRAC**, Professeur, Université du Maine
Co-directeur de thèse :	**M. Nader YAACOUB**, MCF, Université du Maine

List of publications

1. **Synthesis, Mőssbauer characterization, and *ab initio* modelling of iron oxide nanoparticles of medical interest functionalized by dopamine**

   J. Fouineau, K. Brymora, L. Ourry, F. Mammeri, N. Yaacoub, F. Calvayrac, S. Ammar and J.-M. Greneche

   J. Phys. Chem. C, **2013,** 117 (27), pp 14295-14302

   DOI:10.1021/jp4027942

2. **Combined *ab initio* modelling and Fe Mőssbauer spectroscopy approach to characterize the bonding between iron oxide nanoparticles and Aryl Diazonium Salt**

   J. Fouineau, K. Brymora, F. Chau, N. Yaacoub, F. Calvayrac, S. Ammar and J.-M. Greneche

   Submitted to The Journal of Materials Chemistry B

3. **Study of the expected bonding indice in a series of hydrophilic maghemite-based nanohybrids: An experimental and ab-initio modelling combined approach**

   K. Brymora, J. Fouineau, L. Oury, F. Chau, F. Mammeri, N. Yaacoub, F. Calvayrac, S. Ammar and J.-M. Greneche

   Submitted to ...

First and foremost I want to thank my advisor Prof. Florent Calvayrac, the person without whom this thesis would never come to life. It has been an honor to be his Ph.D. student. I appreciate his continuous support, his patience and useful critiques of this research work.

I am also very grateful to my co-supervisor Dr Nader Yaacoub for his valuable suggestions and help during my preparation to defense.

I am particularly grateful for the assistance given by Prof. Jean-Marc Greneche for finding the time to read my manuscript and his suggestions on how to improve the quality of this thesis, as well as Prof. Souad Ammar and Prof. Yvan Labaye for their contribution to this manuscript with their ideas.

I present my sincere thanks to both Prof. Nathalie Vast and Prof. Everett Carpenter for kindly accepting to referee this thesis, and Dr Mai Dinh equally for accepting to be a member of my thesis comittee. I am grateful for their thoughtful and detailed comments.

I would like to acknowledge the financial support provided by 3MPL Doctoral College, IMMM and ANR which allowed me to participate in several national and international conferences.

I also thank my friends for providing support and friendship that I needed during the preparation of this thesis.

I especially thank my Mom for her infinite support throughout everything.

Abstract

This thesis concerns the *ab initio* modeling of ligands and magnetic nanoparticles used in medicine (magnetic hyperthermia, medical imaging). Calculations are performed by the Quantum Espresso software based on density functional theory and LDA+U. The goal is first to understand the binding of ligands on magnetic nanoparticles, the nature of ionicity in the particles, then to describe the change in magnetic anisotropy due to the chemical bondings on surface, and finally to describe the change in optical properties due also to the bonding of various ligands or clusters on the surface of hybrid gold and iron oxide nanoparticles.

After a general introduction, and a discussion of the methods chosen, in the first chapter of results, we show good agreement with experimental findings. In particular, with could predict on which iron site the ligand would preferentially bind, which is of crucial importance in order to understand the magnetic properties of the nanoparticle. Then, we investigate the effect of several ligands, the charge order at the surface of magnetite, the ionicity of the bonds in link with pharmacological requirements, and their effect on the magnetic and electronic properties of the material.

In the next chapter, we address the problem of the *ab initio* computing of the magnetic anisotropy at the surface of a nanoparticle. In literature, this parameter is a phenomenological input in large scale classical calculations based on modified Heisenberg models. Here, on the example of a small cluster (namely Fe13O8) we link various magnetically constrained calculations or calculations done under a magnetic field to a Heisenberg model in order to estimate magnetic properties of the nanoparticle from first principles. We study the change in magnetic properties due the presence of a ligand (dopamine), or of a nearby gold cluster, in link with the next chapter. We discuss the same phenomena on surfaces.

We model in the last chapter the optical response of small gold clusters, gold-coated iron oxide clusters, and hybrid gold and iron oxide clusters using linearized time-dependent density functional theory. We discuss the shortcomings of such a simple method for so complicated systems, and discuss the physical meaning of the results, in link with the previous chapter.

The conclusion of the work present some perspectives on a better modelling of the problem, approaching for instance temperature and pH effects, linkage of the ligands to proteins in order to target tumors, as well as extensions of the work on surface anisotropy.

Résumé

Cette thèse porte sur la modélisation *ab initio* des ligands et des nanoparticules magnétiques utilisés en médecine (hyperthermie magnétique, imagerie médicale ...). Les calculs sont effectués par le logiciel Quantum Espresso basé sur théorie de la fonctionnelle de la densité et LDA + U. L'objectif est d'abord de comprendre la liaison des ligands sur des nanoparticules magnétiques, la nature de l'ionicité dans les particules, puis de décrire le changement d'anisotropie magnétique due aux liaisons chimiques sur la surface, et enfin de décrire la modification des propriétés optiques due également à la liaison de différents ligands sur la surface de nanoparticules hybrides d'or et d'oxyde de fer.

Après une introduction générale et une discussion des méthodes choisies, dans le premier chapitre de résultats, nous montrons un bon accord avec les résultats expérimentaux obtenus sur des nanoparticules. En particulier, nous prédisons sur quel site de fer le ligand pourrait se lier préférentiellement, ce qui est d'une importance cruciale pour comprendre les propriétés magnétiques de la nanoparticule. Ensuite, nous étudions l'effet de ligands couramment utilisés, la mise en ordre des charges à la surface de la magnétite, l'ionicité des liens en comparant aux exigences pharmacologiques, et leur effet sur les propriétés magnétiques et électroniques du matériau.

Dans le chapitre suivant, nous attaquons le problème du calcul *ab initio* de l'anisotropie magnétique à la surface d'une nanoparticule. Dans la littérature, ce paramètre est une entrée phénoménologique dans les calculs classiques à grande échelle basées sur des modèles de Heisenberg modifiés. Ici, sur l'exemple d'un petit agrégat (à savoir Fe13O8) nous relions divers calculs magnétiquement contraints ou des calculs effectués en fonction d'un champ magnétique à un modèle de Heisenberg afin d'estimer les propriétés magnétiques de la nanoparticule à partir des premiers principes. Nous étudions la variation des propriétés magnétiques en fonction de la présence d'un ligand (la dopamine), ou d'un cluster d'or à proximité, en lien avec le chapitre suivant. Nous discutons les mê mes phénomènes sur les surfaces.

Nous modélisons dans le dernier chapitre la réponse optique de petits agrégats d'or ou d'oxyde de fer revêtus d'or, et d'hybrides d'or et d'oxyde de fer en utilisant la théorie de la fonctionnelle de la densité dépendant du temps linéarisée. Nous discutons les lacunes d'une telle méthode simple pour les systèmes si complexes, et discutons signification physique des résultats, en lien avec le chapitre précédent.

La conclusion de ce travail présente quelques perspectives sur une meilleure modélisation du problème, l'approche des effets de la température ou du pH, la liaison des ligands aux protéines afin de cibler les tumeurs, ainsi que des extensions des travaux sur l'anisotropie de surface.

Contents

List of Figures

List of Tables

List of Abbreviations

MRI	Magnetic Resonance Imaging
SPION	Superparamagnetic Iron Oxide Nanoparticles
DFT	Density Functional Theory
TDDFT	Time Dependent Density Functional Theory
LDA	Local Density Approximation
LSDA	Local Spin Density Approximation
GGA	Generalized Gradient Approximation
QE	Quantum Espresso
AMEB	4 - (aminomethyl benzoic acid)
DOPA	3 - hydroxytyramine
PHOS	(3 - aminopropyl) phosphonic acid
APTES	(3 - aminopropyl) triethoxysilane
PBC	Periodic Boundary Conditions
EPLF	Electron Pair Localization Function
DOS	Density of States
PDOS	Projected Density of States
SPR	Surface Plasmon Resonance
NPs	Nanoparticles
IS	Isomer Shift
LYP	Lee-Yang-Parr Functional
LSDF	Local Spin Density Functional
ASW	Augmented Spherical Wave

Chapter 1

Introduction

Cancer is a major cause of death worldwide, according to the World Health Organization the mortality rate in 2008 reached 7.6 million and is estimated to rise to over 13.1 million in 2030 [Globocan 2013]. The perfect cure for cancer does not exist and although the detection and treatment of cancer is presently much easier and more effective than it was in the past, most of the methods used in therapy still wreak havoc on the organisms of patients. To be accurate and hit only the cancer cells leaving undamaged the healthy surrounding tissues instead of devastating the body with toxic drugs, one needs to use a more intelligent method. With nanotechnology, scientists hope for more effective and less invasive cancer treatments.

In recent years, the study of magnetic nanoparticles has focused a great attention due to their existing or possible applications in medicine such as magnetic resonance imaging (MRI), magnetic hyperthermia or targeted drug delivery. The first reason for which magnetic nanoparticles may be used in biomedical applications is the fact that their dimensions are comparable to the size of proteins (5 - 50 nm) or viruses (20 - 450 nm) [Pankhurst *et al.* 2003] thus they can act at the cellular and molecular level. Their size as well as properties are controllable [Nitta & Numata 2013]. Third, they can be controlled by an external magnetic field [Pankhurst *et al.* 2003].

MRI is the most advanced noninvasive tomographic technique used in diagnostics to obtain cross sections of the patient body. Magnetic resonance imaging has wide applications, among others in cancer diagnostics. It does not only allow to detect the tumor, but also to evaluate its stage and to monitor the body's response to the therapy. To improve the images and highlight the structures which are less clear, including blood vessels and tumors, contrast agents are used. An alternative to contrast agents used so far is represented by superparamagnetic iron oxide nanoparticles (SPION) [Xiang & Wang 2011]. SPION contrast agents are based on magnetite and maghemite molecules [Weinstein *et al.* 2010]. The superparamagnetic and paramagnetic

substances are similar as regards the ability of losing magnetization when the magnetic field is removed but the magnetic moment is much higher in the case of the SPION [Mornet *et al.* 2004]. Thus, their relaxation is higher than the one of the traditional MRI contrast agent - gadolinium. Many studies have shown that imaging based on SPION, from the viewpoint of characterized metastases and size of the exposed smallest lesion, is one of the most accurate techniques [Ward *et al.* 2005].

Hyperthermia, in general and primary meaning is defined as a state of increased temperature, artificial hyperthermia has healing properties. The use of hyperthermia is as old as medicine [Mornet *et al.* 2004] and has 5000 years history [Kim *et al.* 2010]. Indeed, one of the greatest precursors of modern medicine, endowed with the nickname "Father of Medicine" - Hippocrates, was convinced of its efficiency[1] and proposed that tumors should be cauterized[2] by application of an hot iron [Hofer 2002]. In the early modern period, hyperthermia was abandoned and re-discovered in the nineteenth century. Nowadays it remains a promising form of cancer therapy and is a way to improve the efficiency of the chemotherapy or radiotherapy, based on raising the temperature of the region of the body affected by a tumor to 40 - 41 °C [Wust *et al.* 2002]. This process takes several hours and the biocompatible, superparamagnetic particles are used with an external magnetic field [Jordan *et al.* 1997]. Magnetic nanoparticles are the best developed in the middle of all the nanometric heat mediators because of their capability to heat when a high-frequency magnetic field is applied[3] [Jordan *et al.* 1993]. Magnetic hyperthermia relies on injecting magnetic nanoparticles directly into the target region of the organism followed by applying an alternating magnetic field to heat the nanoparticles. If the temperature can be held above 42°C for more than 30 min, the cancer is destroyed without damaging the surrounding healthy cells [Pankhurst *et al.* 2003].

The ideal nanoparticles for magnetic hyperthermia would have to exhibit a satisfactory amount of heat at the lowest possible magnetic field because the human tissue can only stand a field about $4.85 \cdot 10^8$ A/(m/s) before their damage or death [Zeng *et al.* 2007]. Under the same magnetic field, nanoparticles with higher magnetization would generate more heat than the ones with lower because the heating power increases with the square of the magnetization [Lacroix *et al.* 2008].

[1] As he described in his aphorism: Quae medicamenta non sanat; ferrum sanat. Quae ferrum non sanat; ignis sanat. Quae vero ignis non sanat; insanabilia reportari oportet (Those diseases which medicines do not cure, the knife cures; those which the knife cannot cure, fire cures; and those which fire cannot cure, are to be reckoned wholly incurable.) [Ito *et al.* 2005].

[2] Medical treatment, based on thermal or chemical coagulation of the living, pathologically affected tissue.

[3] The physical basis for which magnetic nanoparticles are heated in the presence of an external magnetic filed is due to loss processes during the reorientation of the magnetization[Hiergeist *et al.* 1999]

The sketch of therapeutic procedure involving magnetic nanoparticles is presented on Figure 1.1. Magnetic nanoparticles are placed by the drug delivery system (DDS) in the cancer cells, then they can be used as contrast agents for cancer diagnosis in MRI and finally hyperthermia is induced by applying an external alternating magnetic field [Ito *et al.* 2005].

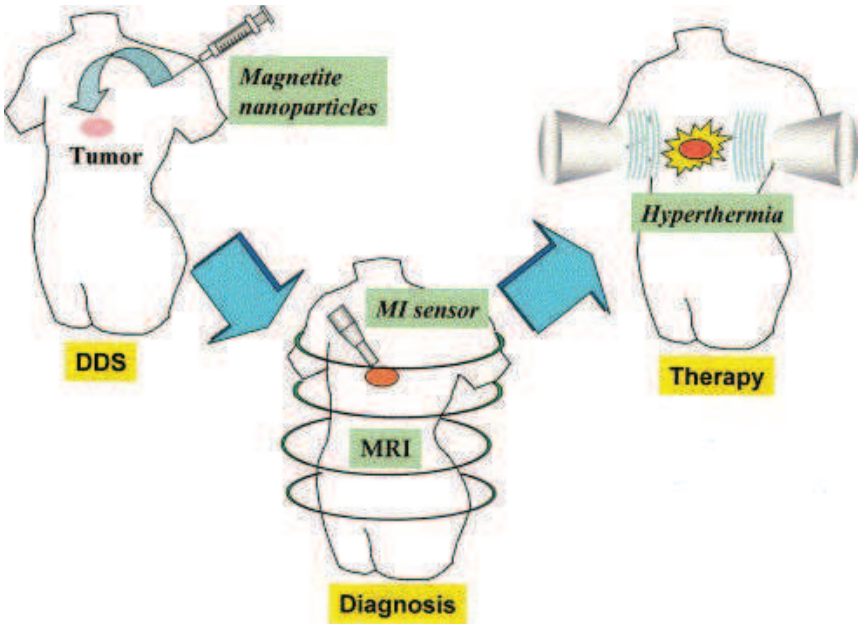

Figure 1.1: Illustration of the therapeutic approach using magnetic nanoparticles. Adapted from [Ito *et al.* 2005].

In 1891, Paul Ehrlich gave a preliminary description of the paradigm of drug delivery [Sattler 2011]. According to the german researcher, drugs have to be transported with the appropriate concentration to the appropriate place and in the appropriate time. So far, this objective is reached only in a small number of clinical trials. However, once again, there is a hope because of the evolution of nanotechnology and the use of nanoparticles to carrying pharmaceuticals. Many of latest publications have shown promising results of targeted drug delivery as a strategy for a better treatment of cancer [Karra & Benita 2012]. The idea of drug delivery by magnetic microspheres in cancer treatment was first presented by [Widder *et al.* 1779]. Their study in rats and further research showed complete and permanent tumor remission [Prijic & Sersa 2011]. Magnetic nanoparticles may be transported to the particular region of the body under an external magnetic field and fixed at the local site while the drug is released via enzy-

matic activity or through changes in physiological conditions [Dobson 2006]. The medication acts only in the target place, thus, the dose as well as the concentration of the drug at nontargeted regions can be reduced. This allows to minimize the side effects [Neuberger *et al.* 2005]. Moreover, when magnetic nanoparticles are targeted to the tumor, the cancer cells may be imaged as well. In order to increase the specificity of target, the drug is linked with another molecule, which is able to recognize and bind to the desired tissue [Berry & Curtis 2003]. The most common type of such molecules are antibodies, proteins, hormones and ligands [Berry & Curtis 2003]. The use of ligand - modified drug loaded magnetic nanoparticles allows to increase the drug delivery into the tumor relative to that into healthy cells [Liong *et al.* 2008]. These ligands have to be not recognizable by macrophages[4] Such a method should give a possibility to target cells within the vasculature [Mornet *et al.* 2004]. It seems to be more likely to succeed when targeting with small ligand molecules due to their ease of use and manufacture [Mohanraj & Chen 2006]. Additionally, the team of Prof. McDonald from the Georgia Institute of Technology demonstrated a new utility of targeted nanoparticles [Scarberry *et al.* 2010] as a method to ttreat metastasis of malignant cancer. They developed a new approach to remove tumor cells from a fluid in the abdominal cavity by filtering them outside the body with the magnetic nanoparticles designed to bind to the tumor cells. The device developed by researchers operates on the fluids collected from the abdomen, to which magnetic nanoparticles are added, then magnetically removed from it, and the filtered liquid is returned back to the abdominal cavity.

During the last decades, much scientific research concerning magnetic nanoparticles has been devoted to several types of iron oxides, but in their midst the most successful and encouraging systems are mixtures of magnetite and its oxidized form maghemite due to their proven biocompatibility [Wu *et al.* 2008]. Iron naturally occurs in the human body, thus nanoparticles containing iron are biocompatible[5] , they can be utilised by the body in metabolic processes [Markides *et al.* 2012]. Other magnetic particles based on nickel or cobalt become toxic and they are not so interesting [Tartaj *et al.* 2003]. Iron oxide nanoparticles have a high surface energy due to a large surface area to volume ratio. Accordingly, they have a tendency to agglomerate in order to minimize the surface energy [Wu *et al.* 2008]. What is more, bare magnetic nanoparticles are characterized by a quick oxidation in air (especially magnetite) [Gao *et al.* 2010], [Wu *et al.* 2008] and this

[4]Connective tissue cells, directly originating from monocytes that have left the blood. Their main task is to defend the body.

[5]In case of an excess of iron in the body of course we will observe his destructive nature. An excess of iron accumulates first in the liver and pancreas, then in brain. Iron interferes with the processes of neurotransmitters what may cause neurological and psychiatric disorders. It is also belived that the main factor causing Alzheimer's disease is an exces of iron in the brain.

leads to the loss of magnetism [Wu *et al.* 2008]. Thus, the functionalization of magnetic iron oxide nanoparticles in order to maintain their stability is very often indispensable and includes grafting or coating. These strategies are significant in order to prevent from aggregation and fast oxidation.

The coating of magnetic iron oxide nanoparticles with a stable metal such as a gold is a very promising and attractive method as it results in a stable nanosystem protected from oxidation and also improves its biocompatibility [Kayal & Ramanujan 2010], [Shevchenko *et al.* 2008]. In the study of [Tamer *et al.* 2013] gold-coated iron nanospheres was showed to detect *Escherichia coli*. Moreover, the coating with gold provides plasmonic properties[6] to the nanoparticles as well. Thus, such a combination for the magnetic, optical and biomedical applications is greatly valuable.

As seen, magnetic nanoparticles are very promising in the cancer treatment and iron oxide based nanoparticles are widely analyzed. In the present work, in order to contribute to the research of magnetic nanoparticles, we performed some modeling. After a discussion of the chosen methods, in the first chapter of results, we show good agreement with experimental findings on maghemite nanoparticles synthesized and functionalized by the team of Souad Ammar (ITODYS Paris 7) and characterized by Mössbauer spectroscopy[7] by Jean-Marc Grenèche and Nader Yaacoub in Le Mans. In particular, we could predict on which iron site the ligand would preferentially bind, which is of crucial importance in order to understand the magnetic properties of the nanoparticle. Then, we investigate the effect of commonly used ligands (which we called citrate, (bi) phosphonate, silane, dopamine, diazonium, etc..for commodity) the charge order at the surface of magnetite, the ionicity of the bonds in link with pharmacological requirements, and their effect on the magnetic and electronic properties of the material.

[6]Described in Chapter 4

[7]Combined *ab initio* modeling and Mössbauer spectroscopy study is attached as an Appendix so it seems necessary to mention about one of the main parameters describing Mössbauer's spectrum - isomer shift. A result of the electric interaction between the charge of the nucleus and the charge of electron shells is nuclear energy levels shift, which change the energy of the quantum transition γ of value δ: $\delta = \delta E_{excitedstate} - \delta E_{groundstate}$. The transition of electrons s have an impact on the value δ. Mössbauer's isomer shift can provide information about the density of the electrons in the core area, wherein one uses frequently a standard source for comparison. One can conclude from isomer shift about the electron shell configuration of the atom, its deegre of valence and nature of the bonds.

Chapter 2

Theoretical choices

A very important element in enabling the development and applications of new materials is the ability to understand their chemical, electrical and physical properties. Numerical modeling allows for the replacement of complicated, expensive measurements and burdensome chemical experiments by computer simulations. In this work, Density Functional Theory (DFT) method was chosen to study the magnetic properties, electronic structure and nature of chemical bonds of magnetite and maghemite surfaces modified by ligands, as well as the optical properties of systems consisting of iron oxide clusters and gold.

Why DFT? Methods developed in the framework of Density Functional Theory are currently the most popular and effective approaches used in solid state physics, quantum chemistry and nanotechnology. This method allows us to compute any of the ground state properties and can be used in a number of calculations performed for atomic and molecular layouts as well as for crystals, which are large, periodic systems and metal surfaces using plane wave basis sets, not forgetting a good accuracy-cost compromise. This method was born in the 1964 [Hohenberg & Kohn 1964] on the basis of quantum mechanics and created the basis for numerical calculations of total energy and density distribution in many body systems. The background of the DFT was formed by Hohenberg - Kohn theorems[1] [Hohenberg & Kohn 1964], which were extended and reformulated by Levy [Levy 1979], [Jones & Gunnarsson 1989]. Levy in 1979 introduced an alternative approach to the minimization problem, called constrained search formulation [2]. The name of this method highlights the fact that for calculating the properties of interacting electrons we do not need to know the wave function [Magnasco 2006]. Electrons are quantum mechanical spin particles. Density Functional Theory allows to compute all the

[1] See Appendix C

[2] Levy demonstrated that first theorem (which according to the Hohenberg - Kohn theorem held only for non - degenerate ground state) may be applied also to the degenerated ground states and the density is not required to be v - representable - it is enough to consider only N - representable densities

properties of a system through electron density [Ramachandran *et al.* 2008]. The electron density ρ_r determines the probability of finding any of N electrons within volume of element dr.

In DFT all properties of the ground state of an interacting electron gas may be described by introducing certain functionals of electron density ρ_r. Regardless of the number of electrons, the electron density always depends only on these three spatial coordinates, so the mathematical structure does not complicate at increasing number of electrons. The main objective of DFT method is to find the value of the functional, because its character is not explicit - it has a non-local character. This search requires some approximation. The formula for the energy in the DFT is as follows:

$$E_{DFT}[\rho] = T[\rho] + E_{ne}[\rho] + J[\rho] + E_{XC}[\rho] \tag{2.1}$$

Here $T[\rho]$ is the kinetic energy of the system of non-interacting electrons with density $\rho(r)$; E_{ne} is the electrostatic interaction of the electron and the nucleus; J is the electrostatic repulsion energy and the functional $E_{XC}[\rho]$ contains the many-electron effects of the exchange and the correlation. The value of each of those potentials is a separate problem to be solved. The last part is referred as exchange-correlation energy. It is assumed that exchange-correlation energy in the inhomogeneous system is locally equal to the exchange-correlation energy of a homogeneous system with the same density. One can calculate the results in two ways: (1) $E_{XC}[\rho] \approx E_{XC}(\rho(r))$ - the so-called Local Density Approximation (LDA) - which assumes exchange-correlation energy dependence of the local density or (2) $E_{XC}[\rho] \approx E_{XC}(\rho(r), \bigtriangledown\rho(r))$ - the so-called Generalized Gradient Approximation (GGA) - which assumes exchange-correlation energy dependence of the local density and its gradient. The introduction of electron spin dependence by using the Local Spin Density (LSD) in approximate functionals and its importance was presented in [Gunnarsson *et al.* 1974], it was found that using LSD improves the unpaired electron description in Na cluster. The solving of the equations is performed in a self-consistent way. Because the potential (input data) depends on the density (output data), the density calculated in the previous step is taken as a input in the next step.

Regrettably, the common DFT approaches of (LDA) and (GGA) are unsuccessful in a correct prediction of the energy gaps between occupied and unoccupied states. It is known as a "band gap problem" [Chan & Ceder 2010]. LDA is not applicable in the case of highly correlated transition metals [Madsen & Novak 2005] and underestimates the width of the band gap by about 50% [Persson & Mirbt 2006], [Bachelet & Christensen 1985]. The true band gap of single particle excitations deviates for Kohn-Sham gap by a large

amount for a system with the empty conduction bands separated by an energy gap from the filled valence bands [Sham & Schlüter 1985], [Levy & Perdew 1985]. It results from insufficiently precise description of electron correlation, which is the result of building an exchange-correlation functional on homogeneous electron gas model. However, the improvement can be achieved by introducing the Hubbard U correction within the LDA+U approach and one obtains the whole band structure practically in agreement with experiment [Persson & Mirbt 2006], [Madsen & Novak 2005]. In this connection, the LDA+U method was chosen to perform the calculations of electronic structure and magnetism due to the complexity of charge order of studied systems and GGA to predict the correct structures (in form of Perdew, Burke and Ernzerhof [Perdew *et al.* 1996a]). In this method the orbital dependence of the Coulomb and exchange interactions is implemented [Anisimov *et al.* 1997]. The assumption of this approach is to separate the valence electrons into two systems: localized d or f electrons (the Coulomb interaction U is taken into account for them), and delocalized s and p electrons (described by LDA) [Singh & Papaconstantopoulos 2003]. A suitably chosen value of the U parameter results in getting the whole band structure almost in accordance with experiments [Persson & Mirbt 2006].

The calculations in this thesis were performed in the framework of Quantum Espresso [Giannozzi *et al.* 2009] code based on DFT, plane waves and pseudopotentials. DFT calculations with all-electron exchange-correlation potential are expensive and core electrons are basically neutral in bonding environments (most physical properties of solids depend on the valence electrons), thus the pseudopotentials were introduced and are used as an approximation for the simplified description of complex systems [Bachelet *et al.* 1982]. Pseudopotentials replace the effect of the core electrons and only the valence electrons are considered. By simulating the core effect on the valence electrons, a significant simplification of computational problem is achieved. In the pseudopotential method, electrons are determined by pseudo-wave functions, which are required to be identical to the real wave functions outside the nuclear core and as smooth as possible inside the core area. In the Quantum Espresso code the scheme proposed by Cococcioni and de Gironcoli [Cococcioni & de Gironcoli 2005] is implemented. It based on a linear response of the system to calculate in an internally consistent way the interaction parameters entering the LDA+U functional.

The better description of the molecular orbitals causes the better results. Molecular orbitals are built by linear combinations of known functions - basis sets. The choice of the basis set can influence both the efficiency of the calculations and accuracy of the results [Brazdova & Bowler 2013]. The Quantum Espresso code [Giannozzi *et al.* 2009] uses a plane wave basis set to model the kinetic energies of the valence electrons. Plane wave

basis sets are popular solution for free electrons in periodic boundary conditions calculations [Lesar 2013]. In calculations that implement plane wave basis sets, a finite number of plane wave functions is used below a chosen cutoff energy [Ramachandran *et al.* 2008]. The cutoff energy specifies the quality of the plane wave basis set [Kaupp *et al.* 2004]. It is common to combine plane wave basis set with the pseudopotential method which results in describing only the valence electrons by plane waves [Ramachandran *et al.* 2008]. The choice of such a combination is due to the fact that the core electrons are likely to concentrate near the atomic nuclei, what causes a large wave function and density gradient near the nuclei, which are difficult to describe by a plane wave basis set.

Dependent Density Functional Theory (TDDFT) method is DFT's extension to describe response properties in presence of an external electric field. TDDFT method to obtain optical properties of iron oxide clusters with gold was used. This method allows us to study the properties of molecules in the excited states of electrons. In 1984 Runge and Gross [Runge & Gross 1984] demonstrated how to extend the idea of ground - state DFT into the time domain, their theorem is analog to the one of Hohenberg - Kohn for static DFT. Later Gross and Kohn [Gross & Kohn 1985] developed a linear response theory. The fundamental variable of TDDFT is the one-body electron density and no longer the many - body wavefunction. It is believed that the chosen methods are the right kind of tools to deal with the issues contained in this work, however their application on strongly correlated materials might be wrong in connection with LDA and GGA.

Chapter 3

Ligand Effects on the Electronic Structure and Magnetism of Iron Oxide Surfaces

3.1 Introduction

In this chapter we will focus on the effects of commonly used ligands, the charge order at the surface of magnetite, the ionicity of the bonds in link with pharmacological requirements and their effect on the magnetic and electronic properties of materials.

Among various magnetic nanoparticles which have been extensively studied in the recent years, iron oxides such as Fe_3O_4 and γ-Fe_2O_3 have considerable interest. Magnetite, with a chemical formula $Fe^{3+}(Fe^{2+}Fe^{3+})O_4$, is the single most important and magnetic mineral naturally occurring on the Earth, on the continents and in the ocean crust. The primary details of magnetite structure were established in 1915; this was one of the first mineral structures measured by X-Ray diffraction method. Magnetite has a face-centered cubic unit cell and inverse spinel structure [1]. It differs from most other iron oxides in that it contains Fe^{2+} and Fe^{3+} cations. The unit cell, with cubic lattice constance a=8.396 Å, contains eight cations of Fe^{3+} on tetrahedral (A) sites, each surrounded by four O^{2-} anions and sixteen cations (Fe^{2+} and the remaining Fe^{3+} randomly distributed) on octahedral (B) sites, each surrounded by six O^{2-} ions. This cation distribution defines as inverse spinel. Magnetite can be converted to maghemite under oxidative conditions or maghemite to magnetite under reducing conditions. Maghemite has a structure similar to that of magnetite, however maghemite is considered as an Fe^{2+} deficient magnetite and

[1] Above the transition temperature ($\sim$ 120 K) Fe_3O_4 crystallizes in an inverse spinel structure with a cubic lattice, below transition temperature Fe_3O_4 undergoes the Verwey transition in which the lattice turns from cubic to monoclinic [Huang *et al.* 2006]

accommodates cationic gaps in octahedral sites Fe^{3+}(tetra)[$Fe^{3+}{}_{(5/3)}$-$\square_{1/3}$(octa)]O_4. Under a certain size, those nanoparticles present zero coercivity [Figuerola *et al.* 2010] which is specifically useful due to the apparition of superparamagnetism and the prevention of the clogging of particles.

Regrettably, bare Fe particles cannot be directly used in the body due to their easiness to aggregate to form larger particles what may result in the formation of thromboses, also their magnetic properties may weaken because they can be easily oxidized. To exceed those issues iron nanoparticles need to be functionalized so that they remain nontoxic, biocompatible, chemically stable and preserve their high magnetic moment. It is therefore interesting to study the role of commonly used ligands at the iron oxide surfaces.

Consequently, the present work deals with investigating the magnetic structure of the surface layer and the magnetic interactions in the surface layers when it is modified by organic materials, together with the nature of the chemical bonding. i.e. ionic or covalent. At the same time, we attempted to answer the question of how gold [2] affects the magnetism of iron oxide and for this purpose non-collinear magnetism calculations were performed.

3.2 Computational Details

In this work, magnetite and maghemite nanoparticles were studied. These nanoparticles are large enough (typical size of 7 nm) that the site where a ligand will bind is almost locally flat. Therefore, the studied systems were modeled as surfaces with periodic boundary conditions and a vacuum in the direction orthogonal to the surface. Various ligands representing various kinds of binding affinity and ways of binding were chosen to functionalize considered nanoparticles:

- 4 - (aminomethyl benzoic acid) (AMEB): σ - donor and π - donor ligand, (fig. 3.1*a*)
- 3-hydroxytyramine (DOPA): σ - donor ligand, (fig. 3.1*b*)
- (3-aminopropyl) phosphonic acid (PHOS): σ - donor and π - donor ligand, (fig. 3.1*c*)
- (3-aminopropyl) triethoxysilane (APTES), (fig. 3.1*d*)
- citric acid (citrate), (fig. 3.1*e*)
- aryl functional groups: phenoxy (C_6H_5O) and phenyl (C_6H_5) radical formations

[2] The plasmonic properties of gold are described in Chapter 5.

In the σ bonding interactions the ligand always acts as a Lewis base (species capable of donating electron density) and the metal as a Lewis acid (species capable of accepting electron density). σ donor is a ligand that bonds to the metal center through a direct σ bond. While all ligands participate in σ bonding, some ligands are adapted in π bonding. By contrast, in the π interactions, ligands containing double or triple bonds may act as π donors and transfer charge in a π bond to the metal or π acceptors by accepting electron from central metal. Therefore, metal-ligand bonding can be separated in three classes:

- σ -donor ligands
- σ-donor and π-donor ligands
- σ-donor and π-acceptor ligands (both effects augment each other - synergic bonding)

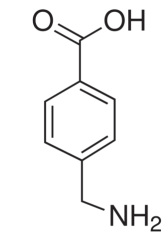

a

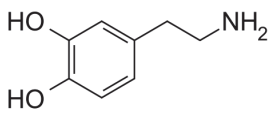

b

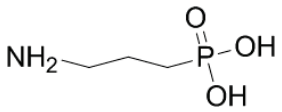

c

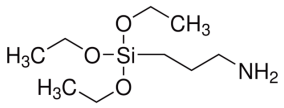

d

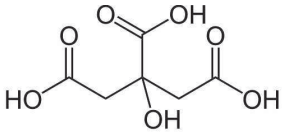

e

Figure 3.1: Structural formulas of chosen ligands.

We used the WebMo interface to the Gaussian09 code [Frisch *et al.*] using the Hartree - Fock method with 6-31+G(d) basis set which is often considered as the best compromise between speed and accuracy in order to perform a quick structural optimization of the chosen molecules (without spin-polarization). Then we checked that the obtained coordinates for the ligands correspond to stable molecules in the pseudopotential approach.

The surface functionalization simulations of magnetite and simplified maghemite were performed in the framework of density functional theory with the local density approximation +U (LDA+U) and generalized gradient approximation (GGA) approaches. To obtain the relaxed structures we used GGA functional and to describe the electronic structure and magnetism we used LDA+U method. It is well established that to determine the ground state of bulk iron the LDA and LSDA methods fail, while GGA predicts the correct structure. For highly correlated materials, LSDA or GGA incorrectly determine them to be small gap semiconductors or metals. The Quantum Espresso [Giannozzi *et al.* 2009] computer code for electronic-structure calculations, based on DFT, plane waves and pseudopotentials (which were taken from the QE website), was used to describe the systems. Quantum Espresso uses periodic boundary conditions [Makov & Payne 1995] which are the best solution to minimize edge effects in a finite systems. In PBCs, the simulation cell is infinitely repeated in 3 directions of space. It means that each atom in the simulation box is interacting with other atoms as well as with their replicas (images) in the contiguous cells. Some corrections can however be included for isolated systems. The studied surfaces were built by taking the simplest unit cells from the Open Crystallography Database [Grazulis *et al.* 2012] and expanded throughout vacuum in the [100] and [111] directions [3]. To allow the use of periodic boundary conditions and minimize the effects from the repeated surfaces the size of the unit cell was doubled perpendicularly to the surface direction.

For the structural optimization of magnetite the GGA density functional from PBE - Perdew Burke Ernzerhof [Perdew *et al.* 1996b] was used and LDA+U method with the Perdew-Zunger [Perdew & Zunger 1981] functional was used for final optimization and electronic structure calculations. The $LDA+U$ parameters were set at U=4.5 eV for iron and the Hund's coupling J parameter was set to zero in accordance with previous papers [Lodziana 2007], [Pinto & Elliott 2006]. Both, the U and J parameters for oxygen were set to zero. The parameters already used and reported in the literature were chosen due to soft balance between U and J which can lead to differences concerning the final magnetic state of the system. Marzari - Vanderbilt cold smearing and a Gaussian smearing factor of 0.02 Ry were used. A grid of 3x3x3 k-points in the first Brillouin zone was used.

[3]To create a [100] and [111] surfaces of magnetite and maghemite we used a Atomistic Simulation Environment [Bahn & Jacobsen 2002] written in Python programming language.

A test of convergence, which relies on successive increase of the cutoff energy in the plane-wave expansion of the pseudo-wave-functions until the total energy no longer changes, was performed (Figure 3.2) From this one can see that a kinetic energy cutoff of 29-30 Ry is sufficient to obtain a good convergence. And therefore, 30 Ry (408 eV) was employed as the cutoff energy and 0.17 as a mixing factor for self-consistency. The spin degree of freedom in the calculations was turned on after having established stable structures. Then the ligands optimized as described above were added at a height of 3 a.u. above the surfaces and a full structural optimization by the standard annealing method of the PWscf code was performed.

Density of states and projected density of states calculations were performed using DFT in the framework of the LDA+U approach and using the Perdew-Zunger pseudopotential for the exchange-correlation functional. The U and J parameters were set with the same values as in other calculations, i.e. 4.5 eV and zero for Fe cations.

The difference in energy in between a full simulation of maghemite (corresponding to 3 simplified cells with 2 Fe cations removed) with forced occupations in LDA+U leading to an insulating state and a simplified cubic cell with a semimetal state is less than 0.001 Ry/cell. Therefore we concluded after discovering this fact far in our work that in order to compute binding energies in a reasonable time the simplified method was the best even if the electronic structure of maghemite might be wrong. It is to be noted that this electronic structure also depends on the magnetic state as reported in [Grau-Crespo *et al.* 2010b] ; those authors got total magnetic moments of 80 μ_B per cell, very close to our results. However, in the next parts, we prefer to present in details results obtained on the magnetite surface, which are very close to the ones obtained on maghemite surfaces.

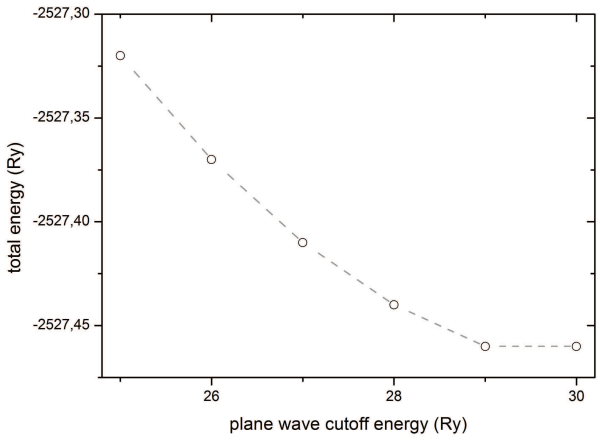

Figure 3.2: Total energy of maghemite grafted by dopamine versus cutoff energy.

3.3 Results and Discussion

3.3.1 Nature of the binding with the surface

The surface ([100] or [111]), the choice of orientation of the surface (oxygen atoms close to the ligands or iron atoms close to them), the initial orientation and position of the ligands were varied. In all cases, all ligands, except citrate, present affinity for the octahedral (B) sites of iron atom and citrate ligand has a preferential binding on the tetrahedral (A) site of the magnetite surface which were the final structures given by full structural optimization, the results of which are presented in figures 3.3 - 3.7 [4].

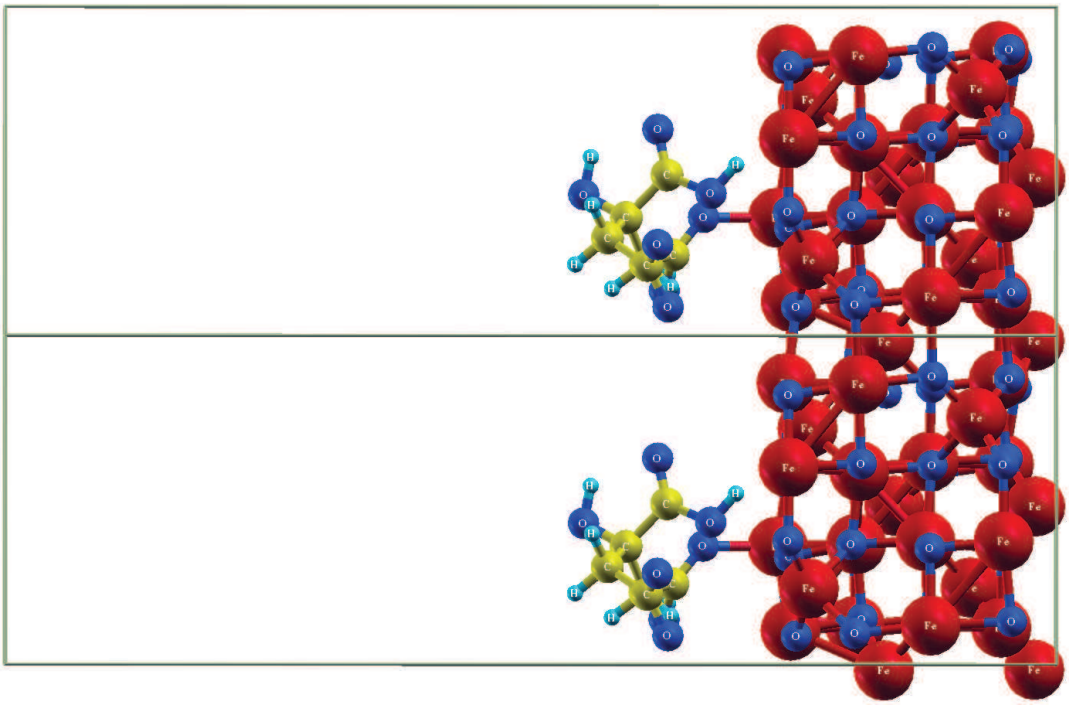

Figure 3.3: Three dimensional view of citric acid ligand at magnetite surface.

[4]Structures drawn using XCrySDen visualization program [Kokalj 1999]

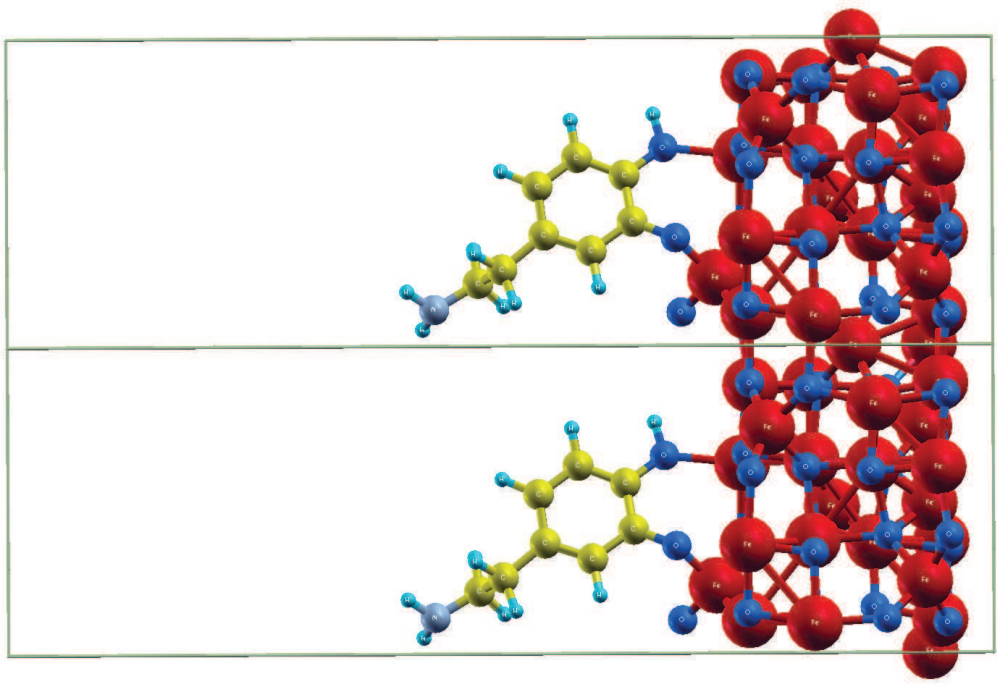

Figure 3.4: Three dimensional view of dopamine ligand at magnetite surface.

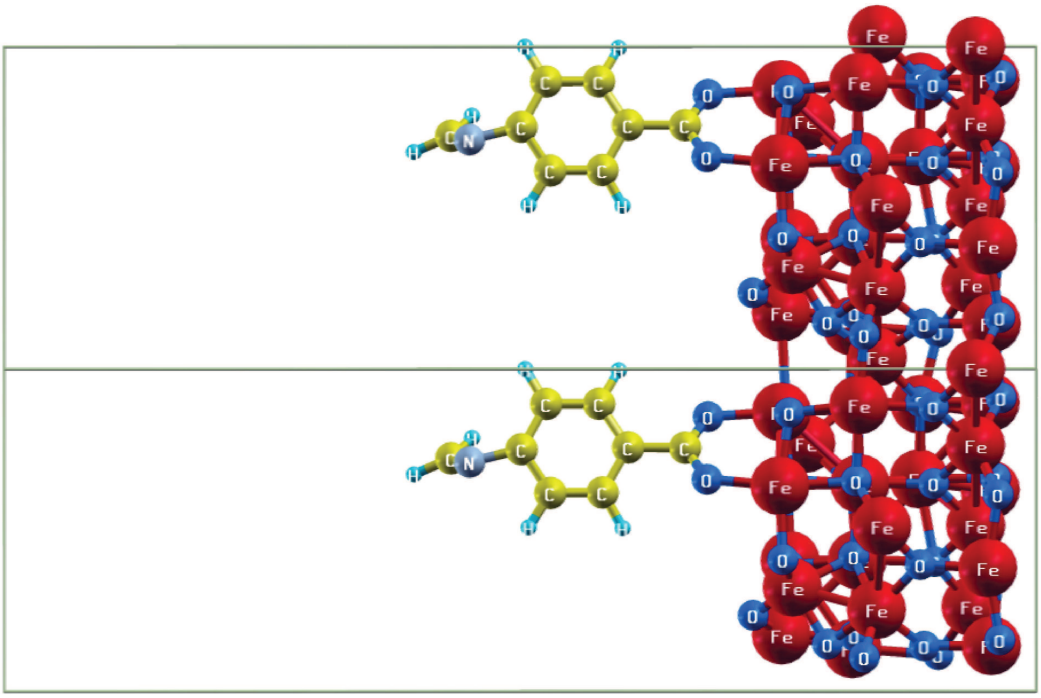

Figure 3.5: Three dimensional view of 4 - aminomethyl benzoic acid ligand at magnetite surface.

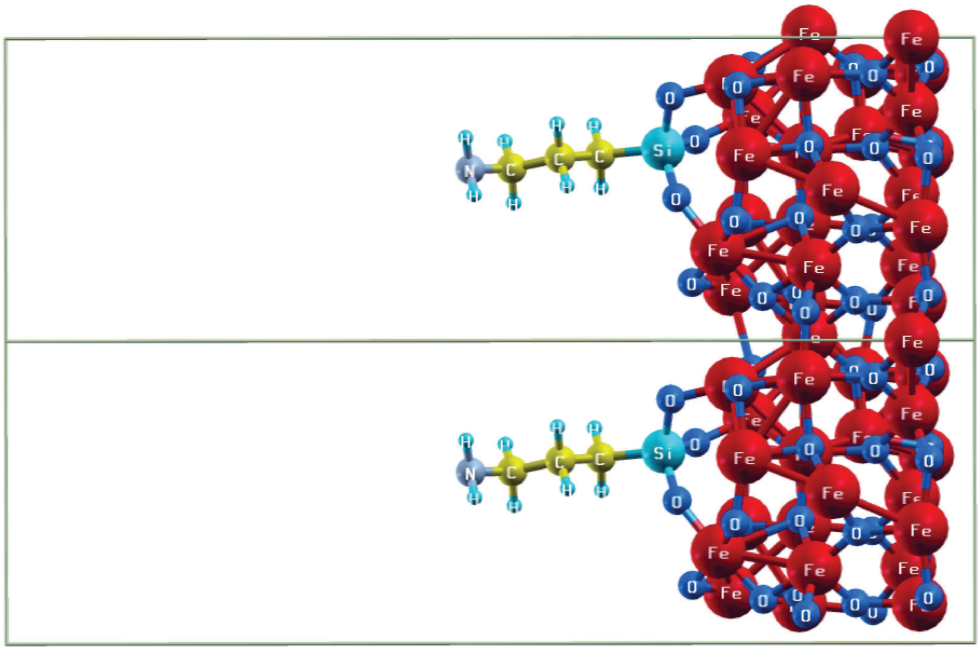

Figure 3.6: Three dimensional view of (3 - aminopropyl) triethoxysilane ligand at magnetite surface.

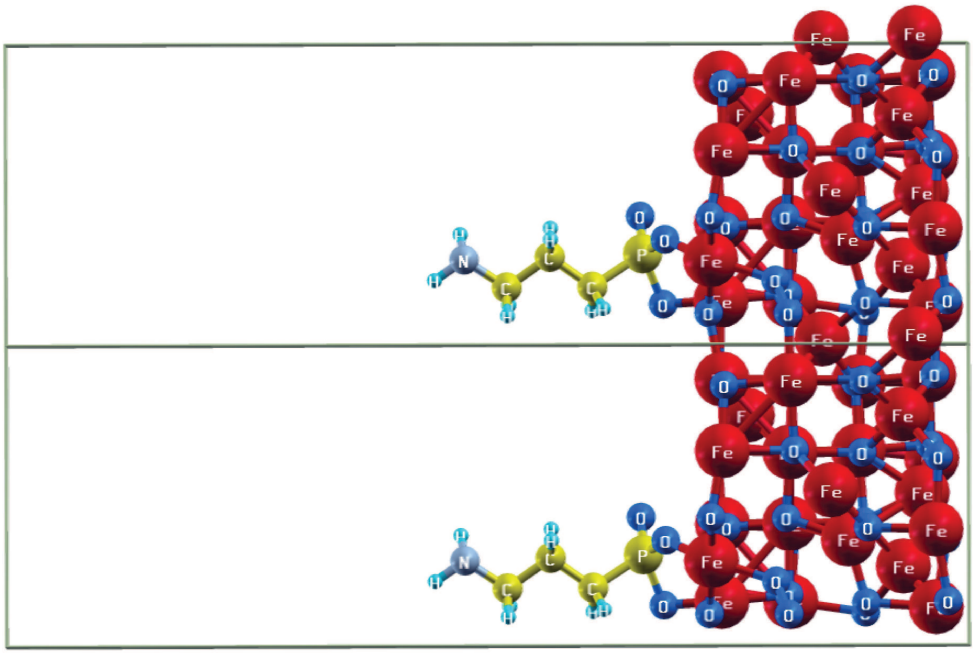

Figure 3.7: Three dimensional view of (3 - aminopropyl) phosphonic acid ligand at magnetite surface.

Table 3.1: Binding energy of studied systems.

Molecule	DOPA	CITRATE	AMEB	PHOS
E [Ry] (molecules alone)	-186.66	-300.89	-184,37	-177.63
E [Ry] (surface Fe_3O_4/ γ-Fe_2O_3)	-2334.98	-2334.98	-2341.27	-2341.27
Sum	-2521.64	-2635.87	-2525,64	-2518,90
E [Ry] (Molecule+Surface)	-2522.08	-2635.98	-2526,05	-2519,23
E [Ry] (Molecule+Surface)-Sum	**-0.44**	**-0.11**	**-0.41**	**-0.34**

The reason could be that the oxidation degree of the iron atoms at the octahedral site differs from the one at the tetrahedral sites. This was also checked using a forced orientation of the ligands on preferential sites; the binding energy was definitely lower in the octahedral case. Trends show that the binding energy is lower for DOPA (table 3.1)

Besides, in the case of dopamine, we found that the binding happens in the surprising configuration of a "bridging", that is, two oxygen atoms binding on two different iron atoms on the surface (Figure 3.3 *b*), where traditional chemistry would have preferred a chelate, with two oxygen atoms from the ligand closer to the same iron atom than to other iron atoms. This was also checked by a systematic variation of the O-C-O angle on the ligand. In this case, the automatic optimization showed that the dopamine molecule could also bind at the surface with the NH_2 group, also at the octahedral site. These results are also coherent with the ones from [Rajh *et al.* 2002], although in the latter case they are obtained either by experimental means (XANES) or by simple *ab initio* modeling of single atom iron oxide clusters attached to ligands.

It was checked if the reason could be the difference in oxidation by computing the change in Lőwdin charges (projecting the final wavefunction on the atomic wavefunction used for pseudopotential generation) of each atom of the system during grafting. The results, presented in figure 3.8, give evidence that there is indeed a partial reduction of Fe^{3+} atoms, the *d* orbitals being reduced, and the *p* orbitals of dopamine, showing a marked increase in charge, especially around the linking oxygen atoms, at the right of the figure. Those results are totally coherent with those from Mőssbauer spectrometry [Fouineau *et al.* 2013] [5].

[5] See Appendix A

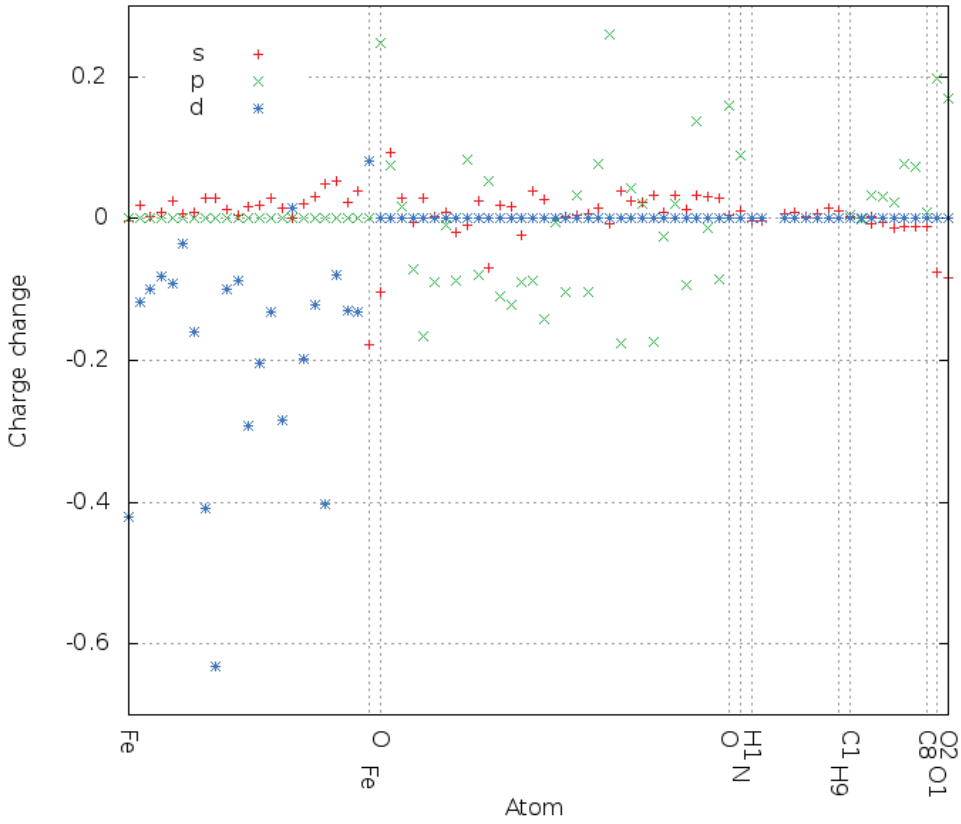

Figure 3.8: Change in the Lőwdin charges for each atom of iron oxide and dopamine after grafting (LDA+U).

We have also computed the reduced gradient of the electronic density according to the method of [Scemama *et al.* 2011] and plotted the isosurface at a value of 0.5. At this value, this method also called Electron Pair Localization Function (EPLF) can show whether bonds are either ionic or covalent by estimating the degree of pairing electrons in the system. One can check in figure 3.9 that the bonding of the atoms in dopamine is, as expected, covalent (no isosurface is present except at the center of the aromatic ring) while the bonding in iron oxide is strongly ionic (high presence of the isosurface). The welcome result is then that the bonding of the dopamine molecule and the iron oxide surface is covalent, which is also a strong requirement for pharmaceutical applications of the considered nanohybrids. In this application, the covalent bonds have an advantage over ionic ones due to the fact that the human body is an aqueous environment and it is known that many ionic compounds are soluble in water, the polarity of water breaking them apart and separating the positive and negative ions from each other. In the body, positive ions are called free radicals, they can react with other radicals (join their unpaired electrons and make covalent bonds) or with molecules that contain only paired electrons.

Most of molecules in the body are non-radicals hence it is likely that free radicals will steal electrons from healthy cells causing cellular damage. The harmful effect of free radicals causing biological damage is termed oxidative stress. This physiological stress on the body was combined with the various pathological conditions including cardiovascular disease, cancer, neurological disorders, diabets, ischemia/reperfusion, other diseases and ageing [Valko *et al.* 2007].

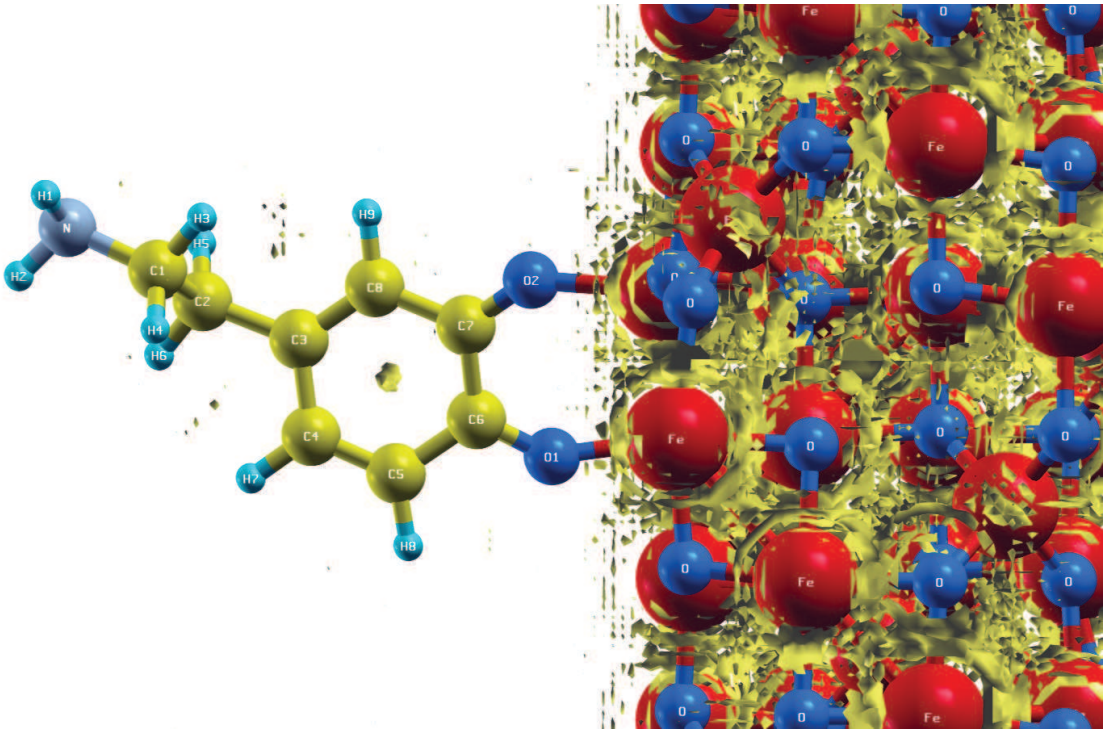

Figure 3.9: Reduced density gradient isosurface at value of 0.5. Red atoms are irons, dark blue - oxygens, yellow - carbons, light blue - nitrogen and blue - hydrogens.

The ionicity of bonds as well as the change in Lőwdin charges were also checked in case of other ligands, namely AMEB, PHOS and citrate at the magnetite surfaces. The graphical visualizations of results are presented in Figures 3.10 - 3.12. Similarly as in the case of dopamine one can see that the bondings of AMEB (Fig. 3.22(c)) is covalent and result of citrate (Fig. 3.11(a)) may indicate ionicity (presence of isosurface also close to citrate molecule). In the case of PHOS (Fig. 3.12(b)), one can see the presence of isosurface near to the carbon atom of ligand what indicate a limiting case between covalent and ionic bond. On the graphs presenting the charge change one can conclude that there is a reduction of Fe^{3+} atoms, the increase in charge is noticeable especially around the linking oxygen atoms.

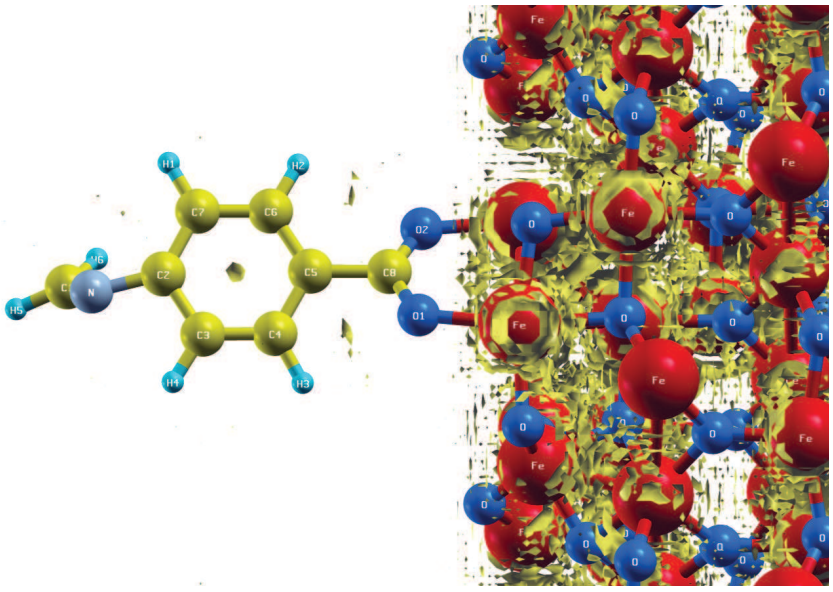

(a)

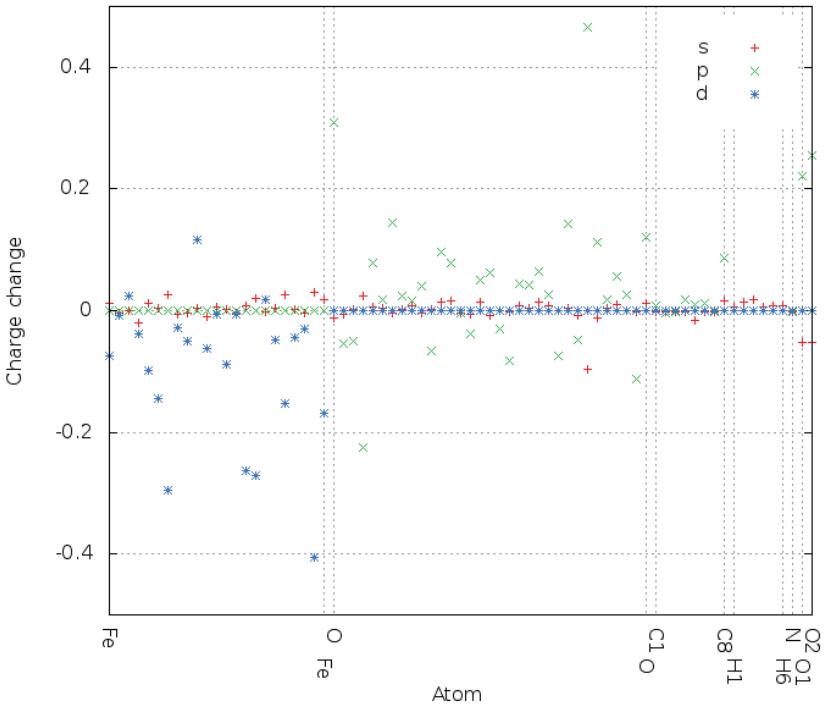

(b)

Figure 3.10: Ionicity of magnetite grafted by AMEB (*a*) the change in Lőwdin charges after bonding (*b*).

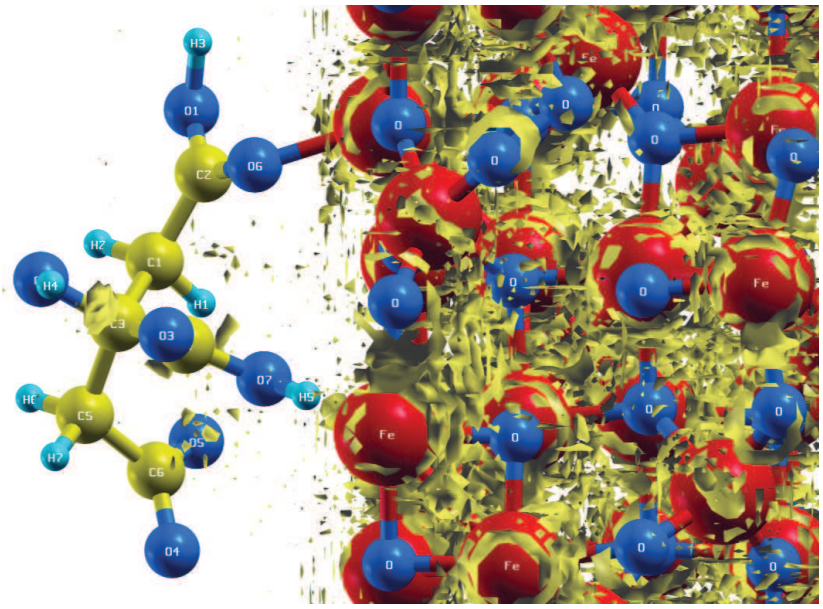

(a)

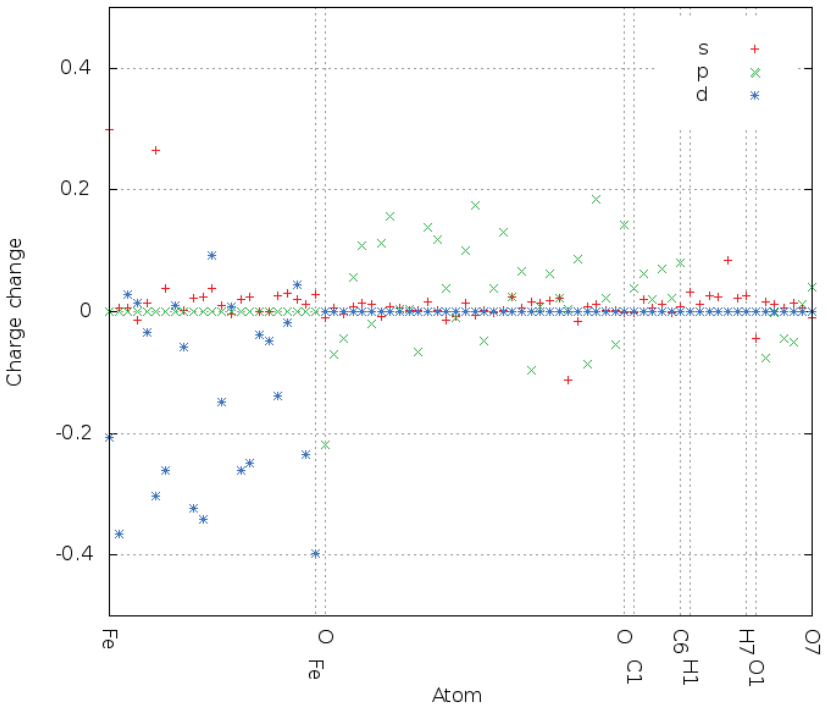

(b)

Figure 3.11: Ionicity of magnetite grafted by citrate (*a*) the change in Lőwdin charges after bonding (*b*).

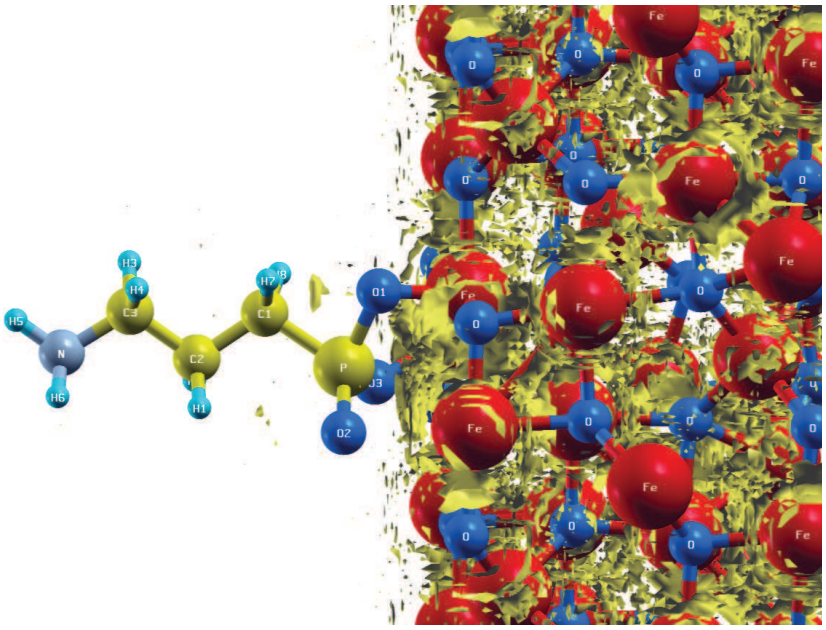

(a)

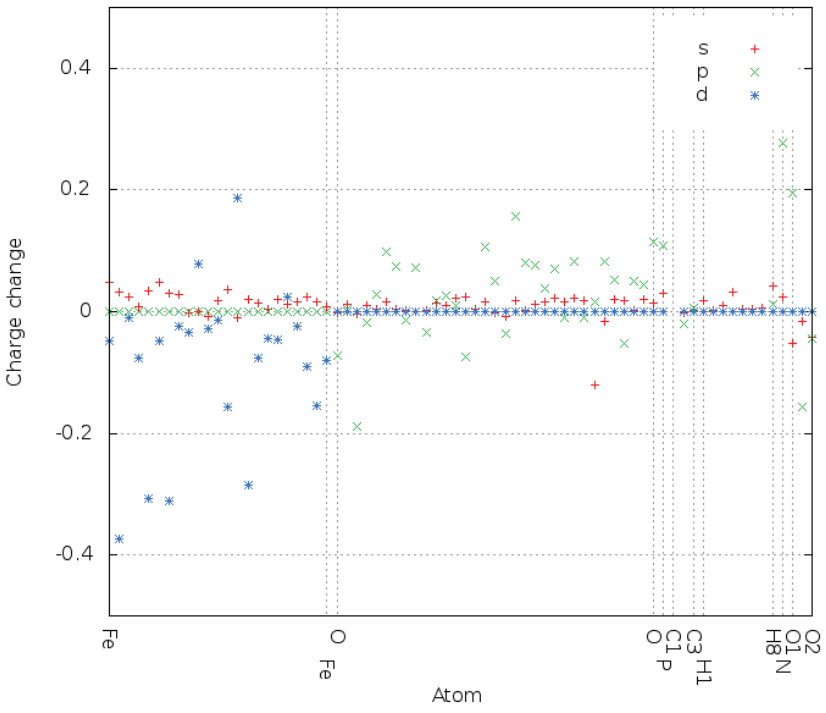

(b)

Figure 3.12: Ionicity of magnetite grafted by PHOS (a) the change in Lőwdin charges after bonding (b).

APTES is one of the common molecule used for surface functionalization [Cheang *et al.* 2012], such systems are nontoxic [Natarajan *et al.* 2008]. APTES molecules can dissolve in polar and nonpolar olvents as well as they have a high solubility in cell membranes. Nanoparticles of silicon dioxide amino - functionalized by APTES were developed for gene therapy [Cheang *et al.* 2012], they are also used to promote protein adhesion and cell growth for biological implants [Howarter & Youngblood 2006], [Bambini *et al.* 2006].

In order to evaluate the preferred binding of the magnetic nanoparticles modified by APTES, the subsequent simulations were performed. At first, the geometry of the systems consisting of maghemite and APTES were fully optimized. Calculations concerned four cases, where hydrogen atoms linked to silicon were successively removed (Figures 3.13 - 3.16).

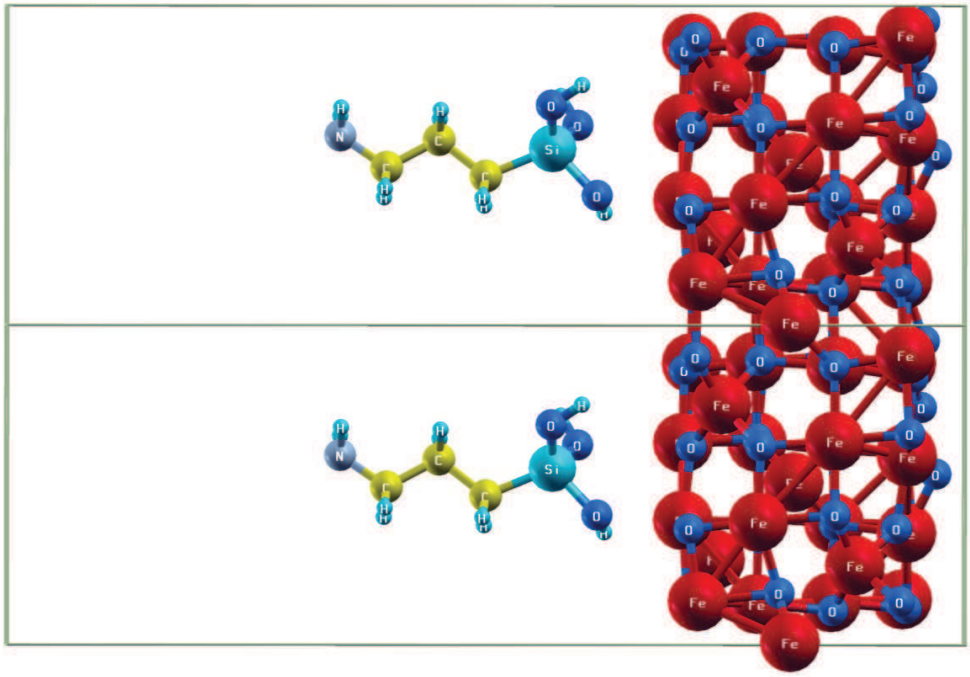

Figure 3.13: Three dimensional view of maghemite surface functionalized by APTES.

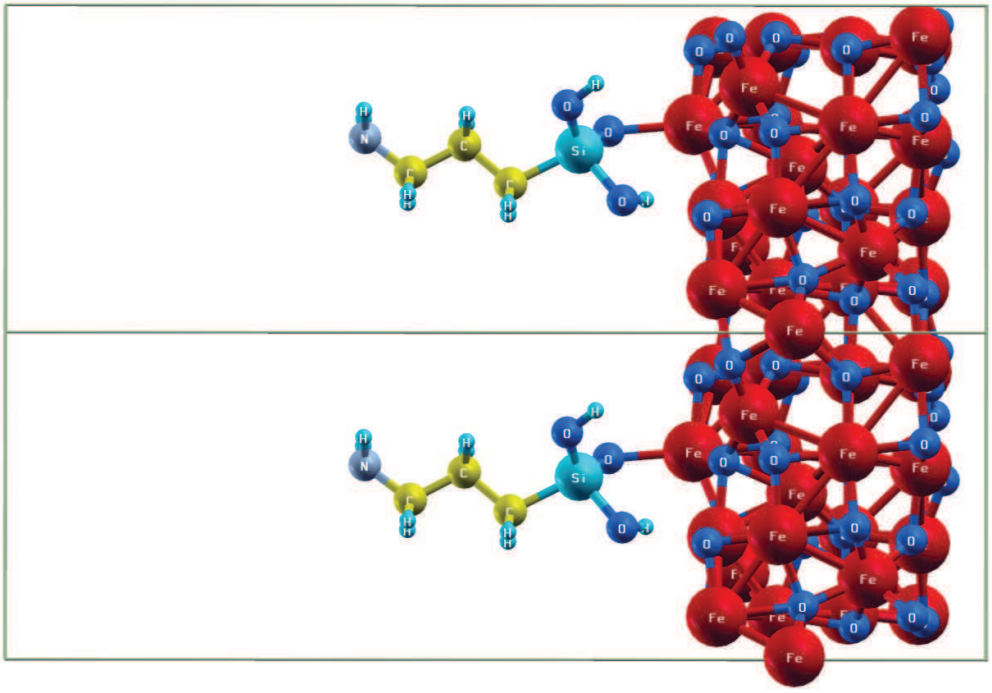

Figure 3.14: Three dimensional view of maghemite surface functionalized by APTES (1 hydrogen atom removed).

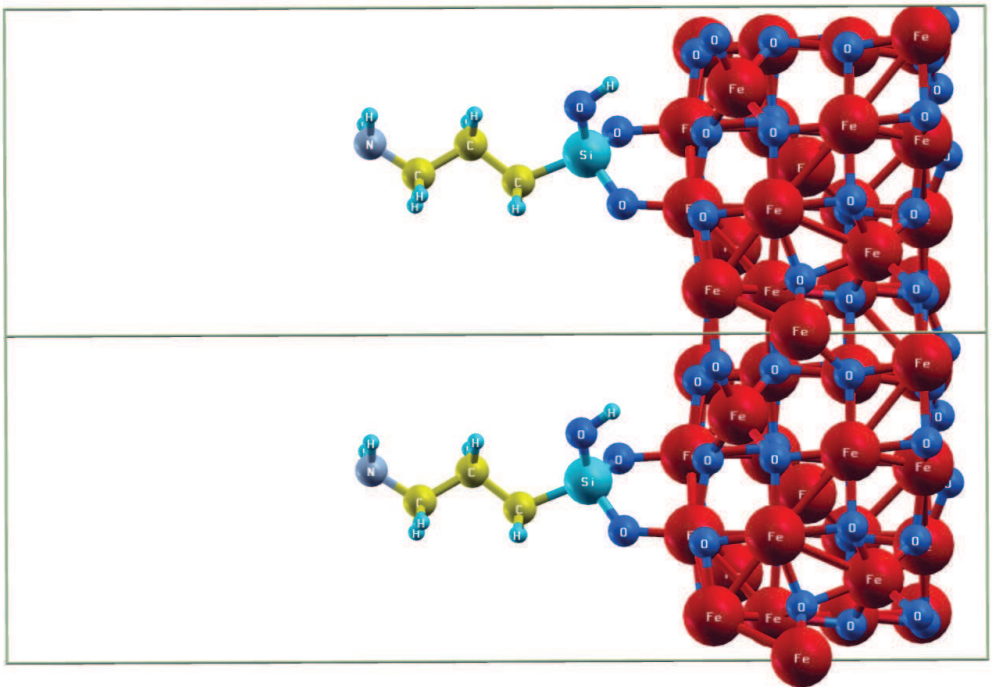

Figure 3.15: Three dimensional view of maghemite surface functionalized by APTES (2 hydrogen atoms removed).

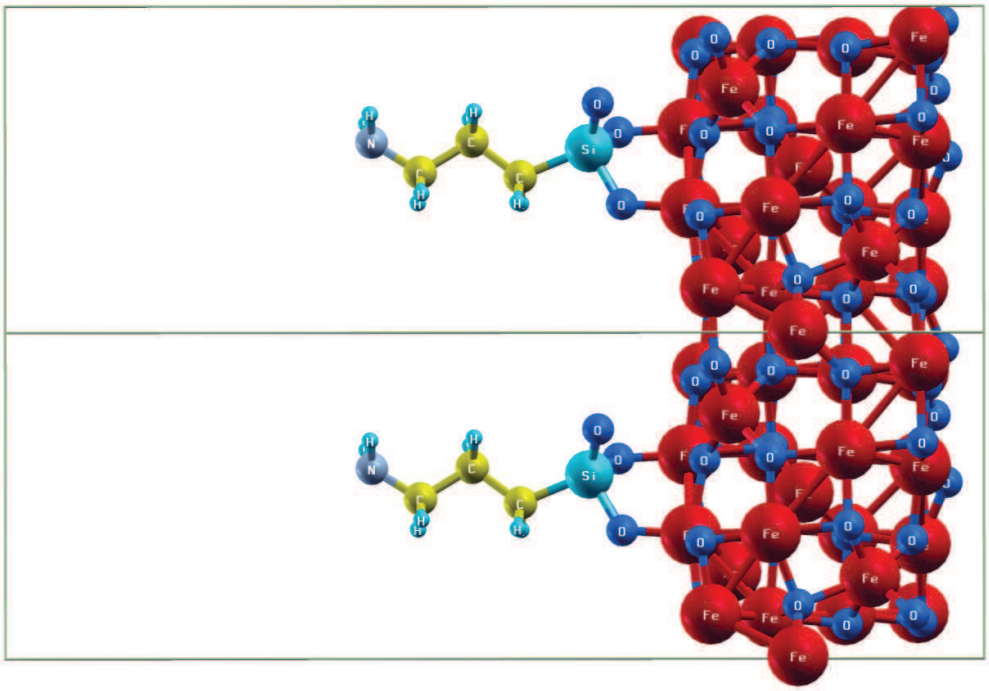

Figure 3.16: Three dimensional view of maghemite surface functionalized by APTES (3 hydrogen atoms removed).

Afterwards, the binding energies were calculated, the results of which are presented in Table 3.2. One can see that the lowest binding energy of -0.88 Ry occurs in the system with APTES molecule without hydrogen atoms linked to silicon, thus it is the strongest combination. This form of APTES was used in further calculations involving maghemite surface functionalization. The ionicity of bonds (Figure 3.17) as well as change in the Lőwdin charges (Figure 3.18) were checked.

Table 3.2: Binding energy as a function of removed H atom.

Molecule	**APTES (3H)**	**APTES (2H)**	**APTES (1H)**	**APTES (0H)**
E [Ry] (molecules alone)	-173.12	-171.72	-170.36	-168.96
E [Ry] (surface maghemite)	-2341.27	- 2341.27	-2341.27	-2341.27
Sum	-2514.39	-2512.99	-2511.63	-2510.23
E [Ry] (Molecule+Surface)	-2514.86	-2513.69	- 2512.45	-2511.11
E [Ry] (Molecule+Surface)-Sum	**-0.47**	**-0.7**	**-0.82**	**-0.88**

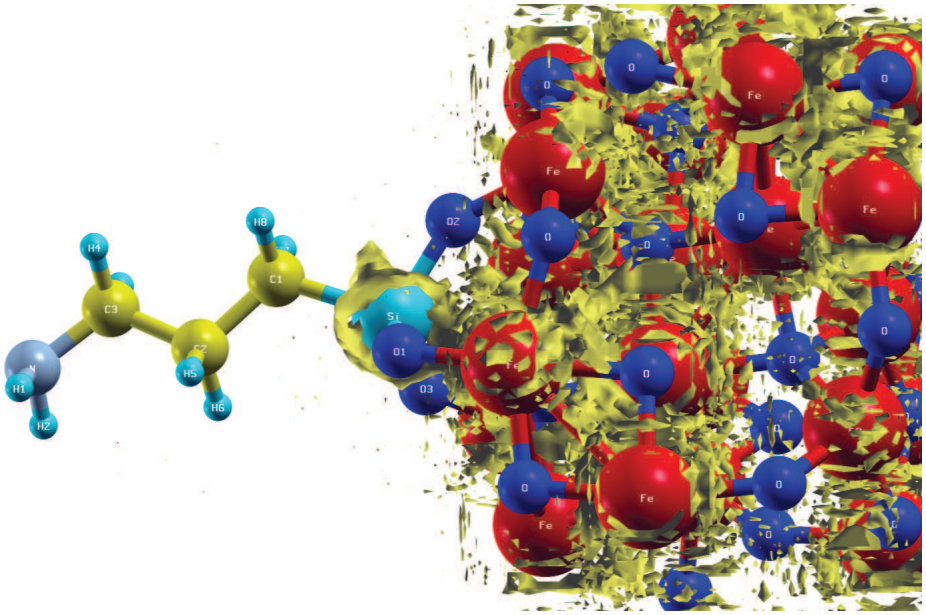

Figure 3.17: Optimized structure of APTES bonded to magnetite surface and reduced electronic density gradient isosurface at value of 0.5.

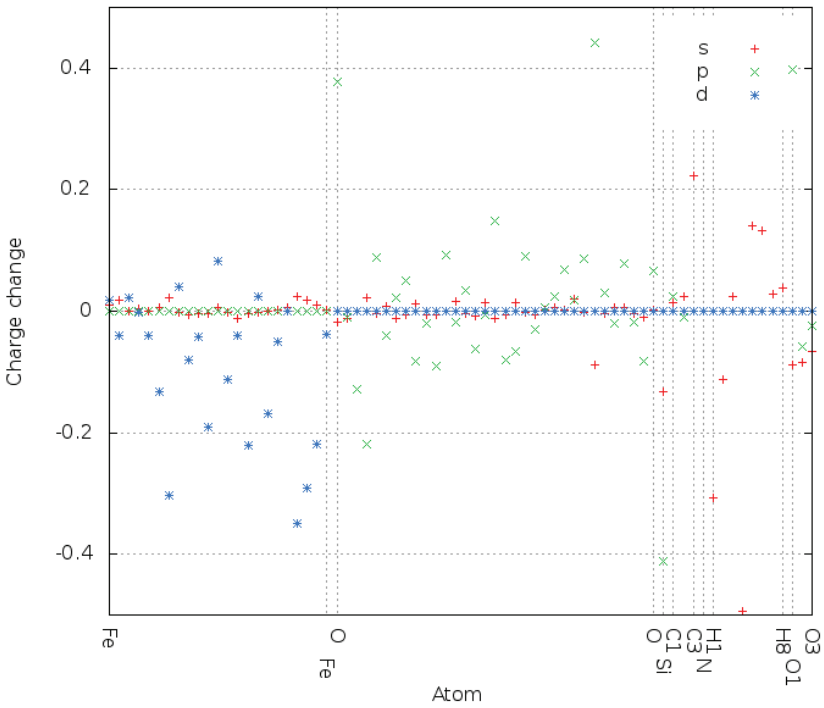

Figure 3.18: The change in Lőwdin charges after grafting magnetite by APTES.

The functionalization of magnetite surface based on the use of aryl functional group was also studied. The aryl diazonium salts have been shown to be useful organic reagents for the surface modifications of carbon-based and metallic substrates. This method has been recently extended to iron oxide nanoparticles, in this case, the nature of aryl and oxide surface linkage is not yet established. In this work, phenoxy (C_6H_5O) and phenyl (C_6H_5) radical were used to functionalize the surface of magnetite. The LDA+U parameters were set to U = 4.5 eV and J = 0.367 eV. A cutoff energy of 30 Ry and a 0.2 Ry mixing factor for self-consistency was used. We used a 3x3x3 sampling of the first Brillouin zone and a Gaussian smearing factor of 0.02 Ry. The absolute pseudo-energies with single systems were determined and then computed binding energies by difference. The values of -0.18 Ry and -0.83 Ry were obtained, respectively for C_6H_5 and C_6H_5O. Thus, the phenoxy group provides the most robust system.

The change in Lőwdin charges of each atom was computed. From the result, presented in Figure 3.19 one can see a partial reduction of Fe^{3+} atoms, the *d* orbitals being reduced, showing increase in charge, especially around the linking oxygen atoms in the case of the phenoxy group. In the case of phenyl ligand, a small change in the *s* orbitals is noticeable, while the reduction of Fe^{3+} atoms is not as important.

The reduced gradient of the electronic density was also computed in order to check the nature of the linkage and plotted the isosurface at a value of 0.5. The results, presented in Figure 3.20, illustrate that the bonding of the atoms in the ligand is covalent and the bonding in iron oxide is strongly ionic (high presence of the isosurface).

From those results one can conclude that those molecules preferentially attach via oxygen-surface covalent bond and provides enhanced chemical stability, what makes them interesting for potential applications. These results were confirmed by an experimental findings [6].

[6] See Appendix B

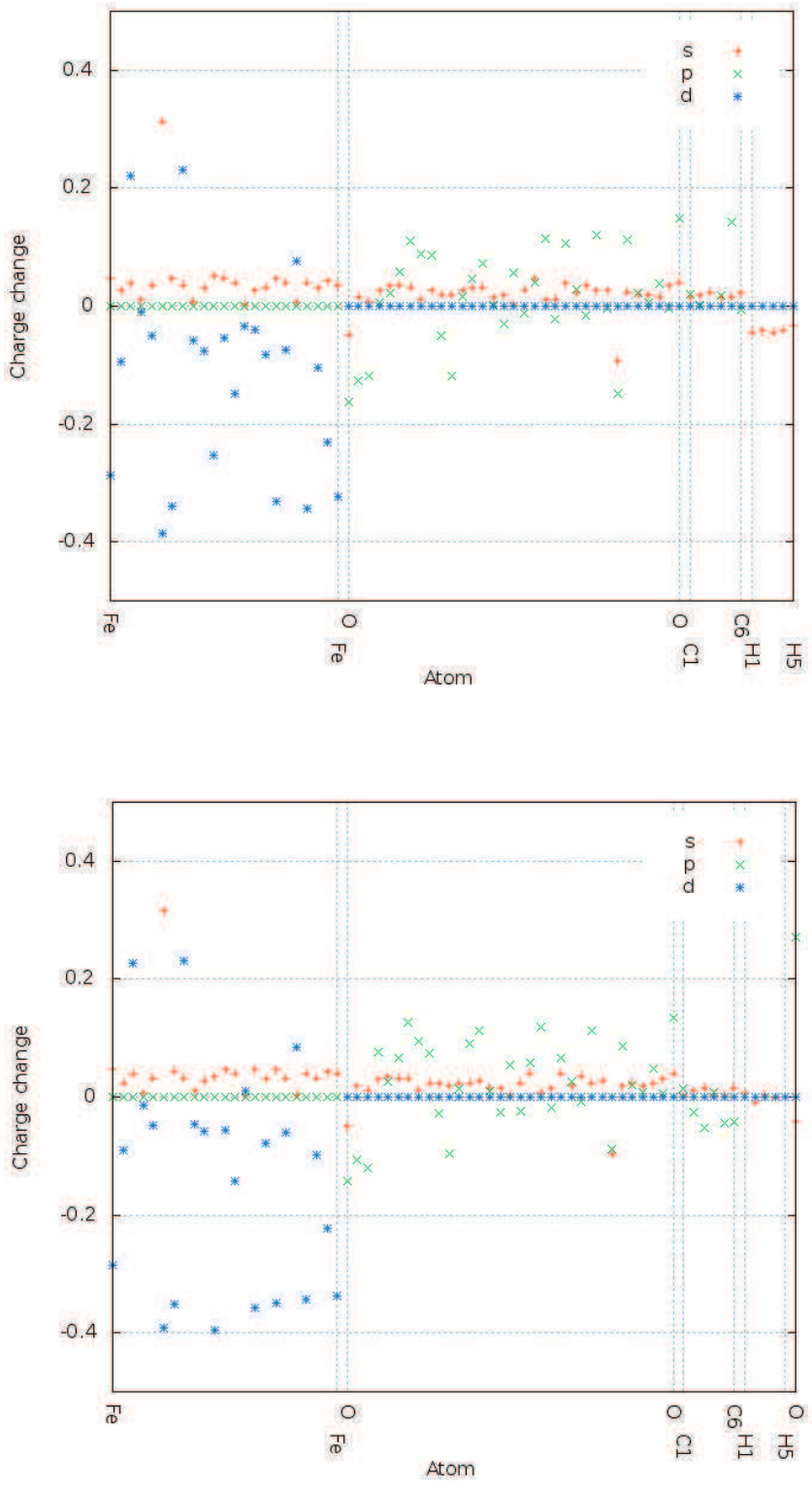

Figure 3.19: The change in Lőwdin charges after bonding.

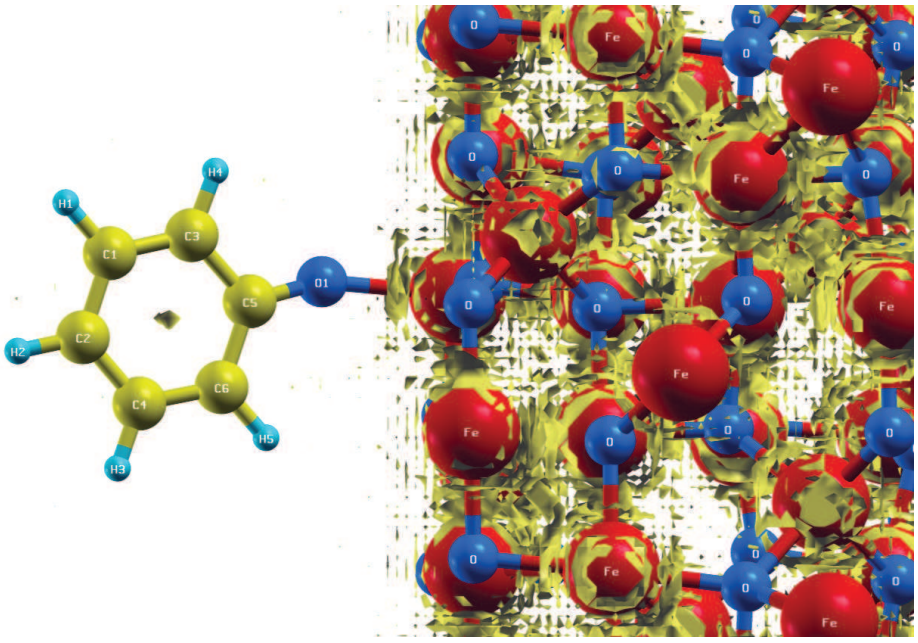

(a)

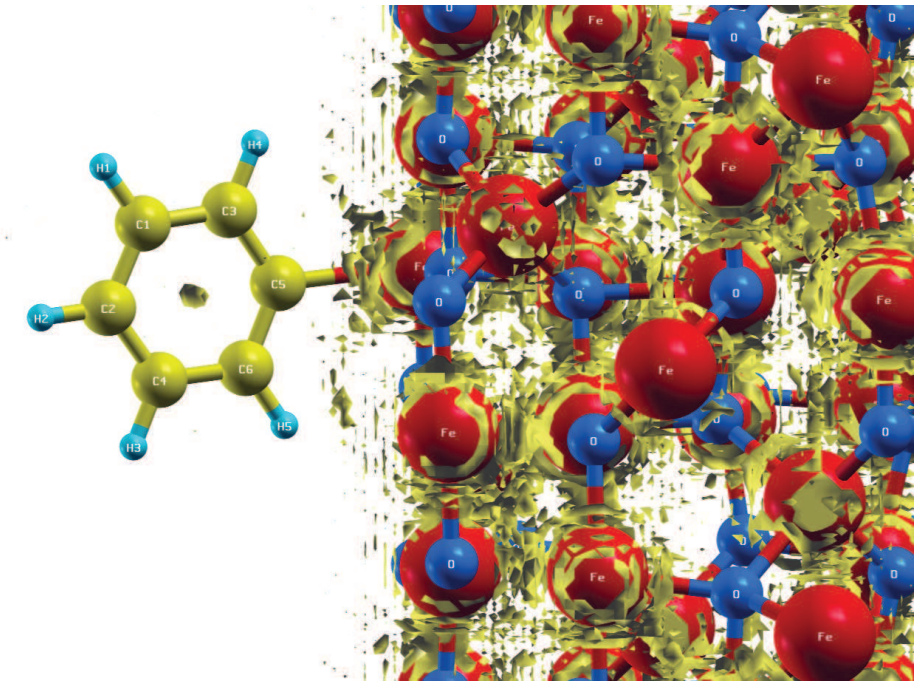

(b)

Figure 3.20: Magnetite surface functionalized by aryl diazonium salts, (*a*) C_6H_5O and (*b*) C_6H_5 as well as reduced electronic density gradient isosurfaces at a value of 0.5.

System	Magnetite surface	Citrate	Dopamine
Total magnetization	75.03 μ_B /cell	92.69 μ_B /cell	83.46 μ_B /cell
Absolute magnetization	83.67 μ_B /cell	97.17 μ_B /cell	90.90 μ_B /cell

Table 3.3: Some quantitative results obtained on the chosen systems

3.3.2 Study of magnetic properties

To study the effect of ligands on the magnetic properties of magnetite, the density of states (DOS) and projected density of states (PDOS) were calculated. From the total density of states plotted in Figure 3.21, one can see that the presence of dopamine does change the small gap of magnetite by adding some conduction electrons, when the presence of citrate does not significantly change the total density of states.

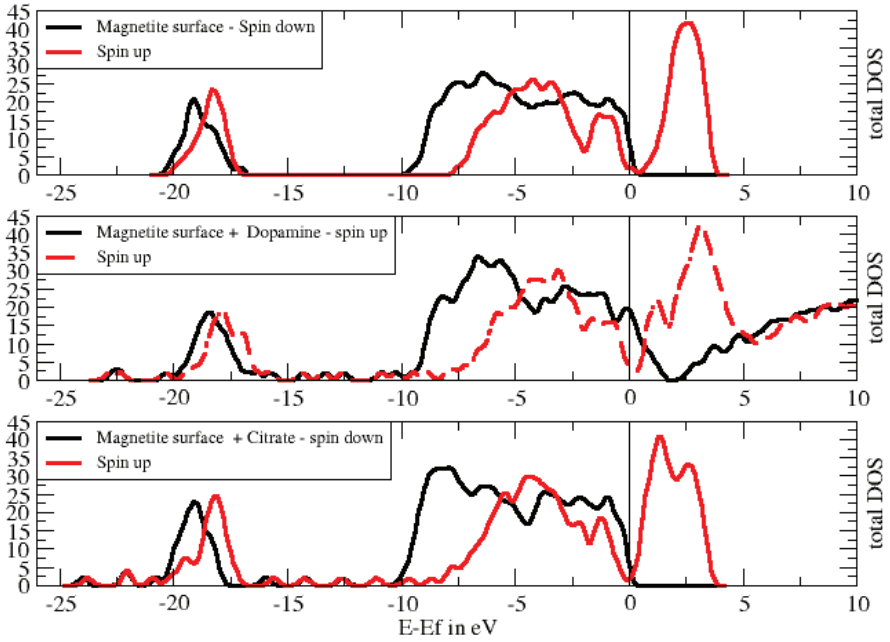

Figure 3.21: Total density of states for three chosen systems.

The difference of spin up and down density of states led us to suspect an effect of functionalization on the magnetization of the systems. Those results are summarized on Table 3.4. Functionalization leads to a marked increase in magnetism, when the value of magnetite surface alone is close to the one obtained by [Lodziana 2007]. This increase in magnetic momenta can be compared to results recently experimentally obtained by [Li *et al.* 2009].

Moreover, in order to clarify the role of *d* orbitals on iron atoms on those effects, in Figure 3.22 typical electronic densities isosurfaces at Fermi energy were plotted .

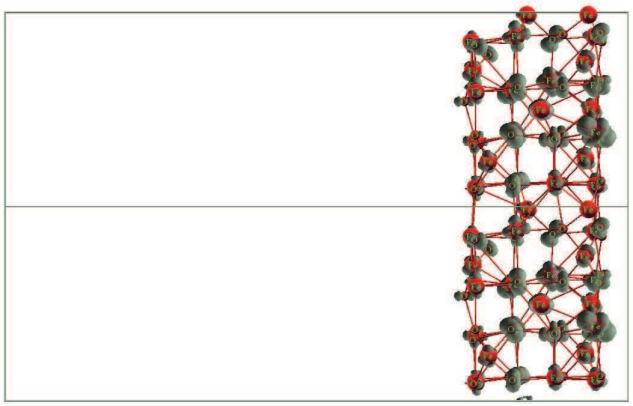

(a)

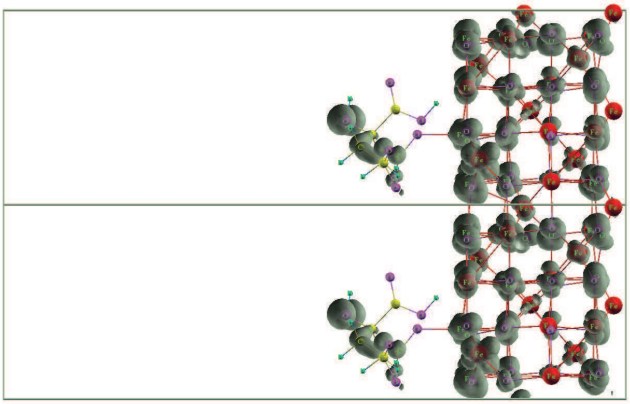

(b)

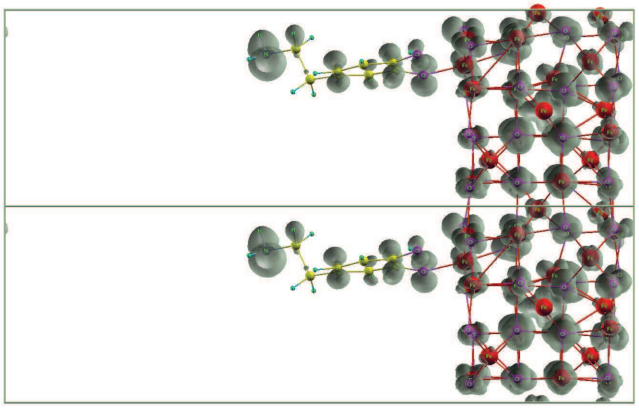

(c)

Figure 3.22: Electronic isosurfaces at the Fermi energy of (a) magnetite surface, (b) magnetite surface functionalized by citrate ligand , (c) magnetite surface functionalized by dopamine ligand.

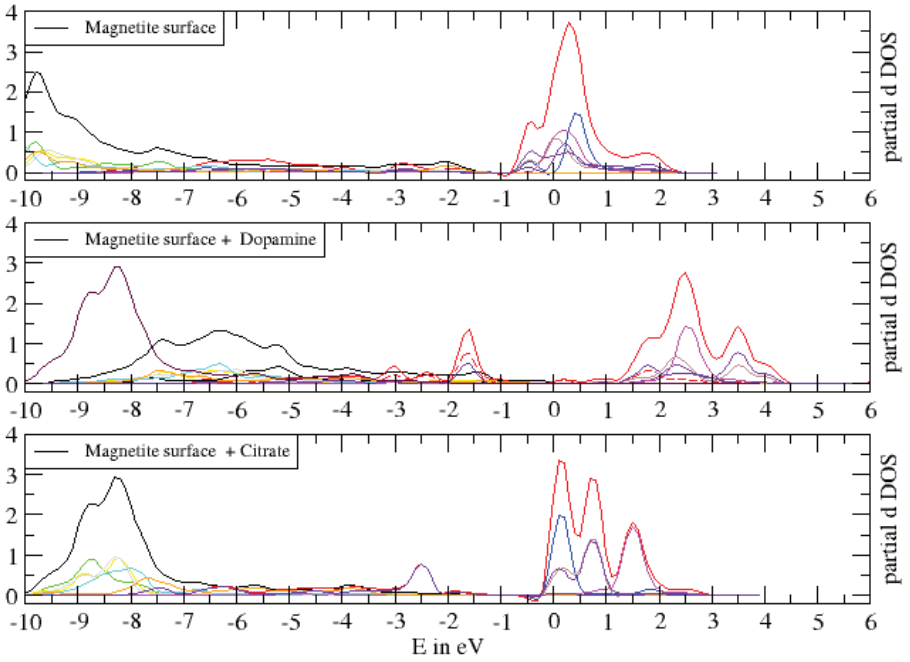

Figure 3.23: Partial density of states projected on a "d" state for an atom of type (A) at the surface

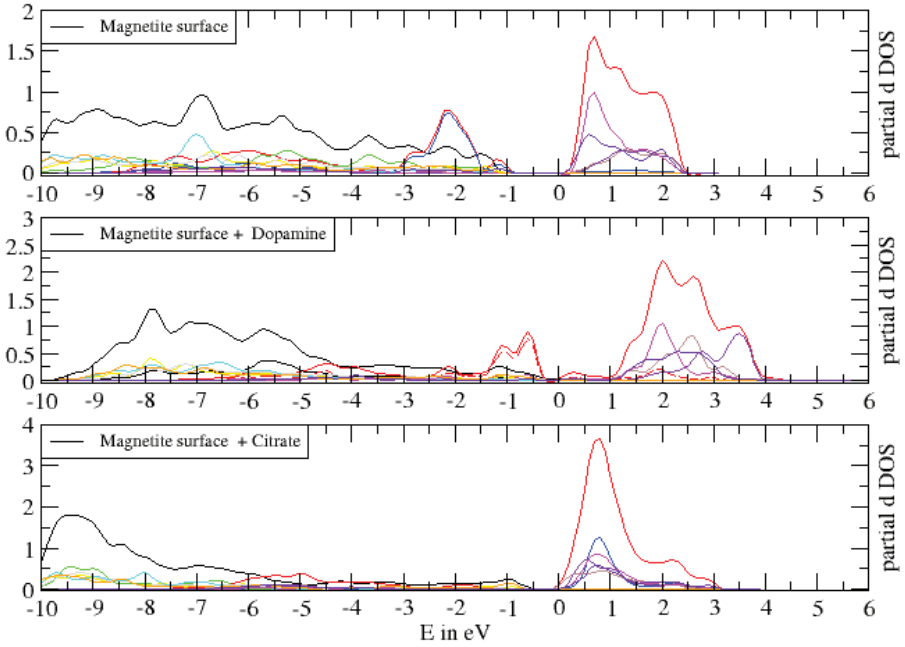

Figure 3.24: Partial density of states projected on a "d" state for an atom of type (B) at surface

One can conclude from those figures the typical π character of orbitals contributed by dopamine to conduction electrons at the surface, versus the lack of contribution of the citrate ligand. In both cases, there is however a change of the d character of electrons contributing to conductivity close to the surface, when in the case of the non-functionalized magnetite surface the conductivity rather comes from bulk electrons. Those results remind us those obtained by [Parkinson *et al.* 2010], about the change in the conducting behavior of magnetite induced by hydrogen adsorption, turning from a semiconductor to a half-metal.

In order to further analyses of those results, projected densities of states for two typical atoms, namely Fe atoms of octahedral (A) types and tetrahedral (B) types were plotted in Figure 3.23 and 3.24. Only d-character wavefunctions are plotted around the chosen atoms, and one can see that the presence of either dopamine or citrate leads to a marked change in the projected densities of states around the chosen atoms, the presence of dopamine shifting the positions of the peaks when the presence of citrate mainly changes the shapes of the peaks. From this it can be concluded that the functionalization by dopamine will induce a stronger change in the magnetic properties of the system than the one by citrate, which, however, tends to induce a stronger magnetization.

3.3.3 Study of the binding of a nanoparticles and a surface of gold

The composition of gold and iron oxide might have important biomedical applications not only due to the optical properties of gold but also due to its negligible cytotoxicity and to the magnetic properties of iron oxide. Therefore, we tested how the combination of those two compounds would change magnetization. The non-collinear magnetism study of iron oxide cluster on the gold layer (Fig. 3.25) was performed. In Table 3.4 the values of the absolute magnetization are summarized. The calculated value of magnetization for iron oxide was 45.56 μ_B /cell and increased to 49.57 μ_B /cell after linking with gold layer. This additional magnetization may result from an interfacial effect.

To check the origin of magnetization enhancement upon the incorporation of gold, post processing calculations of non-collinear magnetism were performed. The obtained outcome (Fig. 3.26), may indicate that magnetization increases as a result of trapping free electrons from gold particles by iron site. This finding suggests that the magnetic properties of iron oxide combined with gold are suitable for applications such as magnetic hyperthermia or contrast agents.

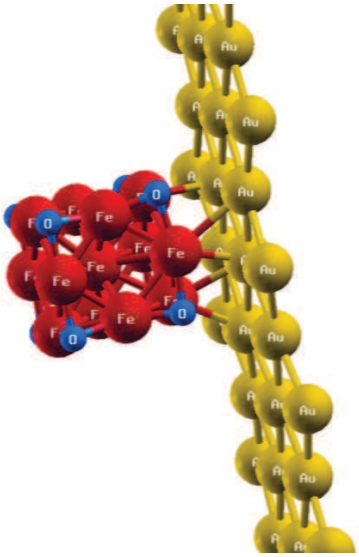

Figure 3.25: Optimized structure of iron oxide cluster on the gold layer.

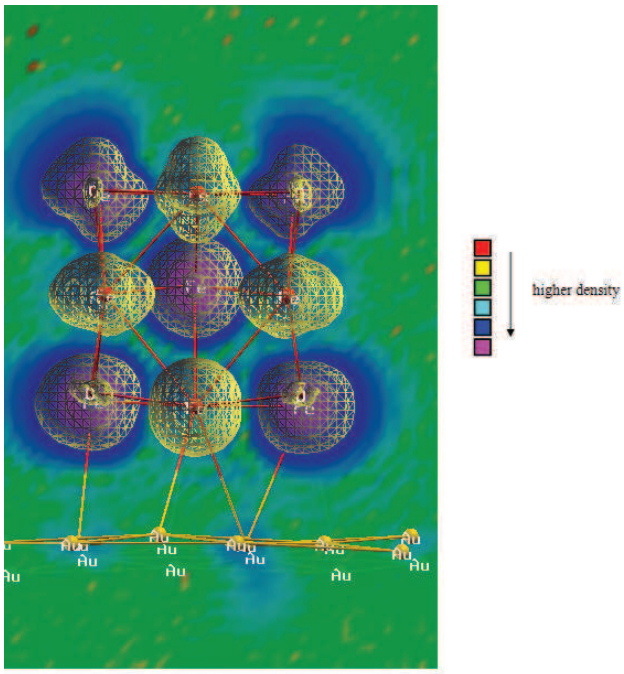

Figure 3.26: Magnetization density of iron oxide cluster with gold layer.

System	Iron Oxide	Gold Layer + Iron Oxide
Absolute magnetization	45.56 μ_B /cell	49.57 μ_B /cell

Table 3.4: Change in magnetization

3.4 Summary and Conclusions

During the recent years, the development of functionalized nanoparticles with specific surface properties has been a subject of research, mainly due to their promising usage in pharmaceutical and biomedical sciences. In this chapter, the surface modification of various ligands has been studied. The way a molecule of biological interest can bind to the surface of iron oxide nanoparticles was shown. The result showing that dopamine preferentially binds on octahedral sites was confirmed and a quantitative assessment of this preference was obtained. The covalent nature of the bond was proved, which makes such ligands efficient for the functionalization of nanoobjects of medical interest. From the carried out calculations, it has been suggested that the system with dopamine is the most stable among the considered systems.

We also predicted that attachment of dopamine and citrate would induce a different change in the electronic properties of the systems, but in both cases an enhancement of magnetization was observed. Therefore, grafting by those ligands can keep the magnetism alive, thus providing the basis for the applications of such functionalized iron oxide nanoparticles in magnetic drug delivery and magnetic fluid hyperthermia. Those findings are confirmed by some recent experimental work.

Results concerning functionalization of aryl diazonium salts suggest that they are highly suitably for further applications because of the formation of strong iron oxide-aryl surface bond, the nature of which is most likely covalent.

It was also observed that is possible to raise the magnetization of nanocomposites by linking the iron oxide with the gold. This result is very important from a medical point of view and promises such applications as targeted medical delivery.

Chapter 4

Magnetic Modeling and Properties of Iron Oxide Nanoparticles

4.1 Introduction

In this chapter, we will perform some *ab initio* computations of the magnetic properties of simple iron oxide clusters, and from those results try to develop a magnetic model of the nanoparticles to which this work is devoted. Indeed, a large number of experimental as well as theoretical effort has been devoted to this problem, as reviewed in [Kodama 1999], or, more generally, to magnetic nanoparticles based on cobalt or nickel.

It has indeed been proven possible to create nanoparticles alternating layers of various materials with different magnetic behaviors (antiferromagnetic - AFM- or ferromagnetic FM, even ferrimagnetic), which will influence the magnetic moment structure at the surface or interface [Tronc *et al.* 2003] . Exchange bias can appear in those cases, corresponding to a shifted hysteresis loop and a ferrimagnetic alignment of the moments near to the center of the nanoparticle as well as a pinning of the magnetic moments on the surface.

Organic ligands on the surface have also a strong influence on the magnetic structure of nanoparticles, as described in the pioneering work of [Berkowitz *et al.* 1975] and related work, such as [Kseolu 2006] also pinning the spins near the surface.

Surface effects alone can change the magnetic structure, as it was demonstrated for instance in the case of cobalt in [Luis *et al.* 2002], cobalt oxide in [Hajra *et al.* 2012], magnetite powders in [Kihal *et al.* 2012], and maghemite nanoparticles in [Nadeem *et al.* 2012]. Those effects have been reviewed, in the case of iron oxide, in [Tronc *et al.* 2000].

From the theoretical point of view, this problem has been considered mainly from the phenomenological side. Typically, Monte-Carlo calculations on the classical Heisenberg model are performed, such as in [van Leeuwen *et al.* 1994] where the results were com-

pared to experimental data obtained on CO-functionalized NiPt clusters, as well as to DFT calculations where magnetic moments were computed in the collinear local density functional approach.

The Monte-Carlo-Metropolis approach was also used in the case of magnetite nanoparticles in [Mazo-Zuluaga *et al.* 2009]. In this work, the authors have demonstrated that the surface anisotropy constant can heavily influence the exchange-bias behavior, but this value remains a parameter, the value of which cannot even be precisely infered from experimental data; only a range of possible values is estimated from the resulting magnetic behavior and comparison to experiment.

Therefore, in this chapter, we will consider two typical situations: an iron oxide cluster small enough to be tackled by non-collinear density functional theory, functionalized by a molecule, or glued to a gold cluster of the same size, or an iron oxide surface. The changes in magnetic behavior are explored using constrained magnetic calculations or external magnetic fields applied to the system, and a possible value for surface anisotropy is estimated from the fit of a classical Heisenberg model on *ab initio* results.

4.2 Computational Details

4.2.1 Structure of the Chosen System

The first objective was to obtain an optimized structure of $Fe_{13}O_8$, which according to mass spectrometry shows higher abundance than other iron oxide clusters with different compositions [Sun *et al.* 2007]. The plane wave basis set was defined by an energy cutoff of 30 Ry (408eV), checked to be enough with the same method used in a previous chapter through the test of convergence (Figure 3.2). A mixing factor of 0.17 was employed. Integration in the first Brillouin zone was performed using 1x1x1 points sampling, since the system is an isolated cluster in a large computational cubic box of size 30 Ångströms and the GGA density functional from PBE [Perdew *et al.* 1996b] was used with the corresponding pseudopotentials computed by A.dal Corso with the "rrkj3" code, taken from the QE website. The optimization procedure was conducted without any symmetry.

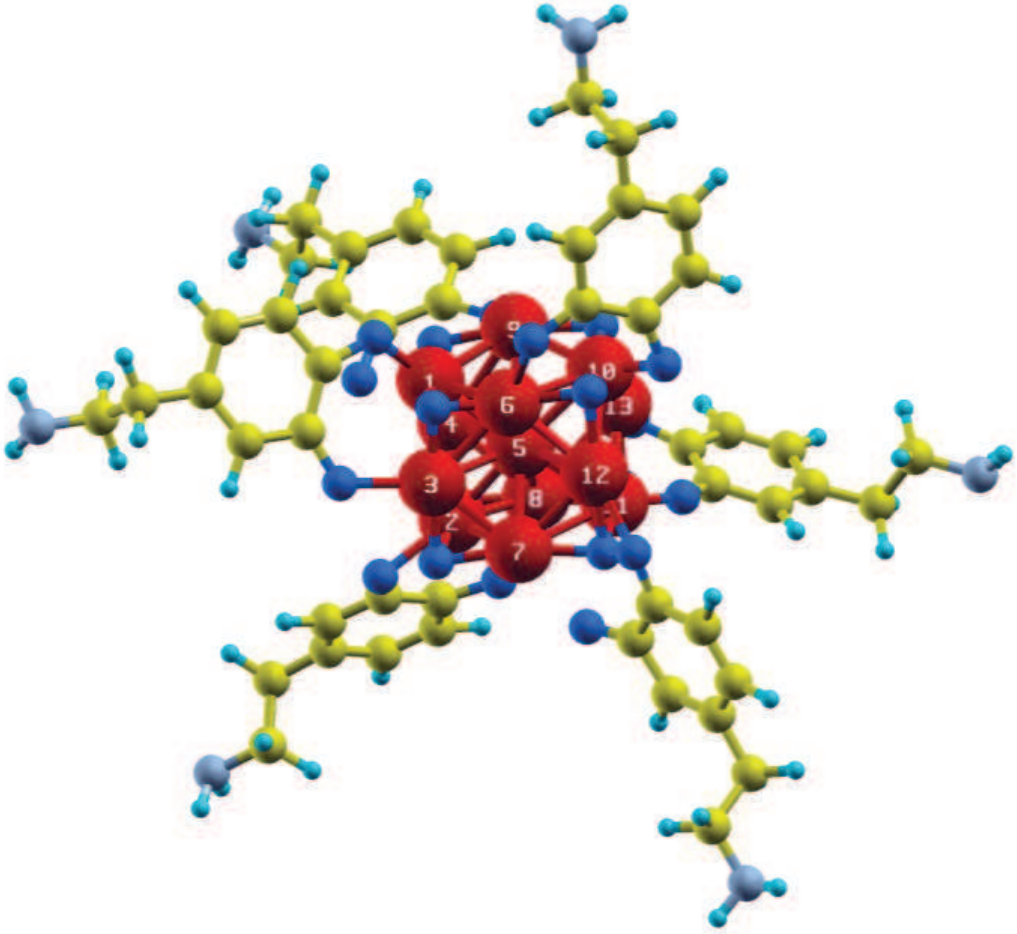

Figure 4.1: $Fe_{13}O_8$ cluster with six dopamine molecules.

4.2.2 *Ab initio* Magnetic Computation

Following a suggestion of Yvan Labaye (Assistant Proffesor at the IMMM, University of Le Mans) we then used Quantum Espresso version 4.2, where it is possible to enforce an external magnetic field with arbitrary magnitude and direction, and computed the resulting change in local magnetic moments (sometimes refered in the literature as "spins", when they are actually expectations on the values of spin components integrated over a sphere of reasonable but arbitrary radius centered on each atom). For this, we used non-collinear density functional theory [Barth & Hedin 1972].

We considered four cases, $Fe_{13}O_8$ alone, with one dopamine molecule added, with six dopamine molecules, and with a gold cluster in the framework of non-collinear magnetism calculations. In the case of magnetic computations we found that a reduction

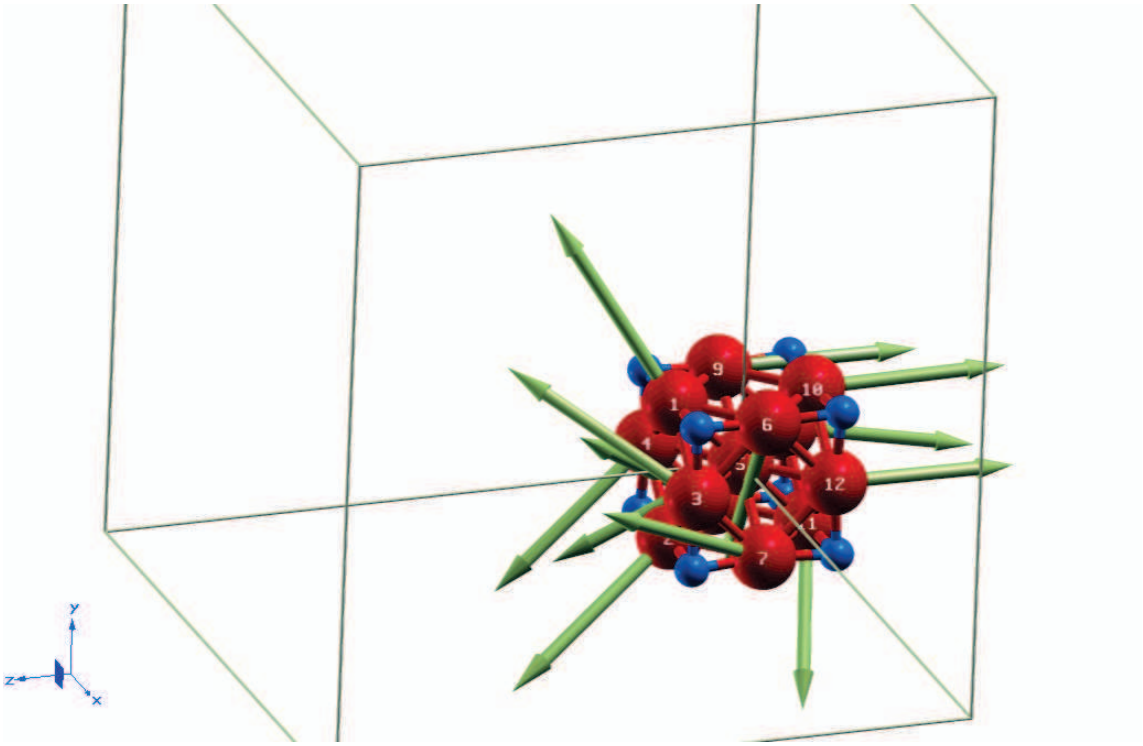

Figure 4.2: The result of a typical noncollinear constrained calculation of the iron oxide cluster ; here we imposed magnetic moments of 5,1 and 45 μ_B on each axis.

of the cutoff energy by half was ensuring consistency of the results, and a 0.17 mixing factor for self-consistency was employed. A smearing factor of 0.02 Ry was used. We performed calculations assuming the systems to be isolated with Martyna-Tuckerman correction [Martyna & Tuckerman 1999]. We checked the result performing calculations with relativistic pseudopotentials with spin-orbit coupling which we generated from the QE distribution suggested values for cutoff (1.4 and 1.6 a.u for Oxygen with 6 active electrons and a projector on empty 3d states), as well as ultrasoft pseudopotentials without spin-orbit as described previously.

Since the possibility to enforce an external magnetic field disappeared in the version 5 of Quantum Espresso, we also did the opposite, namely enforcing an arbitrary magnetization state different from the ground-state result but close to it, and computing the corresponding magnetic field. We used a penalty factor ("lambda") of 0.001 for this purpose in order to speed up convergence under this external constraint, sometimes missing the desired value of the moments by some amount because of the smallness of the penalty factor ; this is not a problem because we are mainly interested in the relationship in between magnetization and magnetic field.

4.2.3 Magnetic Model

The two previous procedures (enforcing either magnetic field or magnetization and computing the other as a result) give a distribution of local magnetic moments $\vec{S}_i$, magnetic fields $\vec{H}$, and total energies H. We then collected these values from QE runs into a single file using some scripting commands, and fitted the parameters from the Heisenberg Hamiltonian used to model magnetite nanoparticles in [Mazo-Zuluaga *et al.* 2009].

This Hamiltonian reads

$$H = -2\sum_{(i,j)} J_{ij}\vec{S}_i\cdot\vec{S}_j - K_V\sum_i \left(S_{x,i}^2 S_{y,i}^2 + S_{y,i}^2 S_{z,i}^2 + S_{x,i}^2 S_{z,i}^2\right) - K_S\sum_k \left(\vec{S_k}\cdot\vec{e_k}\right)^2 - g\mu_B\vec{H}\cdot\sum_i \vec{S}_i \tag{4.1}$$

It is to be noted here that the Zeeman energy (last term) is absent from QE results.

The first sum involves nearest neighbors interactions in between iron atoms. In reference [Mazo-Zuluaga *et al.* 2009] these were computed as from coordination numbers. In the bulk three different coordination numbers appear: $z_{AA} = 4$, $z_{BB} = z_{BA} = 6$, and $z_{AB} = 12$. These numbers apply for the core of the nanoparticle. In our case, these numbers were computed from the coordinates of the iron atoms, enforcing a cutoff radius such that no atom had more than 12 neighbors.

The second term in the Hamiltonian is the core cubic magneto- crystalline anisotropy and reference [Mazo-Zuluaga *et al.* 2009] chose a value of $K_V = 0.002$ meV / spin

The third term accounts for the single-ion site surface anisotropy where the unitary vector reads

$$\vec{e_k} = \frac{\sum_j \vec{P_k} - \vec{P_j}}{|\sum_j \vec{P_k} - \vec{P_j}|} \tag{4.2}$$

with $\vec{P_i}$ the position vector of each iron atom on the surface and the sum runs over iron neighbors of j .

In reference [Mazo-Zuluaga *et al.* 2009] the exchange parameters were set at a value of $J_{AA} = -0.11$ meV, $J_{BB} = +0.63$ meV, and $J_{AB} = -2.92$ meV corresponding to a mix of ferromagnetic and antiferromagnetic interactions. Those values were taken from [Uhl & Siberchicot 1995] where they were fitted on *ab initio* results using a method similar in principle to the one with presently discussed : bulk spin waves were fitted to non-collinear spin calculations.

4.2.4 Fitting Procedure

The results of the *ab initio* calculations (energies) were fitted using the Monte-Carlo Metropolis result method, based on random configurations of the parameters.

We used the basic recurrence generator provided for instance in [Press *et al.* 1992] $I_{n+1} = (aI_n + b)[2^N]$ checking by hand with $N = 3$ for instance that for well chosen a and b one has indeed a one-cycle permutation of the integers, and with $N = 32$ and arbitrary large a and b a set of seemingly random numbers. This fact can be checked with a simple 2D plot of successive numbers : correlations or holes in the distribution are obvious in such representations.

The Metropolis algorithm consists in generating a trial random configuration change (in our case, a change of the Heisenberg parameters) $(q_i' = q_i + \Delta q_i)$ corresponding to a $\Delta E = E'(q_i') - E(q_i)$ change in the virtual energy of the system, the virtual energy E being here some penalty function representing the distance in between the set of energies found with *ab initio* calculations and found with the Heisenberg model applied to the distribution of moments, and accepting this move if a random number y uniformily drawn in between 0 and 1 is lower than $P(\Delta E, T)$.

This reminds of Von Neumann's rejection method, which consists in finding a majorant M to the wished distribution $P(x)$, then in the drawing of uniform random numbers (x, y) with x in a chosen interval and $y < M$. If $y < P(x)$, x is accepted and output from the method, else the method restarts. It is obvious if one draws a graph representing $P(x)$ and illustrates the method on this graph that the result is correct ; however, if M is too large, the method will slow down considerably by rejecting too many couples.

One of the goals of the well known Metropolis algorithm [Metropolis *et al.* 1953], which can be seen as an application of this method is to simulate the evolution of a real physical system described by a set of generalized coordinates (q_i), at a virtual temperature T. The probability of the transition in between two states of this system with an energy difference of ΔE being given by a Boltzmann factor $P(\Delta E, T) = \exp(-\Delta E/(k_B T))$, k_B being the Boltzmann constant.

From our description of the rejection method, one sees that this algorithm is exactly similar and will generate configurations (q_i) of energy $E(q_i)$ with a Boltzmann probability distribution $P(E - E_g, T)$ relative to the state of lower energy E_g of the system. This is interesting *per se* as it allows one to explore the configuration space of a thermodynamical system with an alternative method to molecular dynamics (on the top of that, ensuring detailed balance evolution), but also because, by a progressive annealing, to find heuristically the ground state of an arbitrary system as soon as some virtual energy E can be defined from configuration q_i (in our case, a penalty function and a set of magnetic moments and field).

Minimum search by the Metropolis algorithm has indeed the advantage over other methods such as steepest descent or conjugate gradient that if one starts from a trial state close to a local minimum but far from the global minimum. One still has a chance of finding the global minimum by "jumping" over the barriers separating the local minima valleys thanks to thermodynamical activation, where the other mentioned methods will only be able to find the local minimum. Of course, compared to an exhaustive enumeration of the configurations of the system, the method is only a heuristical one since it has many problem-dependent ingredients and may fail if the initial trial state, the temperature annealing law, or the size of the random trial moves (Δq_i) are badly chosen. Genetic algorithms become thus an interesting alternative to the Metropolis method [Mitchell 1999] .

4.2.5 Fitted Parameters and Penalty Function

The parameters we choose to fit using the Metropolis simulated annealing method were a reference energy H_0 (fit parameter), the set of J_{ij}, enforcing $J_{ij} = J_{ji}$, K_V, K_S and g. We first used a small set of J_{ij} corresponding to a small cutoff in neighborhood search, then increased the number of neighbors to increase the quality of the fit. In order for the results to keep a physical meaning we kept the total number of fitted parameters (maximum of 40) well under number N of samples used to define the virtual energy or penalty function from the energies in Rydbergs

$$E = \frac{1}{N}\sum_{i}^{N} |H_{\text{ab initio}} - H_{\text{Heisenberg}}|$$

We also changed the Hamiltonian to allow for a local change in surface anisotropy ending up with

$$H = H_0 - 2\sum_{(i,j)} \vec{J}_{ij}\vec{S}_i\cdot\vec{S}_j - K_V \sum_i \left(S_{x,i}^2 S_{y,i}^2 + S_{y,i}^2 S_{z,i}^2 + S_{x,i}^2 S_{z,i}^2\right) - \sum_k K_{Sk}\left(\vec{S_k}\cdot\vec{e_k}\right)^2 - g\mu_B\vec{H}\cdot\sum_i \vec{S}_i \tag{4.3}$$

We also had to chose several parameters of the simulated annealing procedure, such as the fictious temperature, the annealing law, and the dependence of random changes to the temperature. The fitting program being quite small, we find it easier to include it as an annex to this dissertation rather than detailing all those empirical choices, nevertheless validated by the goodness of the resulting fit.

4.3 Results and Discussion

4.3.1 Iron Oxide Clusters

We generated sets of $N = 101$ configurations randomly drawn from *ab initio* results corresponding to a total enforced magnetization running from l to 5 μ_B along the x axis, 1 to 5 along the y axis, and 37 to 41 μ_B along the z axis.

The best result (penalty function as defined above less than 10^{-4}Ry) was of course found using the largest number of fitting parameters (full set of J_{ij} and set of surface anistropy constants K_{Sk}). A typical fit of *ab initio* values versus Heisenberg model is given in Figure 4.3; in this case it can be seen that the Heisenberg model seems to model correctly the *ab initio* results. A further confirmation is found in the fact that the g factor is obtained with a value lower than 10^{-2} confirming that the absence of Zeeman energy in the QE code results is found by the fitting procedure.

A histogram of the obtained parameters for the J_{ij} is illustrated in Figure 4.4. It can be seen that those values are close to the ones of reference [Uhl & Siberchicot 1995], with an alternation of ferromagnetic and antiferromagnetic couplings.

The volume anisotropy was found to have a value of -2.10^{-05} a.u, coherent with the one used in [Mazo-Zuluaga *et al.* 2009]. The values for the local surface anisotropy constants are given in Table 4.1. It can be seen that the best fit corresponds to an alternation of positive and negative values for those constants, raising the question of the validity of the Hamiltonian used in [Mazo-Zuluaga *et al.* 2009] where a constant surface anisotropy was used.

Indeed, we found that the model does not adjust as well when we use a constant surface anisotropy, the best penalty found being at a value of $1.13 \cdot 10^{-3}$ Ry. This corresponds to a value of the surface anisotropy of 1.753 a.u and a volume anisotropy of $6.31 \cdot 10^{-05}$ a.u. The latter value is now positive, but the authors of [Mazo-Zuluaga *et al.* 2009] found that the K_S/K_V ratio is the more important parameter to predict the magnetic structure of a nanoparticle of intermediate size. Here, the value of 27780 we find for this ratio hints to a hedgehog type magnetic structure. Maybe the large surface contribution of such a small system as the one we study is responsible of this fact, but at least the value we find is not a free, almost unknown parameter as in the literature. Physically, such a result would correspond to jumps during magnetization reversal, and exchange bias properties. Such results have been experimentally observed and are also reviewed in [Mazo-Zuluaga *et al.* 2009].

When we tried the same method with full spin-orbit coupling and relativistic pseudopotentials, the increased disorder in the magnetic moments resulted in a penalty function of $2 \cdot 10^{-3}$ Ry, with essentially similar results for the fitting parameters.

Fe atom	Surface anisotropy in a.u.
1	0.5592594E-01
2	-0.5450376E-01
3	0.4755301E-01
4	-0.2952414E-01
5	0.4511738E-01
6	0.5525300E-01
7	-0.4852317E-01
8	-0.2241407E-01
9	0.8430323E-01
10	-0.7067873E-02
11	-0.7141519E-01
12	-0.7437612E-01
13	-0.8089262E-01

Table 4.1: Local surface anisotropy constants

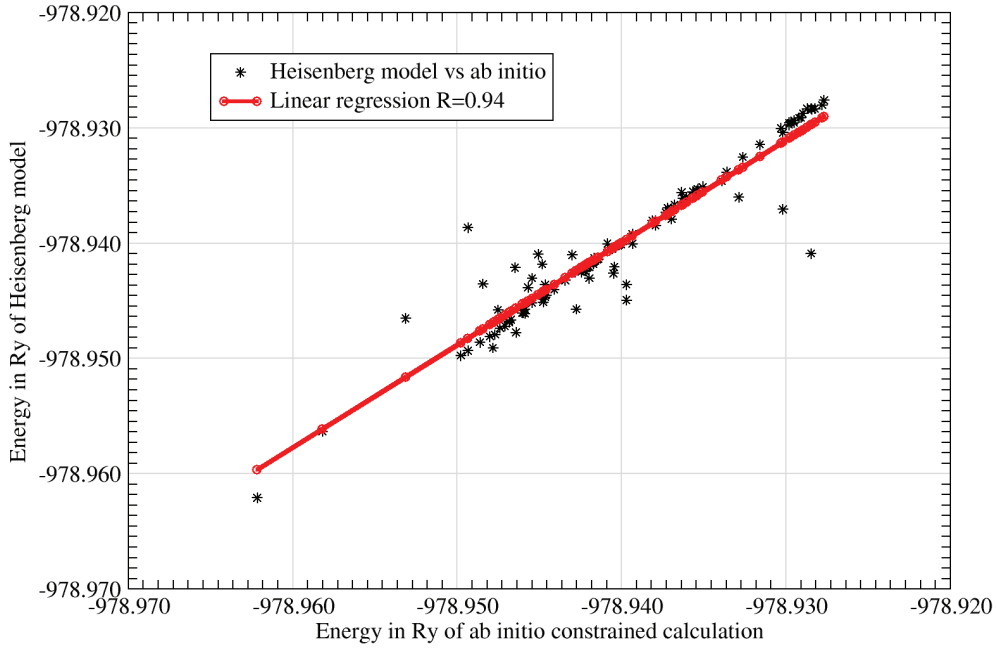

Figure 4.3: Results of the *ab initio* calculations fitted using the Monte-Carlo Metropolis (without spin-orbit).

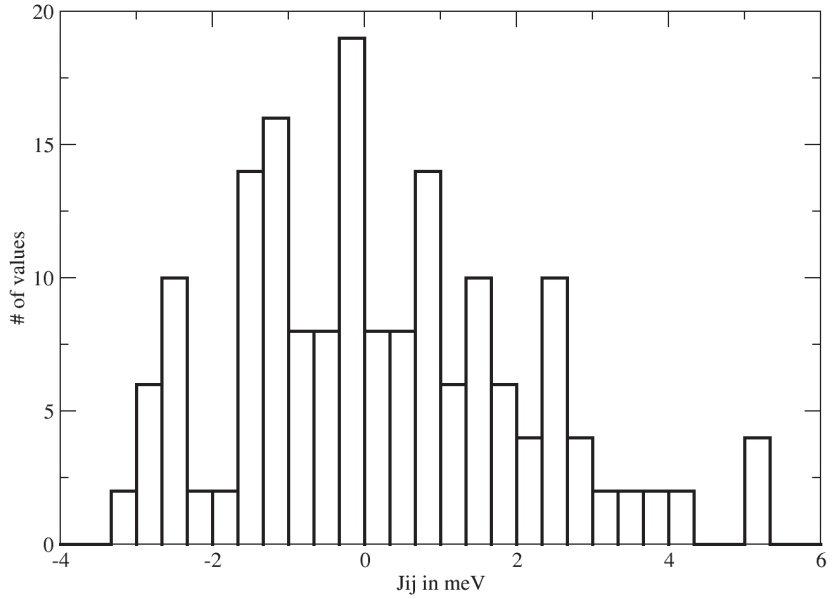

Figure 4.4: Histogram of exchange constants found by the fitting procedure on the iron oxide cluster.

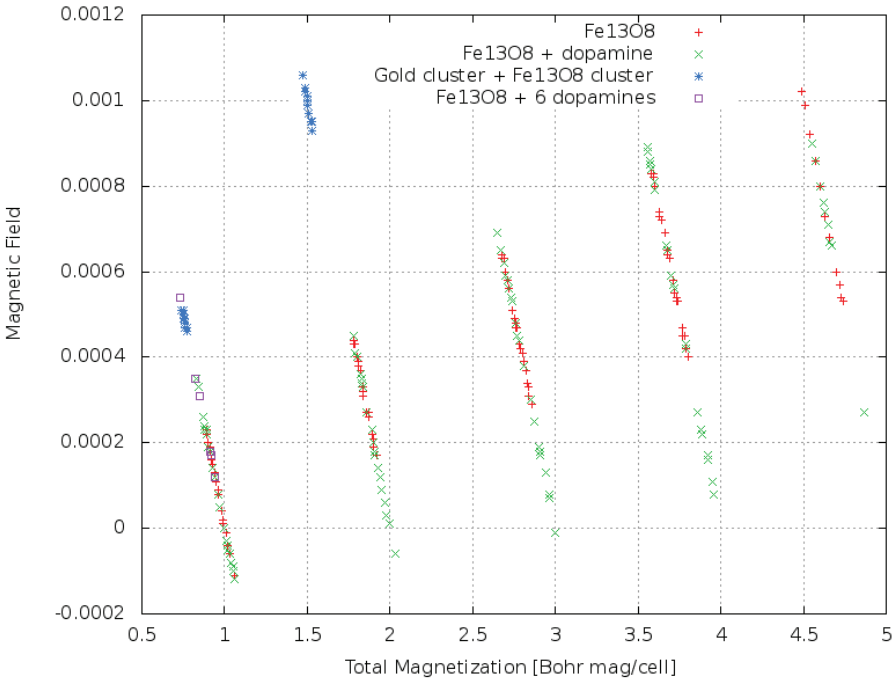

Figure 4.5: Magnetic susceptibility of studied systems.

4.3.2 Iron Oxide Clusters and Dopamine

We then added a dopamine molecule next to the cluster from the previous section and, after optimizing the atomic positions, tried the same fitting procedure with a Heisenberg model. It turned out that we could not achieve a fit with a penalty function better than $5 \cdot 10^{-3}$ Ry, which more or less corresponds to the distribution of energies in the *ab initio* results, and unrealistic coupling constants as well as a strongly unstable distribution of surface anisotropy constants. We concluded that a Heisenberg model may be too simple to describe such a system, where electrons donated by the dopamine molecule can lead to some itinerant magnetism, or at least to some symmetry breaking.

In order to address the latter point, we added 6 dopamine molecules symmetrically distributed around the cluster. The simulation time was found to be too large to compute as many constrained points as in the previous section, but, by plotting the magnetization versus the magnetic field, as can be seen in Figure 4.5, we could check that the susceptibility of the system seems to be unchanged from this functionalization.

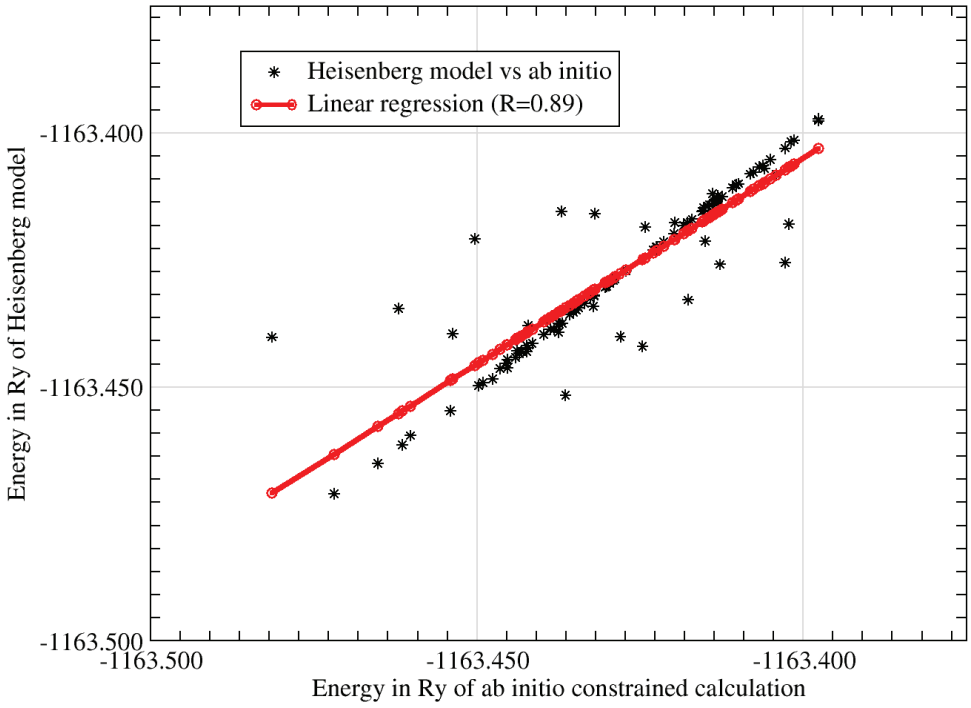

Figure 4.6: The results of the *ab initio* calculations on the iron oxide cluster functionalized with one dopamine molecule fitted using the Monte-Carlo Metropolis (without spin-orbit).

4.3.3 Iron Oxide Clusters and Gold Cluster

In order to answer a question of Prof. Souad Ammar, we also tried a system discussed in more details in the next chapter, namely a small gold cluster (which could act as a nanoantenna in plasmonics) glued to the iron oxide cluster. In this case, the Heisenberg model did not fit very well either the computed *ab initio* values of energies. However, as can be seen in Figure 4.5, although the absolute values of external magnetic field to achieve the same total magnetization along the x axis are strongly different than in the previous cases (with or without dopamine), the slope of the curve seems to be rather the same.

4.4 Conclusions

In this chapter, we have tried to fit using the Metropolis simulated annealing method a classical Heisenberg model of magnetism including surface anisotropy effects on magnetically constrained, non collinear *ab initio* results obtained a small iron oxide cluster functionalized or not by one or several dopamine molecules or a nearby small gold cluster. We conclude that the Heisenberg model seems to apply well to the simpler system (namely, a free iron oxide cluster), allowing to give some absolute values of the surface anisotropy constant, although a locally varying surface anisotropy alternating positive and negative values seem to provide a better description.

This could allow to describe the magnetic behavior of a nanoparticle of size 1 to 10 nm, which *ab initio* calculations cannot tackle for the time being because of computing power limitations, hoping that the large surface proportion of iron atoms in the small cluster we have studied does not too much influence the results.

In the case of functionalized cluster by one or several molecules of dopamine, or by a nearby gold cluster, the Heisenberg picture does not apply as well as for the simpler system, but we could nevertheless observe that the linear relation in between magnetic field and magnetization was unchanged in all those cases even if absolute values changed.

Having studied for some part the magnetic effects, in the next chapter we will focus on the optical excitation of the gold cluster.

Chapter 5

Time Dependent Density Perturbation Theory Study on Gold-Coated Iron Oxide Clusters: Optical Properties

5.1 Introduction

As mentioned in the earlier part of the work, iron oxide nanoparticles have increasing potential in medicine (MRI contrast agents, magnetic hyperthermia, targeted drug delivery and detoxification) [Nohyun & Taeghwan 2012]. However, one of the problems with particles in this size is their instability over a long period of time. Indeed they tend to form agglomerates to reduce the energy and are easily oxidized in air what causes the loss of magnetism and dispersibility. A coating layer is needed to protect magnetic nanoparticles against degradation. A system consisting of iron oxide nanoparticles coated with gold is very attractive due to unique properties of both the iron oxide (magnetic) and gold (surface plasmon resonance).

The optical properties of gold have been appreciated for a long time. Since ancient times, it has been established that adding gold nanoparticles to glass causes the change of its color and these changes depend on the size of the particles. The most famous example of glass obtained by medieval glaziers is the one in ruby-colored glass (known as "Cranberry Glass or "Rubino Oro"). Recently, the team of professor Zhu Huai Yong from the Australian Queensland University of Technology, who investigates old stained glass, discovered that the gold-colored glass does not only looks beautiful and does not change its hue, but is also a nano-catalyzer degrading air pollution under the influence of light [Chen *et al.* 2008].

During the exposure of gold nanoparticles (size of 10-100 nm) to optical radiation, begins the process whereby the free electrons in the conduction band of gold resonate in response causing them to absorb and scatter light [Pissuwan *et al.* 2006]. The specific frequency at which the amplitude of oscillations is maximum is known as surface plasmon resonance (SPR). The property of the plasmon resonance of gold nanoparticles followed by conversion of light into heat is very promising for photo-thermal therapeutic medicine. However, the plasmon resonance, usually modeled with the Mie theory for large gold NPs is usually in the middle of the visible spectrum (500-600 nm) which limits their optical properties for *in vivo applications* [Huang *et al.* 2011] since the tissues of human body are transparent to near infrared light [Pissuwan *et al.* 2006]. Nevertheless, the conducted study has indicated that absorption is dependent on the detailed structure [Zhang & Noguez 2008] of nanorods and this problem can be solved by red-shifting into the infrared region of the electromagnetic spectrum.

Gold nanoparticles became particularly important in research on the diagnosis and treatment of cancer not only because of their specific optical properties but also due to their simple preparations, which can be adapted to the needs by changing their size or shape as well as their biocompatibility (the inability of the organism to detect them and launch an immune response) in clinical conditions [Huang & El-Sayed 2010]. Moreover, gold nanoparticles, due to their plasmonic properties, act as nanoantenna what makes them very promising in the field of optical biosensors.

The gold coated iron oxide nanoparticles became an interesting field of experimental studies [Panaa *et al.* 2007], [Zhou *et al.* 2001] as well as theoretical ones [Sun *et al.* 2006], [Sun *et al.* 2007].

In spite of these works, a theoretical study of the effect of gold functionalization on optical properties of iron oxide nanoclusters is still lacking.

In the present work, by combining *ab initio* Density Functional Theory and Time Dependent Density Functional Perturbation Theory the optical properties of gold interacting with $Fe_{13}O_8$ clusters were studied.

5.2 Computational Details

To perform all the calculations we used the Quantum Espresso [Giannozzi *et al.* 2009] computer code based on density functional theory, plane waves and pseudopotentials. The procedure of structure optimization of iron oxide cluster was described in previous chapter. Figure 5.3(a) shows the optimized structure of the considered cluster. Subsequently, the $Fe_{13}O_8$ cluster was successively coated with 6, 12 and 32 gold atoms resulting in completely wrapped iron oxide($Au_{50}Fe_{13}O_8$), the structure of which is presented in Figure

5.3(b). The same optimization procedure was used for the second system consisting of $Fe_{13}O_8$ iron oxide and Au_{20} gold clusters.

Then we performed time dependent density functional theory calculations using Perdew-Zunger LDA and corresponding ultrasoft, scalar relativistic pseudopotentials generated with the Vanderbilt code from the QE distribution and 11 electrons for gold. To simulate the spectroscopic properties of the chosen systems, we used the turboTDDFT code as an implementation of the Liouville Lanczos approach to time dependent density functional theory. The turboTDDFT code is distributed as a component of Quantum Espresso. In this new method, the spectrum is calculated over wide frequency range but the computational effort is just several times greater than the one needed by a single ground-state DFT or static DFPT [Malcolu *et al.* 2011]. The standard ground state DFT calculations had to be performed first in order to compute the optical spectrum. The gamma points computations using real valued wavefunctions were used. Those calculations were required to obtained all the relevant information about the system, which are read by the turbo-lanczos code at the start. The last step to obtain the spectra of the systems was the execution of the postprocessing program turbo-spectrum.x. We used an extrapolation technique that allows one to substantially reduce the number of Lanczos recursion steps (1500 in our case) needed to calculate well converged optical spectra [Rocca *et al.* 2008].

We performed a computation of a simple sodium cluster (Na_9^+) with PBE DFT and pseudopotentials with 1 active electron per atom in order to check the accuracy of turbo-lanczos code in predicting the optical response. The result is presented in Figure 5.2 which can be favourably compared to previous experimental and theoretical results [Calvayrac *et al.* 2000] at least for the relative intensity of the peaks, the positions being slightly red-shifted.

Of course, for more strongly correlated systems such as iron oxide the GW method [Hedin 1965] is better in principle but although Yambo [1] worked good on Na we do not have success in the case of gold. We neglected spin orbit coupling for gold in this case because of numerical cost but we plan to check results in the future.

[1] A FORTRAN/C code for many0body calculations in solid state and molecular physics [Marini *et al.* 2009].

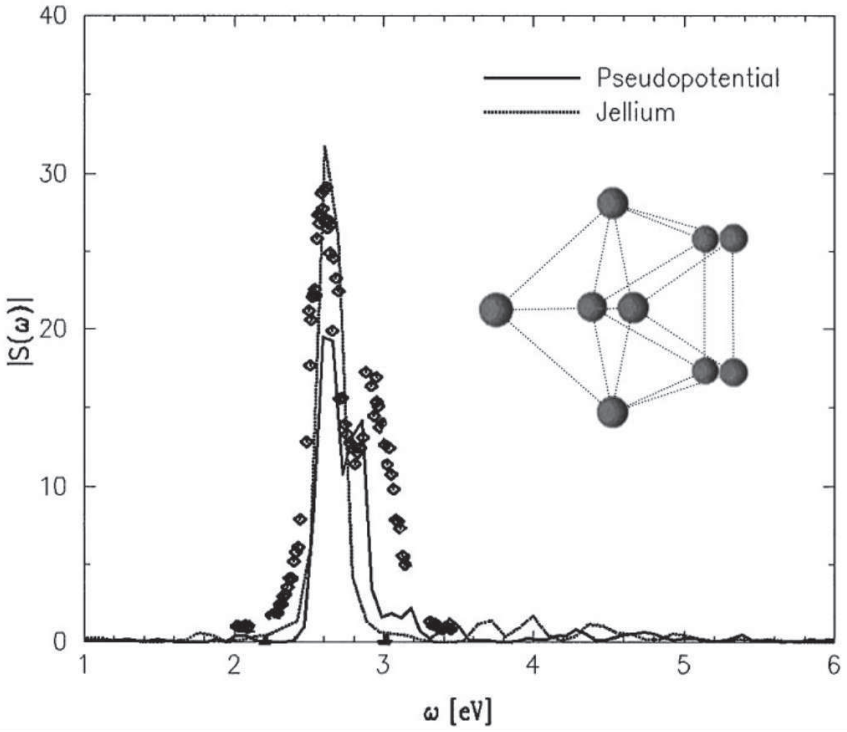

Figure 5.1: The optical response of Na_9^+ obtained by [Calvayrac *et al.* 2000] and compared to experimental data (diamonds).

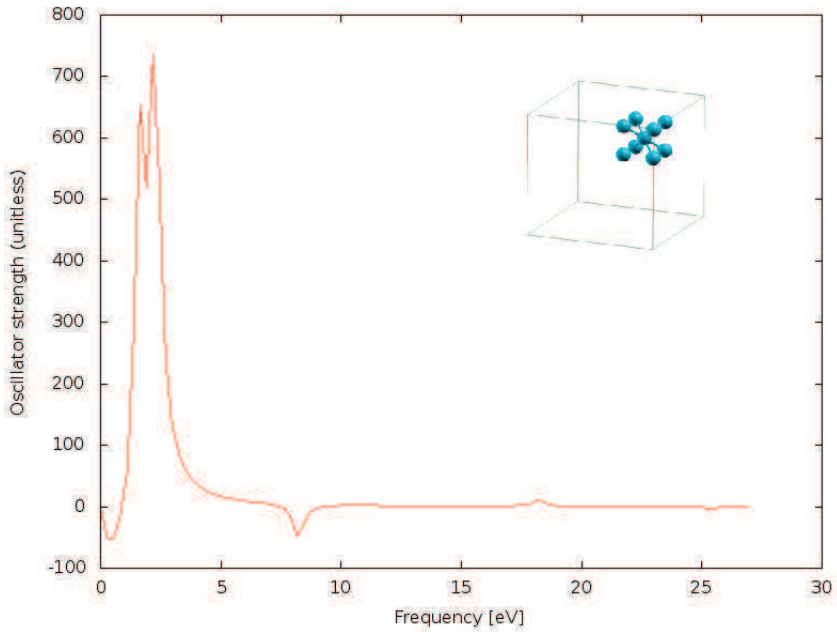

Figure 5.2: Absorption spectrum of Na_9^+.

5.3 Results and Discussion

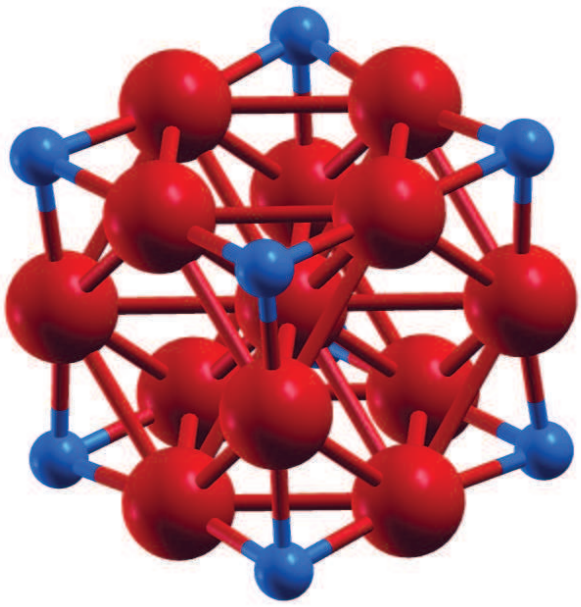

(a) $Fe_{13}O_8$

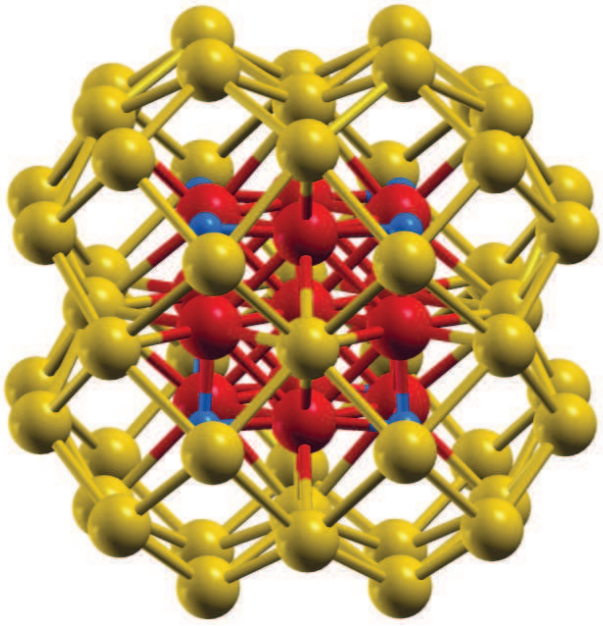

(b) $Au_{50}Fe_{13}O_8$

Figure 5.3: Optimized structures of (a) the un coated and (a) fully coated $Fe_{13}O_8$ clusters.

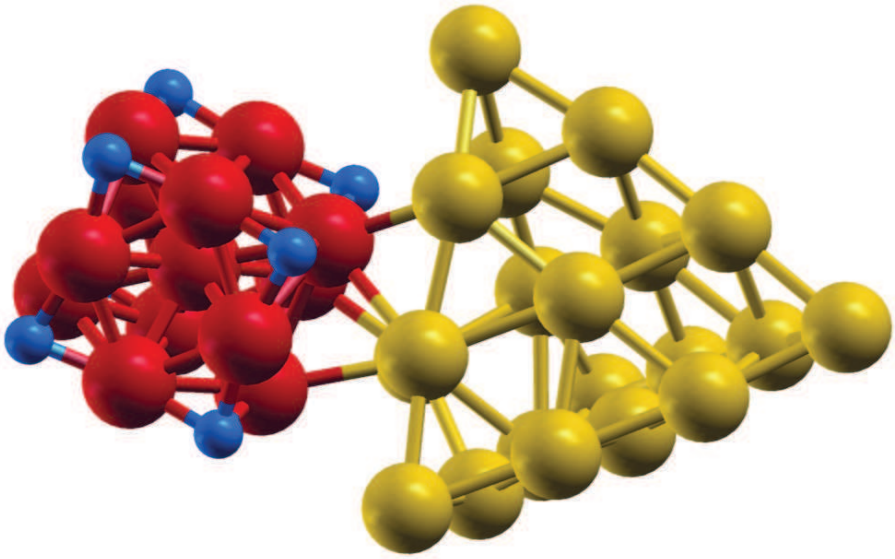

Figure 5.4: Optimized structure of $Fe_{13}O_8$ and gold clusters.

The shapes of the optimized structures are illustrated in Figures 5.3 and 5.4. In the structure of iron oxide cluster we found that nonequivalent Fe atoms: the central atom and two atoms on the surface. The equilibrium structure of $Fe_{13}O_8$ agrees with some previous works [Sun *et al.* 2000], [Wang *et al.* 1999].

The obtained spectrum of the iron oxide cluster coated by gold (Figure 5.5) shows a significant excitation peaks at the frequency of 2 eV what corresponds to values of about 500 nm, a value commonly admitted in literature for the plasmon resonance of large (more than 2nm) gold clusters. For smaller systems the Mie theory do not apply, and quantum theoretical results are sparse. When we compare Figure 5.5 to the UV-vis spectra on Figure 5.6 obtained by [Korobchevskaya *et al.* 2011] we observe a red shift of peak in our result. Nevertheless, the change in the position of the plasmon resonance due to the size of the nanoparticles is never greater than 20% [Kreibig & Vollmer 1995], so our results fall in a reasonable range and indicate that gold-coated iron oxide nanoparticles exhibit the same optical properties as pure gold systems.

One can wonder about the utility of the optical properties of such materials in photothermal therapeutic medicine because of the so-called optical window (therapeutic window). It is a spectral range between 600 nm and 1300 nm [Tsai *et al.* 2001]. In this region the light absorption of most mammalian tissues is low and transparent to light, it so can be relatively deeply penetrated. Below 600 nm they are opaque due to absorption of hemoglobin in the blood [Lin *et al.* 2010].

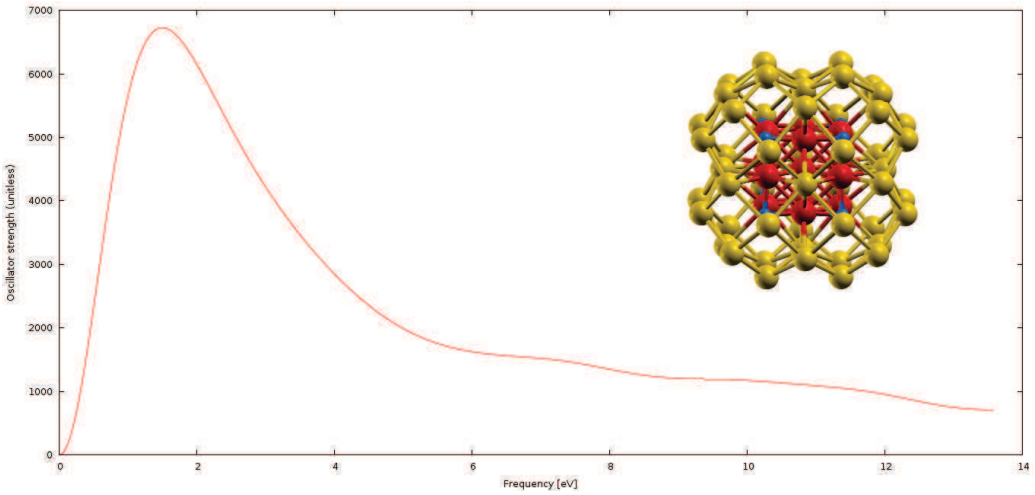

Figure 5.5: Absorption spectrum of studied systems.

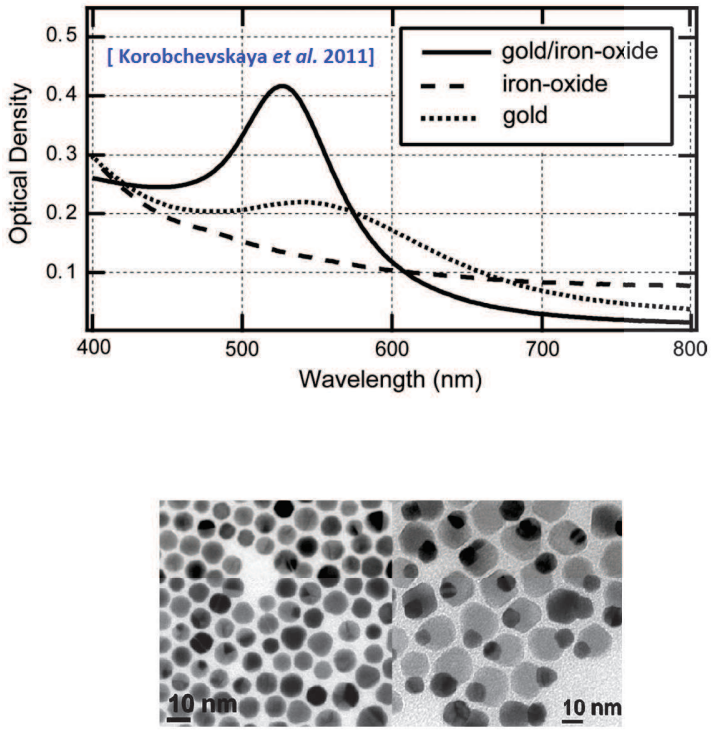

Figure 5.6: UV-vis spectra of the gold, iron oxide and iron oxide/gold as well as the transmission electron microscopy images of Au (left) and gold/iron oxide nanocrystals (right) from [Korobchevskaya *et al.* 2011].

In the case of combined clusters of gold and iron oxide, our results mainly exhibit an extremely broad peak in the visible region which only disappears in the far UV. For the moment we do not know if this result is physically realistic or if there is some artefact in our calculations ; we plan to check this in the near future using either relativistic calculations, GW calculations, or full non-linearized time-dependent density functional theory, either in the QE implementation or in the PWTELEMAN project.

5.4 Conclusions

In this chapter we investigated the optical response of iron oxide clusters with gold in the framework of Time Dependent Density Functional Theory. The results demonstrate the potentials of the systems consisting of iron oxide and gold in the treatment of cancer - localized cancer cell heating as well as the employment of them as contrast agents in magnetic resonance imaging.

The obtained data in the case of iron oxide cluster capped by gold indicate a red-shift of the absorbance which would be needed for clinical use because of the optical window in the body.

Chapter 6

Summary and Perspectives

6.1 Summary

In this work we have applied *ab initio* method to investigate the ligands and magnetic nanoparticles used in medicine. Calculations were performed by the Quantum Espresso software based on density functional theory and LDA+U approach.

Firstly, we predicted on which iron site the ligand would preferentially bind. The obtained results showed that all ligands, except citrate, present affinity for he the octahedral sites of iron atom and citrate ligand has a preferential binding on the tetrahedral site of the iron oxide surface. We assumed that the reason could be that the oxidation degree of the iron atoms at the octahedral site is differs from that at the tetrahedral sites. We checked that by forcing orientation of the ligands and we found that binding energy was lower in the octahedral case. In the case of dopamine the binding energy was the lowest and we found that binding happens in the configuration of a "bidentate", where traditional chemistry would have preferred a chelate. To check if the reason could be difference in oxidation, we computed the change in Lőwdin charges of each atom. The results indicate a partial reduction of Fe^{3+} atoms, d orbitals were reduced as well, the p orbitals of dopamine show a increase in charge. Those results are fairly coherent with those from Mőssbauer spectrometry [Fouineau *et al.* 2013]. Our findings suggested that the system with dopamine is the most stable among the considered systems. We also computed the reduced gradient of the electron density in order to investigate the nature of the ionicity in the particles. In all cases the bondings are covalent what is a favorable result because of the requirements for pharmaceutical applications. Only in case of the citrate we could notice a presence of the isosurface close to ligand what may rather indicate a ionic nature. The proved covalent nature of bonds makes such ligands efficient for the functionalization of nanoobjects of medical interest. We studied the preferred binding of the magnetic nanoparticles modified by APTES, our findings show that the

lowest binding energy occurs in the system with APTES ligand without hydrogen atoms linked to silicon, thus is the strongest combination.

We also checked the change in Lőwdin charges and ionicity, the results are similar to previous findings. From the obtained results of density of states we can see that the presence of dopamine does change the small gap of magnetite by adding some conduction electrons, when the presence of citrate does not significantly change the total DOS. The functionalization leads to a marked increase in magnetism. Therefore grafting by those ligands can keep magnetism alive, thus providing the basis for the applications of functionalized iron oxide nanoparticles in magnetic drug delivery or magnetic hyperthermia. Those results can be compared to results recently experimentally obtained by [Li *et al.* 2009] when the value of magnetite surface alone is close to the one obtained by [Lodziana 2007]. Results concerning functionalization of aryl diazonium salts suggest that they are highly suitably for futher applications because of the formation of strong iron oxide-aryl surface bond, the nature of which is most likely covalent. We also observed that is possible to raise the magnetization of nanocomposites by linking the iron oxide with gold, such result is very important from a medical point of view and promises such applications as a targeted medical delivery.

In next chapter we extended our study to perform non-collinear *ab initio* computations of the magnetic properties of simple iron oxide clusters functionalized or not by one or several dopamine molecules or a nearby small gold cluster, and from those results we have tried to develop a classical Heisenberg model of magnetism including surface anisotropy effects. We conclude that the Heisenberg model seems to apply well to the simpler system (namely, a free iron oxide cluster), allowing to give some absolute values of the surface anisotropy constant, although a locally varying surface anisotropy alternating positive and negative values seem to provide a better description. This could allow to describe the magnetic behavior of a nanoparticle of size 1 to 10 nm, which *ab initio* calculations cannot tackle for the time being because of computing power limitations, hoping that the large surface proportion of iron atoms in the small cluster we have studied does not too much influence the results.

In the case of functionalized cluster by one or several molecules of dopamine, or by a nearby gold cluster, the Heisenberg picture does not apply as well as for the simpler system, but we could nevertheless observe that the linear relation in between magnetic field and magnetization was unchanged in all those cases even if absolute values changed.

It was observed that is possible to raise the magnetization of nanocomposites by linking an iron oxide cluster with a gold cluster.

In the last chapter of results we have simulated the optical response of small gold clusters, gold-coated iron oxide clusters and hybrid gold and iron oxide clusters using

linearized time-dependent density functional theory.

6.2 Perspectives

Human organisms are programmed to live 120 years. So far, for various reasons, almost anyone is unable to reach such a beautiful age, although we live longer and longer. In the 20th century, the average of live extended by 35 years and medical doctors expect that in the 21st century, the age of 100 years will be a norm thanks to the achievements of medicine. Each person is different, just as different are tumor lesions. Patients with the same disease respond differently to the same treatment. In some cases therapy can have positive effects in the second may not give any effect at all or cause side effects. Scientists answer to this problem may be personalized nanomedicine [Liu 2012], [Stegh 2013]. Drugs tailored to a specific group of patients had already appeared on the market. An example of the effectiveness of personalized targeted therapies is trastuzumab-modified nanoparticles treatment of breast cancer that acts in those with an excess of the HER2 protein [Chen *et al.* 2009], [Steinhauser *et al.* 2006].

Targeted therapies require the use of precise diagnostic methods. There is even a new term: theranostic, resulting from the combination of two words: diagnosis and therapy. A study of Swedish researchers [Porsch *et al.* 2013] inform how nanoparticles can be combined with the appropriate drugs to ensure the effective delivery of the active substance into the tumor cells. They also point out that this cancer treatment enables the detection of chemotherapy in a patient using MRI.

Effectiveness of the personalized nanomedicine depends on the variety of nanomaterials, which allow us to customize materials to individual and specific requirements of each patient. Superparamagnetic iron oxide nanoparticles and plasmonic gold nanoparticles studied in this work are one of the candidates for such applications. Since the tumor environment is more acidic than healthy tissues, the release of the drug depending on the pH would be very attractive [Gautier *et al.* 2013]. In this context, a particularly interesting perspective to the present work would be a more detailed modeling of pH, solvent or temperature effects, connecting to a multiscale modeling of the biological medium surrounding the nanoparticles.

Appendix A - Synthesis, Mőssbauer characterization, and *ab initio* modelling of iron oxide nanoparticles of medical interest functionalized by dopamine

THE JOURNAL OF PHYSICAL CHEMISTRY C

Article

pubs.acs.org/JPCC

Synthesis, Mössbauer Characterization, and Ab Initio Modeling of Iron Oxide Nanoparticles of Medical Interest Functionalized by Dopamine

J. Fouineau,[†,‡] K. Brymora,[‡] L. Ourry,[†] F. Mammeri,[†] N. Yaacoub,[‡] F. Calvayrac,*[,‡] S. Ammar-Merah,[†] and J.-M. Greneche[‡]

[†]ITODYS UMR CNRS 7086, Université Paris Diderot, Rue Jean-Antoine de Baïf, 75205 Paris, France

[‡]LUNAM, IMMM UMR CNRS 6283, Université du Maine, Avenue Olivier Messiaen, 72085 Le Mans, France

ABSTRACT: Polyol made from about 10 nm sized maghemite nanoparticles was functionalized by a hydrophilic catechol derivative, namely, dopamine. Infrared spectroscopy confirmed the grafting, whereas X-ray diffraction and transmission electron microscopy did not show either structural or microstructural change on the iron oxide particles. ^{57}Fe Mössbauer spectrometry allowed, giving a quantitative assessment of the bonding preferences of dopamine on the iron oxide surfaces, the π-donor character of this ligand to be experimentally evidenced for the first time. These results are supplemented by ab initio modeling, expanding on previous work by considering various iron oxide surfaces and orientations. Perspectives of the work are discussed.

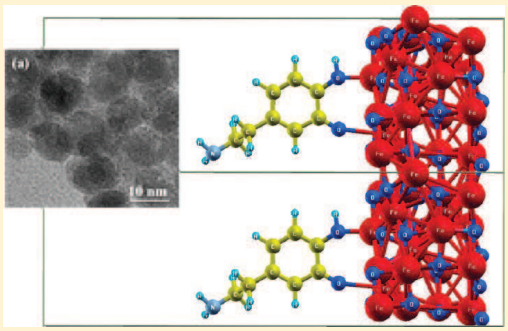

1. INTRODUCTION

During the last decades, great attention has been devoted to a better understanding of the intimate structural, chemical, and physical (magnetic, catalytic, optical...) properties of nanoparticles (NPs). Some relevant applications of such advanced materials require an extreme control of their properties, linked to the physicochemical conditions enforced during the synthesis procedure, ensuring a high reproducibility, a monodispersity in size, as well as a long-time thermal stability of NPs, even after subsequent surface modifications. It is now well-established that magnetic NPs have demonstrated promising properties for in vivo diagnostic purposes and in vivo therapeutic goals.[1] Indeed, as nanovectors, nanoparticles may provide more effective and more convenient routes for drug delivery with lower therapeutic toxicity, but it is then necessary to clearly understand the surface state of NPs and the chemical bonding mechanism between the nanoparticles and the grafted molecules. A large surface-to-volume ratio ensures a better grafting of organic materials and gives rise to a more efficient transport in the biological media as human tissues, blood vessels, and cells. In addition, nanoparticle-based imaging contrast agents originate molecular scale detection and consequently allow the diagnostics of abnormalities earlier than in the case of traditional methods.

For such a purpose and among the already tested magnetic NPs, γ-Fe_2O_3 maghemite iron oxides have created a great interest for the last 20 years due to their chemical stability, low toxicity, and excellent biocompatibility. But more importantly, their main advantages are their effective potential for hyperthermia and contrast enhancing signal for magnetic resonance imaging. Indeed, the structure of these oxides derives from that of spinel magnetite, with formula Fe_3O_4, and both exhibit a ferrimagnetic ordering at room temperature. Magnetite structure consists of a fcc oxygen lattice, where iron cations occupy the tetrahedral (A) and octahedral (B) interstitial sites as follows: $(Fe^{3+})_A[Fe^{2+}Fe^{3+}]_BO_4$, whereas maghemite one consists of a spinel lattice where B sites accommodate with cation vacancies resulting from ferrous cations oxidation into ferric ones: $(Fe^{3+})_A[Fe^{3+}_{1.67}\square_{0.33}]_BO_4$. Nanometer-sized, magnetite, and maghemite oxides exhibit a superparamagnetic behavior with a size-dependent blocking temperature, T_B. For most of the previously listed biomedical applications, T_B value is lower than 300 K.

In addition, judiciously functionalized by various organic ligands, maghemite NPs can be stabilized in water, thus increasing their circulation time in the organism. The resulting nanohybrids must be still biocompatible and have interactive features on the surface to react with the system in which they are distributed. Organic ligands bearing amine groups are particularly required. Amine groups are known to be reactive. They allow different electrophilic addition reactions or nucleophilic substitution and can be used to couple biomolecules of therapeutic interest in these magnetic nanoparticles.[2] Thus maghemite NPs may be attached to drugs, proteins, enzymes, antibodies, and may be subsequently directed through an organ, a tumor, or a tissue. In previous

Received: March 21, 2013
Revised: June 4, 2013
Published: June 5, 2013

dx.doi.org/10.1021/jp4027942 | J. Phys. Chem. C 2013, 117, 14295−14302

work, dopamine (*DA*) has been used to functionalize iron oxide NPs.[3−5] It is a catechol derivative substituted by an alkyl amine group. Catechol has a very high affinity to ferric cations and is considered to be a robust molecular anchor to link functional molecules to the surface of iron oxide magnetic nanoparticles.[6,7] Catechol grafting on iron oxide surfaces was already characterized by spectroscopy methods, mainly X-ray absorption near-edge spectroscopy (XANES)[6] and Fourier transform infrared spectroscopy (FTIR).[4,5] Both of these methods give qualitative results but do not yield quantitative results on the bonding efficiency. In both of those works, ab initio modeling has also been used, using either a single iron atom linked to a molecule or a small iron oxide cluster.[3,4]

Focusing on *DA* grafting on iron oxide NPs, typically 10 nm sized, and well-crystallized maghemite, we want to first investigate the magnetic structure of the surface layer, which strongly differs from that of the core, and then the magnetic interactions in the surface layer when it is modified by organic materials, together with the nature of the chemical bonding, that is, ionic or covalent, with the latter one being preferred because it is stronger. Experimental and numerical approaches were combined to follow the surface phenomena. Namely, ^{57}Fe Mössbauer spectrometry, which is a selective and nondestructive technique, was chosen to discriminate core and surface Fe species through their electronic and magnetic hyperfine characteristics (provided that the size of nanoparticles is less than about 20 nm). Indeed, in iron oxides such as maghemite the magnetic coupling is affected by indirect exchange (superexchange) via the oxygen atoms of the spinel lattice. A rearrangement of the atomic surface structure can lead to a modification of the magnetic coupling and can therefore lead to significant changes in magnetic and electronic properties. These changes are easily viewable by Mössbauer spectroscopy in the case of nanoparticles, as the surface is enhanced.

Ab initio calculations on surfaces are able to bring relevant information on the electronic transfer between the molecules and the surface of either maghemite or magnetite, which can be correlated with experimental results. It is thus interesting to validate such a hybrid approach to predict numerically some further scenario using different organic materials for functionalization, speeding up the cycle of experimental design and validation, which is time- and chemical-product-consuming. To the best of our knowledge, this is the first time that such an approach using the Mössbauer experimental tool was explored.

2. EXPERIMENTAL SECTION

2.1. Synthesis. *NPs Synthesis.* Maghemite-like iron oxide γ-Fe_2O_3 nanoparticles (NPs) were prepared by a two-step process. First, magnetite Fe_3O_4 particles were prepared by the polyol method, which consists of a forced hydrolysis of acetate iron $Fe(CH_3COO)_2$ (ACROS Organics, 95%), in a polyol, diethylene glycol $(HO(CH_2)_2O(CH_2)_2OH$ (Sigma-Aldrich, 99%).[5,8] Typically, 4.35 g of metallic salt was dissolved in 250 mL of diethyleneglycol. About 0.45 g of distilled water was added to ensure the hydrolysis reaction. The mixture was then heated (6 °C min^{-1}) to ebullition and maintained under reflux for 3 h. After cooling to room temperature, the recovered black powder, whose composition is expected to be close to that of magnetite, was washed three times by hot water to achieve its oxidation to maghemite. The resulting brown particles, the composition of which is expected to be close to that of maghemite, were then dried in air at 50 °C overnight and stored without any precautions.

Hybrids Preparation. 100 mL of water and 100 mg of NPs were mixed in a test tube. This solution was left for ∼30 min in an ultrasonic bath to disperse the aggregates that could have formed as well as possible. Then, 5.0 g of 3,4-dihydroxyphenylethylamine hydrochloride, also called dopamine hydrochloride, (ACROS, 99.00%) (Figure 1), was added. The

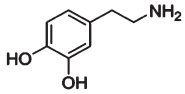

Figure 1. Structural formula of the 4-3,4-dihydroxyphenylethylamine hydrochloride ligand.

obtained mixture was sonicated for 45 min. To wash excess molecules and recover the formed nanohybrids a large excess of acetone was added to the solution. A magnet was then placed below the test tube to attract all of the NPs to the bottom. Two additional washes were performed in the same way. The resulting nanohybrids were air-dried.

2.2. Characterization. The as-produced particles and their related nanohybrids were characterized by X-ray diffraction (XRD) on a PANalytical X'pert Pro in the 2θ (deg) range 20−100 with a scan step of 0.05 using the CoKα radiation (λ = 1789 Å). The cell parameter and the size of coherent diffraction domain (crystal size) were determined with MAUD software,[9] which is based on the Rietveld method combined with Fourier analysis, well-adapted for broadened diffraction peaks.

The morphology of the prepared NPs was studied on a JEOL-100-CX II transmission electron microscope (TEM) operating at 100 kV. Specimens for TEM observation were prepared by evaporating at room temperature a drop of particles suspension in ethanol deposited on amorphous carbon-coated copper grids. The particle size distribution was obtained from TEM images using a digital camera and the SAISAM software (Microvision Instruments).

Hydrodynamic mean size of the particles before and after DA grafting was determined by dynamic light scattering method (DLS) using a Zeta Nanosizer Malvern instrument operating with a laser of 633 nm wavelength after their dispersion in distilled water. Their surface charge was also measured using specific cells with the same equipment.

To confirm *DA* grafting, we carried out Fourier transform infrared (FT-IR) spectroscopy on both fresh and functionalized iron oxide particles using a Bruker Equinox spectrometer in the range 700−4000 cm^{-1}. KBr pellets on dried samples were prepared and the spectra were recorded in transmission mode at room temperature.

The ^{57}Fe Mossbauer spectra of all of the samples were also recorded using a ^{57}Co/Rh γ-ray source mounted on an electromagnetic drive and using a triangular velocity form. They were obtained at 300 and 77 K in a zero magnetic field. The hyperfine structure was modeled by a least-squares fitting procedure involving Zeeman sextets and quadrupolar doublets composed of Lorentzian lines. The isomer shift (IS) values were referred to α-Fe at 300 K. The samples consist of a powder of ∼40 mg located in sample holder.

2.3. Ab Initio Modeling. We turn to ab initio molecular modeling of these systems to provide new information on the electronic exchange between the molecules and the surface of maghemite NPs. The particles were considered to be large

enough that the site where a ligand will bind is almost locally flat. Therefore, the system NP+DA was modeled as a surface with periodic boundary conditions and a vacuum in the direction orthogonal to the surface. We used the Gaussian09 software[10] with the ab initio Hartree–Fock method with 6-31+G(d) basis set to check that we had stable configurations of dopamine.

The spinel iron oxide surfaces were built from the Open Crystallography Database[11] crystal structures for maghemite and magnetite,[12,13] expanded with vacuum in the [100] and [111] directions, doubling the size of the cell in the considered direction to avoid effects from the replicated surface from the periodic boundaries conditions. We then added a dopamine molecule at a height of 3 au above the surface, trying various orientations. The density functional theory calculations of the iron oxide surfaces were performed with the Quantum Espresso (QE) suite, based on density functional theory.[14] The software uses the Pwscf code for electronic–structure calculations using and a plane-wave basis set and ultrasoft pseudopotentials with nonlinear core correction, eight active electrons for Fe (chosen as scalar relativistic), and valence electrons only for the other atoms. These pseudopotentials were taken from the QE site. We used for structural optimization the PBE-generalized gradient approximation (GGA) density functional[15] and for final optimization and electronic structure calculations the local density approximation (LDA)+U method with the Perdew–Zunger functional and corresponding pseudopotentials, a U value of 4.5 eV,[16,17] and occupations of the d orbitals to ensure an insulating state. We used Marzari–Vanderbilt cold smearing and a Gaussian smearing factor of 0.02. We used a 3 × 3 × 3 sampling of the first Brillouin zone, which seemed to be the minimum quality to ensure consistency of the results after convergence analysis. With the same method, the energy cutoff was set to 30 Ry and a 0.17 mixing factor for self-consistency was used to ensure convergence when the spin degree of freedom was released. We then used BFGS structural optimization with the default convergence parameters of QE. A typical calculation took about 1000 CPU hours on a contemporary computer.

3. RESULTS AND DISCUSSION

3.1. Structural and Microstructural Analysis. The XRD patterns of the as-produced iron oxide particles and their related hybrids are very close to each other. They show broadened diffraction peaks unambiguously attributed to the iron oxide with cubic spinel structural group: in this stage, it remains difficult to clearly attribute to either Fe_3O_4 magnetite or γ-Fe_2O_3 maghemite (Figure 2). Indeed, the refined cell parameter and mean coherent diffraction domain size, using MAUD program, were found to be 8.372(5) Å and 10 nm, respectively, which is a priori consistent with an intermediate solid solution between Fe_3O_4 and γ-Fe_2O_3. Note that the color of the obtained power is red-brown and not black, suggesting that the produced solid solution is closer to the maghemite phase than the magnetite one. Mössbauer spectrometry permitted us to distinguish unambiguously the chemical composition of the obtained phase using the electronic density of ^{57}Fe atoms. It matched unambiguously with that of Fe^{3+} species in agreement with the production of maghemite. (See the 57Fe Mössbauer Spectrometry section.) An attentive observation of the hybrid pattern evidences, in the 30–50° 2θ range, a small bump, suggesting an amorphous contribution that can be assigned to *DA* grafting.

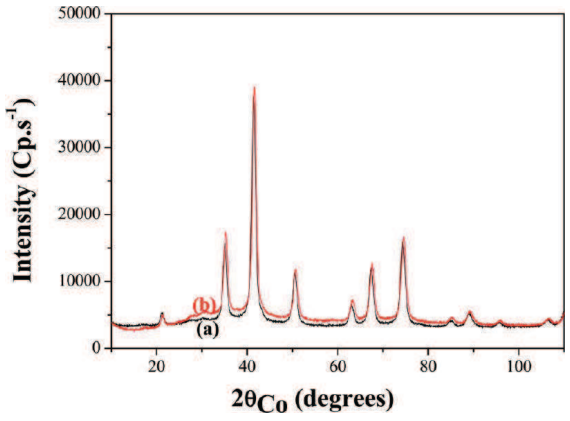

Figure 2. XRD patterns of the as-produced maghemite particles (a) and their related nanohybrids resulting from *DA* grafting (b).

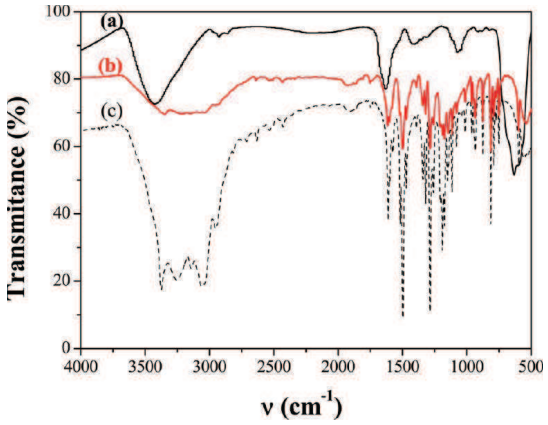

Figure 3. FTIR spectra of the as-produced maghemite particles (a) and their related nanohybrids resulting from *DA* grafting (b) compared with that of free *DA* (c).

Table 1. Hydrodynamic Diameter of Bare and Functionalized Iron Oxide Nanoparticles Dispersed in Distilled Water and Their ζ Potential

NPs	$\langle D_{DLS}\rangle$ (nm)	zeta potential (mv)	[NPs] (g/L)
Fe_2O_3	242	+12.8	25×10^{-3}
DA-Fe_2O_3	45	+2.2	25×10^{-3}

To confirm *DA* grafting, the FTIR spectra of the as-produced brown particles and their related hybrids were compared with that of fresh *DA* (Figure 3). The prefunctionalized NP spectrum is very poor. One can mainly detect the spinel Fe–O vibration bands below 700 cm^{-1} and those assigned to residual adsorbates. Clearly, hydroxyl OH (strong ν(OH) at 3425 cm^{-1}), alkyl CH_3 (very weak and sharp stretching band at 2920–2860 cm^{-1}), and carboxylate COO bands (strong ν_{as}(COO) and weak and broadened ν_s(COO) at 1625 and 1405 cm^{-1}, respectively),[18] assigned to water and acetate adsorbed species at the surface of the particles are observed. In comparison, the postfunctionalized NPs spectrum is richer. A number of changes were observed. The most notable of which is the disappearance of the acetate features with the appearance of additional bands relative to the catechol species such as the

dx.doi.org/10.1021/jp4027942 | J. Phys. Chem. C 2013, 117, 14295–14302

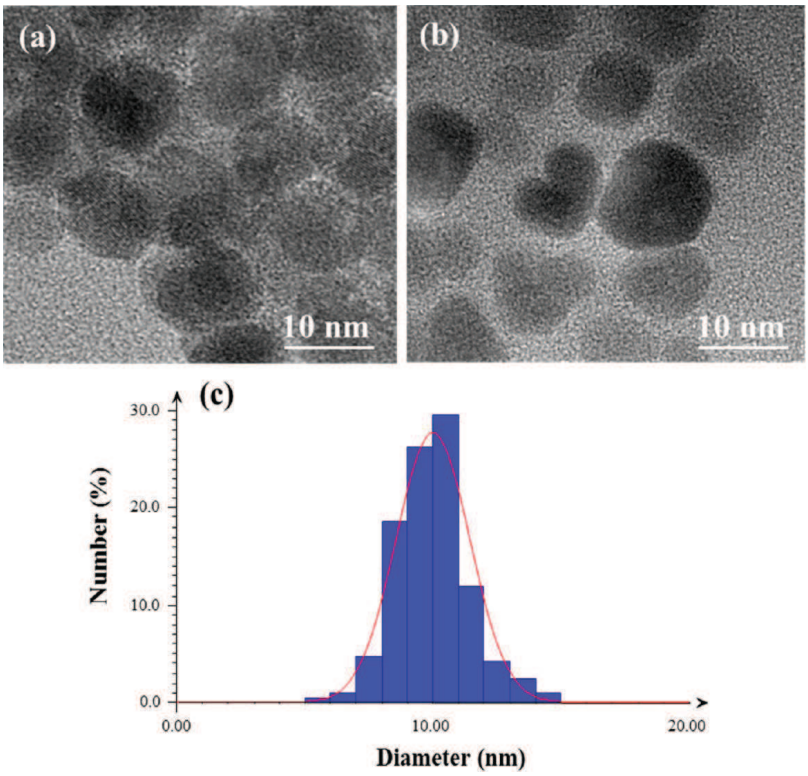

Figure 4. TEM images of the as-produced maghemite particles (a) and their related nanohybrids resulting from DA grafting (b). The size distribution of the iron oxide particles, as inferred from SAISAM program, is given for indication (c).

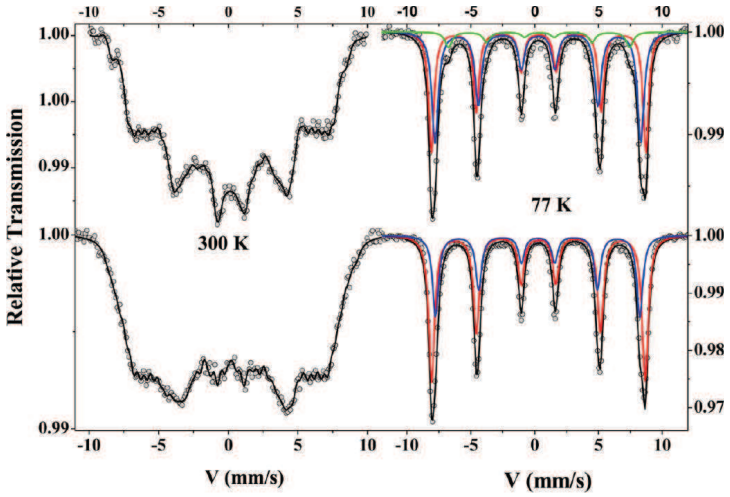

Figure 5. Fe Mossbauer spectra of the as-produced maghemite particles (bottom) and their related nanohybrids resulting from *DA* grafting (top) recorded at 300 (left) and 77 K (right).

aryl C−O stretch (~1290 cm^{-1}), the aromatic ring features (~1500 cm^{-1}), and the N−H bending (~1600 cm^{-1}). It should also be noted that for the postfunctionalized particles some of the catechol bands appear to be slightly red-shifted by about 10−20 cm^{-1} (see, in particular, the aryl C−O stretch), suggesting an effective chemical bonding on the surface of particles. Additionally, the CH groups of grafted organic species are indicated by the intensity increase in the sharp bands in the range 2800−2900 cm^{-1}.

Finally, the strong characteristic band of the spinel Fe−O vibration is very likely overlapped by the dopamine bands appearing in the same energy range.

Thermogravimetric analysis was also performed on bare iron oxide particles and their related hybrids and permitted us to

dx.doi.org/10.1021/jp4027942 | *J. Phys. Chem. C* 2013, 117, 14295−14302

Table 2. Summary of Refined Values of Hyperfine Parameters Obtained at 77 K (Isomer Shift δ, Quadrupolar Shift 2ε, Hyperfine Field B_{hyp}, and Ratio %)

77 K	δ (mm·s^{-1}) ± 0.01	2ε (mm·s^{-1}) ± 0.01	B_{hyp} (T) ± 0.5% ± 1	% ± 2
as-prepared				
(1) Fe_B^{3+}	0.45	0.00	51.7	64
(2) Fe_A^{3+}	0.41	−0.02	49.4	36
grafted				
(1) Fe_B^{3+}	0.46	−0.01	51.8	53
(2) Fe_A^{3+}	0.41	−0.01	49.6	38
(3) Fe_B^{x+} (!) $2 < x < 3$	0.50	−0.04	41.0	9

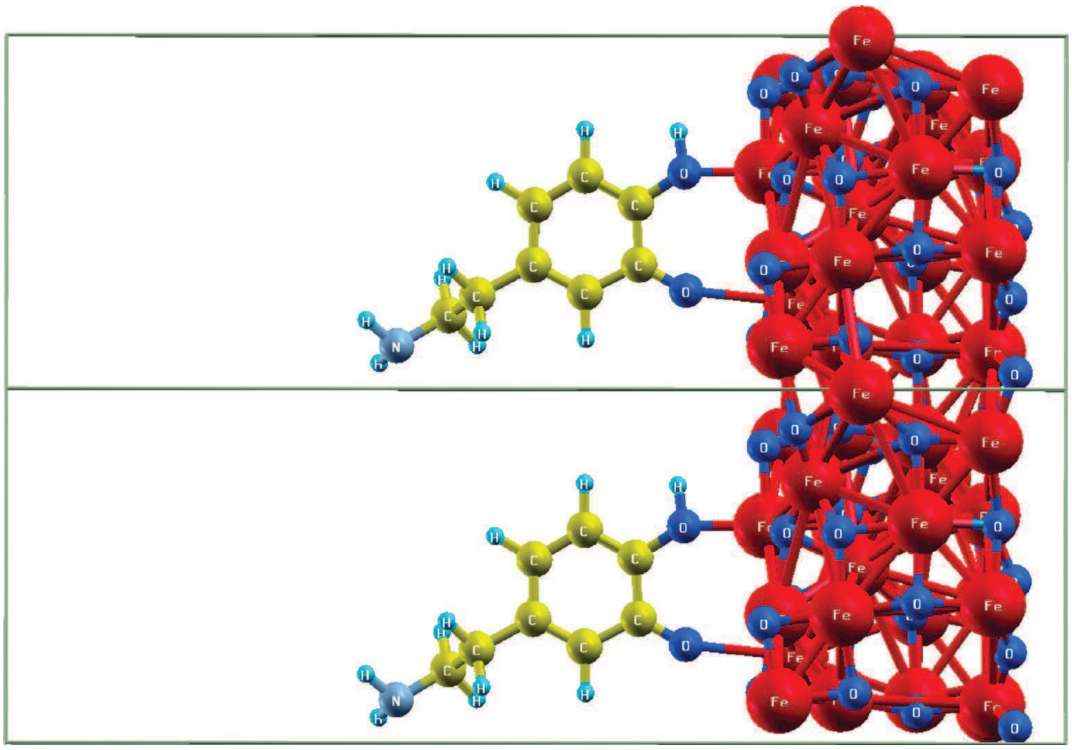

Figure 6. Three-dimensional view of the studied surfaces for ab initio calculations considering *DA* molecules grafted on maghemite structure.

also confirm *DA* grafting and to quantify it. *DA* content was found to be ∼9 wt %.

On the basis of these results, the microstructure of both samples was investigated. Whereas both powders appeared to be constituted by roughly spherical, highly crystallized, and almost uniform in size single crystals with an average diameter of 10 nm (standard deviation lower than 15%), the particles functionalized by *DA* seemed to be less agglomerated. This feature must be underlined because it is the signature of efficient sterical packing at the surface of the hybrid NPs, which maintains them far from each other despite their strong attractive magnetic interactions. This property is needed in medical applications. The hydrodynamic diameter and the zeta potential of the as-produced particles dispersed in distilled water and their related hybrids after ultrasonication are given in Table 1. The obtained hydrodynamic size of bare maghemite particles is larger than that observed by TEM (Figure 4). This is because, even in the absence of any external magnetic field, the magnetic dipole−dipole interactions between 10 nm sized crystals can cause their aggregation. The reached average diameter in this medium is micrometer-size ranged[8] with a positive surface charge close to zero (Table 1). These values change drastically when the particles are coated by dopamine (Table 1). The hydrodynamic diameter in water decreases down to about 45 nm with a close-to-zero surface charge.[5]

3.2. ^{57}Fe Mössbauer Spectrometry. Zero-field Mössbauer spectra of the as-prepared NPs was recorded at both 300 and 77 K and compared with those of their related hybrids to evidence any chemical environment change on Fe species (Figure 5). Mössbauer spectrometry is well-known as a local probe technique suitable to discriminate the chemical environment, electronic structure, and magnetic properties of different Fe species, through the hyperfine interactions. Because of its sensitivity and specificity, it is the best tool for investigating the influence of the grafted dopamine molecule on the electronic properties of iron-based materials as a result of the surface/volume ratio enhancement.

dx.doi.org/10.1021/jp4027942 | J. Phys. Chem. C 2013, 117, 14295−14302

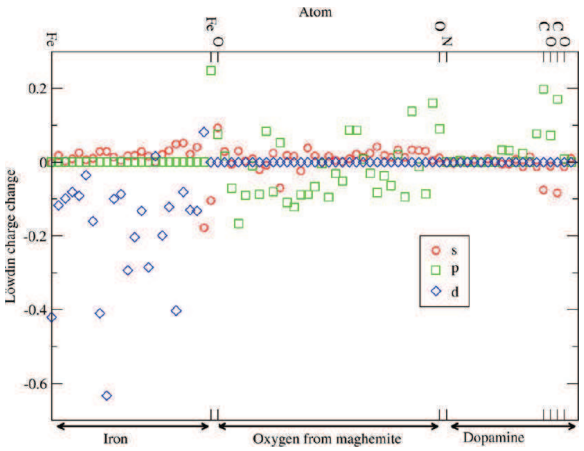

Figure 7. Change in the Löwdin charges of iron oxide and dopamine after grafting (LDA+U).

As illustrated in Figure 5, 300 K Mössbauer spectra exhibit broadened lines magnetic sextets. The broadening is due to the presence of superparamagnetic relaxation phenomena. The spectra should be decomposed into two main components due to the presence of tetrahedral and octahedral positions, but the lack of resolution prevents a clear physical fitting model. The only relevant parameters are the mean values of isomer shift and hyperfine field. One estimates at 0.33(1) mm/s the isomer shift of bare NPs, suggesting rather pure maghemite phase and 0.37(1) mm/s that of grafted NPs, suggesting a priori some electron transfer from Fe^{3+} to Fe^{2+} states; in addition, one notes a decrease in the mean hyperfine field (35.6(5) T down to 30.4(5) T) resulting from the increase in the distance between NPs favoring faster relaxation phenomena. Figure 5 (right bottom) shows that the hyperfine structure of bare NPs at 77 K can be described by means of pure magnetic components, clearly attributed to Fe^{3+} species located in the tetrahedral A site (the smallest isomer shift δ) and in the octahedral B site (the largest isomer shift δ), in perfect agreement with those of maghemite. The proportion of each component site was also estimated (Table 2). The B sites component provides 64(1) % of the final result, and the A sites component provides only 36(1)%. More accurate estimation would require in-field Mössbauer measurements, allowing resolving the hyperfine structure into two distinguishable magnetic components because of the ferrimagnetic behavior. On the contrary, the Mössbauer spectrum obtained on the grafted sample clearly requires an additional magnetic component, as illustrated in Figure 5 (right top). From the refined values of the hyperfine data listed in Table 2, one unambiguously identifies a new Fe species, characterized by a significant increase in the isomer shift up to δ = 0.50 mm/s and a decrease in the hyperfine field. In addition, the proportions of the Fe components allow us to conclude that some octahedral Fe sites are influenced by the presence of dopamine. The slight increase in the isomer shift, which depends on the s-electron density at the ^{57}Fe nucleus, is attributed to an electron transfer from the dopamine molecule to the octahedral Fe sites located at the surface of the maghemite NP. The decrease in the hyperfine field is probably due to the chemical bonding with the diol DA group. Furthermore, the percentage of 9(1)% enables us to see that the third Fe species is located in octahedral positions of the maghemite mesh. Indeed, whereas the percentage contribution of the tetrahedral sites slightly increases to 38(1) %, the contribution of the octahedral sites occupied by Fe3+ ions

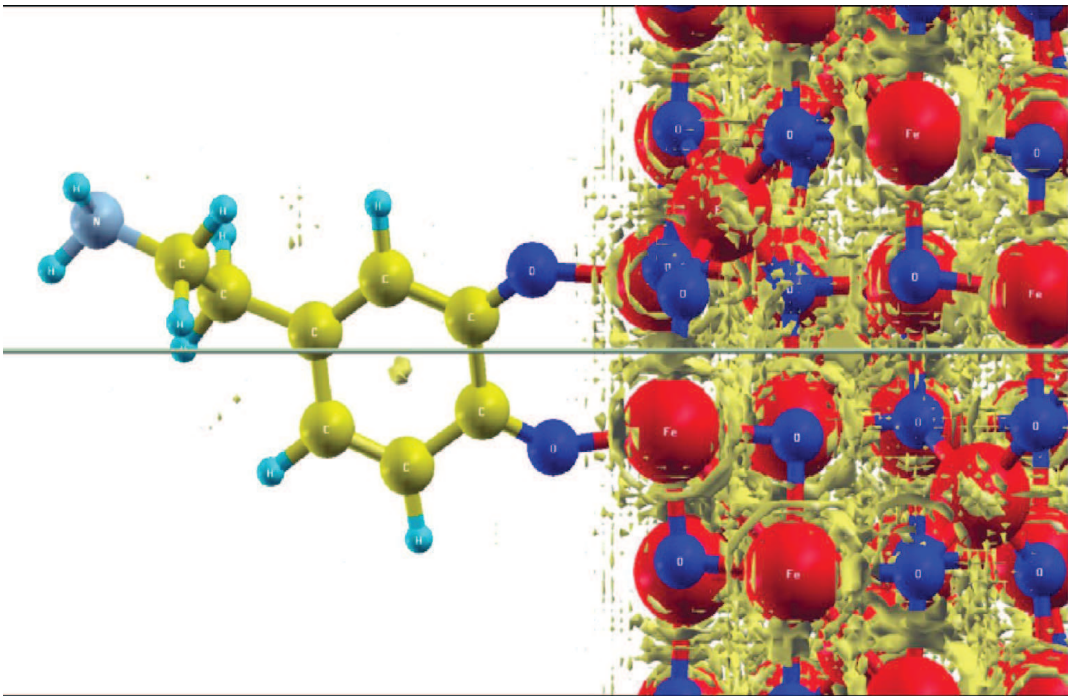

Figure 8. Ionicity of the system, estimated by 0.5 isosurface of reduced density gradient (EPLF) in LDA+U following ref 21.

dx.doi.org/10.1021/jp4027942 | J. Phys. Chem. C 2013, 117, 14295−14302

decreases to 11(1)%, which roughly corresponds to the percentage of the new sextuplet. Those results are coherent with the results reviewed in refs 19 and 20, especially the ones obtained with XANES.[3]

3.3. Ab Initio Modeling. To be as exhaustive as possible, we considered both magnetite and maghemite iron oxide surfaces. We checked that we could reproduce magnetite and maghemite crystals with structural values within 1% of experimental data. In the case of surfaces with or without ligands, structural changes were found to be a little larger (∼5%), but we checked that those results were stable when the number of layers of iron oxide was changed, as was the topology.

We varied the surface ([100] or [111]), the orientation of the surface (oxygen atoms close to the ligands or iron atoms close to them), the initial orientation, and the position of the ligands. In all cases, dopamine presented a preferential affinity for the octahedral sites of iron oxide, which was the final structure given by full structural optimization, the results of which in the case of maghemite are presented in Figure 6. This was also checked using a forced orientation of the ligands on preferential sites; the binding energy was definitely lower in the octahedral case. Besides, in the case of dopamine, we found that the binding happens in the surprising configuration of a "bidentate", that is, two oxygen atoms from the ligand closer to the same iron atom than to other iron atoms (Figure 6), where traditional chemistry would have preferred a bidentate, with two oxygen atoms binding on two different iron atoms on the surface. We also checked this by a systematic variation of the O−C−O angle on the ligand. In this case, the automatic structural optimization also showed that the *DA* molecule could also bind at the surface with the NH_2 group, also at the octahedral site. These results are also coherent with the ones from ref 3, although in the latter case they were obtained either by experimental means (XANES) or by a simple ab initio modeling of single-atom iron oxide clusters attached to ligands.[3,4] We suspect that the reason could be that the oxidation degree of the iron atoms at the octahedral site is different than the one at the tetrahedral sites. This was checked by computing the change in Löwdin charges (projecting the final wave functions on the atomic wave functions used for pseudopotential generation) of each atom of the system during grafting. The results, presented in Figure 7, show that there is indeed a partial reduction of Fe^{3+} atoms, the d orbitals being reduced, and the p orbitals of dopamine, showing a marked increase in charge, especially around the linking oxygen atoms, at the right of the Figure. Those results are totally coherent with those from Mössbauer spectrometry. We also computed the reduced gradient of the electronic density according to the method of ref 21, plotting the isosurface at a value of 0.5. At this value, this method also called electron pair localization function (EPLF) allows us to characterize whether chemical bonds are ionic or covalent. One can check in Figure 8 that the bonding of the atoms in dopamine is, as expected, covalent (no isosurface is present except at the center of the aromatic ring), and the bonding in iron oxide is strongly ionic (high presence of the isosurface). The welcome result is then that the bonding of the dopamine molecule and the iron oxide surface is covalent, which is also a strong requirement for pharmaceutical applications of the considered nanohybrids.

CONCLUSIONS

We showed for the first time that Mössbauer spectrometry enables a quantitative understanding of the way a ligand of biological interest such as a catechol derivative, namely, dopamine, can bind to the surface of iron oxide NPs, namely, maghemite. These results are coherent with results from various ab initio calculations expanding previous work. The synthesis and functionalization by dopamine of the iron oxide NPs was performed in a simple and reproducible way using soft chemistry methods. The products were characterized using TEM, XRD, FTIR, and Mössbauer spectrometry. The latter confirmed the results of previous work showing that dopamine preferentially binds on octahedral sites, and a quantitative assessment of this preference was obtained. Ab initio modeling confirmed these results, expanding on previous work by using various possible iron oxide surfaces. The covalent nature of the bond was proved. It would be interesting to include a modeling taking into account pH or ionic charge of the colloid in which the *DA*-grafted maghemite NPs were dispersed, as well as temperature effect, using a multiscale approach. This is in progress.

AUTHOR INFORMATION

Corresponding Author

*Fax: +33 2 43833518. Tel: +33 243832626. E-mail: florent.calvayrac@univ-lemans.fr.

Notes

The authors declare no competing financial interest.

ACKNOWLEDGMENTS

The authors thank Drs A. Chevillot, S. Nowak, and P. Beaunier for their technical support in FTIR, XRD, and TEM characterization. They want to thank GENCI/IDRIS and CRIHAN national and regional facilities for computational time (projects x2010096171, x2011096171, x2012096171 and 007, respectively).

REFERENCES

(1) (a) Mornet, S.; Vasseur, S.; Grasset, F.; Duguet, E. Magnetic Nanoparticle Design for Medical Diagnosis and Therapy. *J. Mater. Chem.* **2004**, *14*, 2161−2175. (b) Corot, C.; Robert, P.; Idée, J.-M.; Port, M. Recent Advances in Iron Oxide Nanocrystal Technology for Medical Imaging. *Adv. Drug Delivery Rev.* **2006**, *58*, 1471−1504. (c) Laurent, S.; Dutz, S.; Häfeli, U. O.; Mahmoudi, M. Magnetic Fluid Hyperthermia: Focus on Superparamagnetic Iron Oxide Nanoparticles. *Adv. Colloid Interface Sci.* **2011**, *166*, 8−23.

(2) Gupta, A. K.; Gupta, M. Synthesis and Surface Engineering of Iron Oxide Nanoparticles for Biomedical Applications. *Biomaterials* **2005**, *26*, 3995−4021.

(3) Rajh, T.; Chen, L.; Lukas, K.; Liu, T.; Thurnauer, M.; Tiede, D. Surface Restructuring Of Nanoparticles: An Efficient Route For Ligand-Metal Oxide Crosstalk. *J. Phys. Chem. B* **2002**, *106*, 10543−10552.

(4) Shultz, M. D.; Reveles, J. U.; Khanna, S. N.; Carpenter, E. E. Reactive Nature of Dopamine as a Surface Functionalization Agent in Iron Oxide Nanoparticles. *J. Am. Chem. Soc.* **2007**, *129*, 2482−2487.

(5) Basti, H.; Ben Tahar, L.; Smiri, L.; Herbst, F.; Vaulay, M.-J.; Chau, F.; Ammar, S.; Benderbous, S. Catechol Derivatives-Coated Fe_3O_4 And γ-Fe_2O_3 Nanoparticles as Potential MRI Contrast Agents. *J. Colloid Interface Sci.* **2010**, *341*, 248−254.

(6) Jordana, R. B.; Xub, J.-H. Substitution and Oxidation Kinetics in Substituted Catechol-Iron (111) Systems. *Pure Appl. Chem.* **1988**, *60*, 1205−1208.

(7) Xu, C.; Xu, K.; Gu, H.; Zheng, R.; Liu, H.; Zhang, X.; Guo, Z.; Xu, B. Dopamine as a Robust Anchor to Immobilize Functional Molecules on the Iron Oxide Shell of Magnetic Nanoparticles. *J. Am. Chem. Soc.* **2004**, *126*, 9938−9939.
(8) Hanini, A.; Schmitt, A.; Kacem, K.; Chau, F.; Ammar, S.; Gavard, J. Evaluation Of Iron Oxide Nanoparticle Biocompatibility. *Int. J. Nanomed.* **2011**, *6*, 787.
(9) Lutterotti, L.; Matthies, S.; Wenk, H. MAUD: A Friendly Java Program For Material Analysis Using Diffraction. *IUCr: Newsletter of the CPD* **1999**, 21.
(10) Frisch, M.; Trucks, G.; Schlegel, H.; Scuseria, G.; Robb, M.; Cheeseman, J.; Scalmani, G.; Barone, V.; Mennucci, B.; Petersson, G.; et al. *Gaussian 09*, revision A.1; Gaussian, Inc., Wallingford, CT, 2009.
(11) Grazulis, S.; Daskevic, A.; Merkys, A.; Chateigner, D.; Lutterotti, L.; Quirós, M.; Serebryanaya, N. R.; Moeck, P.; Downs, R. T.; Le Bail, A. Crystallography Open Database (COD): An Open-Access Collection of Crystal Structures and Platform for World-Wide Collaboration. *Nucleic Acids Res.* **2012**, *40*, D420−D427.
(12) Greaves, C. A Powder Neutron Diffraction Investigation of Vacancy Ordering and Covalence In γ-Fe_2O_3. *J. Solid State Chem.* **1983**, *49*, 325−333.
(13) Guo, H.; Barnard, A. S. Surface Structure and Environment-Dependent Hydroxylation of the Nonpolar Hematite (100) from Density Functional Theory Modelling. *J. Phys. Chem. C* **2011**, *115*, 23023−23029.
(14) Giannozzi, P.; Baroni, S.; Bonini, N.; Calandra, M.; Car, R.; Cavazzoni, C.; Ceresoli, D.; Chiarotti, G. L.; Cococcioni, M.; Dabo, I.; et al. QUANTUM ESPRESSO: a Modular and Open-Source Software Project for Quantum Simulations of Materials. *J. Phys: Condens. Matter* **2009**, *21*, 395502.
(15) Perdew, J. P.; Burke, K.; Ernzerhof, M. Generalized Gradient Approximation Made Simple. *Phys. Rev. Lett.* **1996**, *77*, 3865−3868.
(16) Perdew, J. P.; Zunger, A. Self-Interaction Correction to Density-Functional Approximations for Many-Electron Systems. *Phys. Rev. B* **1981**, *23*, 5048.
(17) Pinto, H.; Elliott, S. Mechanism of the Verwey Transition in Magnetite: Jahn−Teller Distortion and Charge Ordering Patterns. *J. Phys: Condens. Matter* **2006**, *18*, 10427.
(18) Nakamoto, K. *Infrared and Raman Spectra of Inorganic and Coordination Compounds*, 4th ed.; Wiley: New York, 1986.
(19) Yuen, A. K.; Hutton, G. A.; Masters, A. F.; Maschmeyer, T. The Interplay of Catechol Ligands with Nanoparticulate Iron Oxides. *Dalton Trans.* **2012**, *41*, 2545−2559.
(20) Figuerola, A.; Di Corato, R.; Manna, L.; Pellegrino, T. From Iron Oxide Nanoparticles Towards Advanced Iron-Based Inorganic Materials Designed for Biomedical Applications. *Pharmacol. Res.* **2010**, *62*, 126−143.
(21) Scemama, A.; Caffarel, M.; Chaudret, R.; Piquemal, J.-P. Electron Pair Localization Function (EPLF) for Density Functional Theory and ab Initio Wave-Function-Based Methods: A New Tool for Chemical Interpretation. *J. Chem. Theory Comput.* **2011**, *7*, 618−624.

Appendix B - Combined *ab initio* modelling and Fe Mőssbauer spectroscopy approach to characterize the bonding between iron oxide nanoparticles and Aryl Diazonium Salt

RSC Publishing Journal of Materials Chemistry B

Combined ab initio modelling and 57Fe Mössbauer spectrometry approach to characterize the bounding between iron oxide nanoparticles and Aryl Diazonium Salt

Journal:	*Journal of Materials Chemistry B*
Manuscript ID:	TB-COM-05-2013-020749
Article Type:	Communication
Date Submitted by the Author:	28-May-2013

Complete List of Authors: Fouineau, Jonathan; Paris Diderot University, ITODYS, UMR-CNRS 7086
Brymora, Katarzyna; Université du Maine, IMMM, CNRS UMR-6087
Chau, François; Paris Diderot University, ITODYS, UMR-CNRS 7086
Yaacoub, Nader; Université du Maine, IMMM, CNRS UMR-6087
Calvayrac, Florent ; LUNAM Université du Maine, IMMM - UMR CNRS 6283
Ammar, Souad; Paris Diderot University, ITODYS, UMR-CNRS 7086
Grenèche, Jean-Marc; Université du Maine, LPEC

Cite this: DOI: 10.1039/c0xx00000x

www.rsc.org/xxxxxx

Communication

Combined *ab initio* modelling and ^{57}Fe Mössbauer spectrometry approach to characterize the bounding between iron oxide nanoparticles and Aryl Diazonium Salt

Jonathan Fouineau,[a,b] Katarzyna Brymora,[b] François Chau,[a] Nader Yaacoub,[b] Florent Calvayrac,[b,*] Souad Ammar,[a] Jean-Marc Grenèche,[b]

Received (in XXX, XXX) Xth XXXXXXXXX 200X, Accepted Xth XXXXXXXXX 200X
DOI: 10.1039/b000000x

The use of aryl diazonium salts as a new generation of surface modifiers and coupling agents for binding synthetic polymers or biomacromolecules to nanoparticle surfaces is nowadays seriously considered in view of developing efficient biomedical probes. Even if the robustness of the resulting linkage in the produced nanohybrids is not at all controversial, its nature remains still under investigation particularly in the case of metal oxide surfaces. In this paper, using combined *ab initio* modelling and ^{57}Fe Mössbauer spectrometry we established, for the first time, the metal-oxygen-carbon bonding when aryl diazonium salts are coupled to iron oxide nanoparticles.

Magnetic nanoparticles (NPs) provide many exciting opportunities in biomedical applications if high-quality materials, mainly regarding size and size distribution, crystallinity, magnetic features, and surface functionalization, can be elaborated. [1] For instance, their notoriety as heating agents for magnetic hyperthermia, contrast agent for magnetic resonance imaging (MRI) or drug vector under magnetic guidance is essentially related to a satisfying compromise between a relevant magnetization and a suitable size for medical use. These magnetic NPs are mainly iron oxide, magnetite or maghemite, with formula Fe_3O_4 or Fe_2O_3, the latter being usually obtained by the oxidation of the former.

Both have a spinel cubic structure, the oxygen forming a fcc lattice and iron cations occupying the tetrahedral (A) and octahedral (B) interstitial sites as follows $(Fe^{3+})[Fe^{2+}Fe^{3+}]O_4$ for magnetite and $(Fe^{3+})_{tetra}[Fe^{3+}_{1.67}Fe^{2+}_{0.33}]_{octa}O_4$ for maghemite, where the round and square brackets represent A and B sites, respectively. This structure confers them magnetic properties with a ferrimagnetic ordering at room temperature with relatively a magnetization as bulk materials (about 90 and 74 emu g^{-1}, respectively). [2,3] As NPs, they exhibit a superparamagnetic behavior with a size dependent blocking temperature, most of the time lower than room temperature, which can be very useful for the mentioned applications. They are considered as almost safety at reasonable doses since iron is one of the most abundant transition metal in human body (average adult possessing ca. 5 g).

To ensure effective control over their colloidal stability in water and physiological medium, they were usually functionalized using organic ligands bearing chelating groups such as carboxylates, [4] amines and hydroxyls, [5] phosphates and phosphonates, [6] and sulfonates and thiols. [7] These anchoring groups of the chelate type may fail on metal oxide surfaces in aqueous or protic media due to the hydrolytic instability of the surface attachment and/or the dynamic nature of the interaction. Therefore, developing efficient functionalization chemical strategies to obtain strong and stable linkages between the iron oxide NPs surface and the organic coating still remains challenging, particularly when this anchoring serves as a platform to conjugate biomolecules such as drugs and/or targeting agent for specific *in vivo* application.

For this purpose, a novel grafting method was explored. It is based on diazonium salts chemistry. Aryl diazonium salts have been shown to be useful organic reagents for the surface modification of carbon-based and metallic (Au, Pt, Pd, Ru, and Ti) substrates, affording strong carbon- or metal-carbon linkages. [8] The resulting hybrids, dispersed in different media, evidenced a great stability confirming the robustness of the built links. This method has been recently extended to metal oxides, namely iron metal oxide nanoparticles. [9] In that case, the nature of the aryl and oxide surface linkage is not yet established even if a metal-oxygen-carbon bonding remained the most probable.

From a general point of view, very few experimental techniques exist to evaluate the adsorbates chemical bonding. All of them are based on a spectroscopic analysis of the organic species such as FTIR (PM-IRAS), [10] Raman (SERS) [11] and XPS. [12] Surprisingly, tools based on the analysis of the substrate were seldom considered. Focusing on magnetic iron oxide NPs, ^{57}Fe Mössbauer spectrometry appears as the best non-destructive technique able to discriminate, as the surface is enhanced, core and surface Fe species through their electronic and magnetic hyperfine characteristics. Coupled to *ab initio* modelling, with a special emphasis on the surface, relevant information on the electronic transfer between the molecules and the outer layer of NPs can be obtained. To the best of our knowledge, this approach was used only once to characterize dopamine-maghemite nanohybrids. [13]

For such a purpose, we prepared maghemite γ-Fe_2O_3 NPs by using the polyol process as previously described by Basti et al. [14] The particles consist of roughly spherical and almost uniform in size particles with an average diameter of 10 nm as illustrated in the recorded Electron Transmission Microscopy (TEM) image, using a JEOL-100-CX II TEM microscope operating at 100 kV, (Figure 1). These particles were functionalized by a hydrophilic amine aryl derivative using diazonium salt chemistry.

Typically, 4-(*tert-butyl* ethylcarbamate)benzenediazonium tetrafluoroborate salt, [BF_4^-, $^+N_2$-C_6H_4-C_2H_4-NH-Boc] was prepared from the commercially available 4-aminophenethylamine, following a simple procedure. [15] First the aliphatic amine was selectively protected by reaction with $(Boc)_2O$ (Boc = $(CH_3)_3C$-O-CO-). [16] 4-aminophenethylamine (10 mmol) was mixed to $(Boc)_2O$ (10 mmol) in dichloromethane (5 mL) and stirred for 16 hours. The solvent was evaporated and the recovered yellow solid was characterized by ^1H NMR spectroscopy (400 MHz, $CDCl_3$) δ (ppm) : 6.95 (d, 2 Har), 6.60 (d, 2 Har), 4.56 (bs, NH), 3.59 (bs, NH), 3.29 (m, 2 H), 2.65 (m, 2 H), 1.43 (s, 9 H). The crude solid (2.50 mmol) was then mixed at 0°C to 2.70 mL of HBF_4 (20.60 mmol) in 2 mL of a solution of $NaNO_2$ (207 mg, 3.00 mmol), in deionized water, under magnetic stirring for 30 minutes. The resulting dark brown solution was subsequently filtered and washed with a solution of $NaBF_4$ in ,deionized water (5 wt.-%). The brown-orange obtained powder was dried and stored at -5 °C. It was characterized by FTIR spectroscopy (KBr pellets). IR spectra evidenced the N_2^+ vibration band at ν (cm^{-1}) = 2280 and 2260 cm^{-1}.

To prepare the hybrids, γ-Fe_2O_3 NPs were mixed with the as-produced and dried aryl diazonium salt (which might be explosive) according to the procedure described elsewere.[9] Typically, 100 mg of as-produced maghemite were sonicated in a NaOH (0.1 M) aqueous solution for 20 minutes. Then, [BF_4^-, $^+N_2$-C_6H_4-C_2H_4-NH-Boc] (167 mg, 0.50 mmol) already dissolved in 10 mL of water was added and the mixture was sonicated for 20 minutes at 25°C. We observed a gas evolution during the sonication that could be attributed to N_2 gas resulting from ultrasonically assisted surface treatment by the diazonium salt. The resulting hybrids were then washed by 5 cycles of centrifugation/redispersion (using an ultrasonic bath for 15 min at each step) in water first then ethanol before drying in air. The Boc protecting group was then removed by acidic cleavage according to a typical procedure. Hybrids (20 mg) in dichloromethane (75 mL) were submitted to sonication for 5 minutes and trifluoroacetic acid (2 µL, 0.34 mmol) was added. The mixture was then stirred (mechanically) for 4 hours and washed with dichloromethane by centrifugation/redispersion (4 cycles) before drying in air.

The adsorption of the aryl diazonium salt on the surface of maghemite NPs was investigated by FTIR studies (KBr pellets) on a Bruker Equinox spectrometer. The recorded spectrum on the hybrids was compared to those of bare γ-Fe_2O_3 and free [BF_4^- ,$^+N_2$-C_6H_4-C_2H_4-NH-Boc] (Figure 2).

The spectrum of NP-C_6H_4-C_2H_4-NH_2 appears as a combination of the spectra of pure NPs (band below 800 cm^{-1} attributed to the different vibration modes of the Fe-O skeleton [17,18]) and that of the aryl group (bands at 1600 cm^{-1}), confirming the presence of a phenyl grafting on the surface of the γ-Fe_2O_3 nanoparticles. We note that the relative band of aryl group was shifted from 1582 cm^{-1} in the free aryl diazonium salt to 1600 cm^{-1} in the hybrid particles. This shift can be explained by the liberation of the electron withdrawing group -N_2^+. The most striking difference is the disappearance of the N≡N stretching mode near 2280 cm^{-1} in hybrids, indicating the release of N≡N as a consequence of the cleavage of the diazonium moieties. [9] Besides, thermogravimetry analysis carried out in the 20-800 °C temperature range (10°C/min) under a flow of air at 80 ml/min, using a SETARAM equipment, evidenced a weight loss of about 22% on heating aryl-coated γ-Fe_2O_3 NPs to 800 °C while the uncoated NPs showed a weight loss of only 4%. This result suggests a high grafting density of aryl group on the nanoparticles surface. Finally, X-ray diffraction (XRD) analysis performed on a Panalytical diffractometer equipped with a X'celerator detector and a Cobalt X-ray tube (λ = 1.7889 Å), on bare and hybrid NPs, confirmed that the aryl grafting does not affect *a priori* the crystal structure of the iron oxide phase. XRD patterns recorded before and after surface treatment are typical of a pure spinel phase, consistent with maghemite.

This is also confirmed using Fe local probe analysis route, namely ^{57}Fe transmission Mössbauer spectrometry. As illustrated in Figure 3, the 300 K Mössbauer spectra exhibit broadened lines resulting typically from the presence of superparamagnetic relaxation phenomena: the lack of resolution makes impossible the estimation of the proportions of iron cations located in A and B sites, respectively. But the mean values of the isomer shift which are unchanged before and after grafting are typical of Fe^{3+} species, confirming thus the presence of the maghemite. In addition, the difference between the mean values of hyperfine field estimated at 300 K can be explained by the change of the distance between particles because of the grafting of aryl group at the surface of nanoparticles, favoring an increase of dipolar interactions making faster the relaxation phenomena, i.e. decreasing the hyperfine field values. When cooling the samples at 77 K, the Mössbauer hyperfine structures split into asymmetrical sextets (see Figure 3) while the spectrum recorded at 77 K on the hybrid nanoparticles is close to that of bare γ-Fe_2O_3 ones. The asymmetry allows the spectra to be decomposed into two components, which should be attributed to octahedral and tetrahedral Fe sites on the basis of larger, and smaller isomer shift values, respectively. It is important to note that an accurate estimation of their proportions should require an in external magnetic field spectrum at low temperature, that allows to split the sextet into two well resolved components, because of the ferrimagnetic behavior of present powders.

As listed in Table 1, the refined average values of isomer shift and hyperfine fields (together with those of each components) are very close to each other in both samples and typical to Fe^{3+} cations, confirming thus previous results obtained at 300 K. In all evidence the aryl group is attached to the surface of maghemite through a carbon-oxygen-iron link, as supposed in previous work. [9]

These experimental results were confirmed by *ab initio* calculations. The surface functionalization of maghemite by the aryl functional group was simulated using phenoxy (C_6H_5O) and phenyl (C_6H_5) radical formations, in the framework of density

functional theory, with the local density approximation +U approach and the Quantum Espresso suite [19] and LDA [20] ultrasoft pseudopotentials taken from the distribution. The magnetite surfaces were built from the Open Crystallography Database structures, expanded by a cell tripling vacuum in the [001] direction and annealed after addition of the ligands with the BGFS procedure. The accuracy of our numerical procedure was previously well tested. [13] The LDA+U parameters were set to U = 4.5 eV and J = 0.367 eV. A cutoff energy of 30 Ry was used in the plane-wave expansion of the pseudo-wave-functions and a 0.2 mixing factor for self-consistency was used. We used a 3x3x3 sampling of the first Brillouin zone and a Gaussian smearing factor of 0.02. Results show a binding energy for the phenoxy group of -0.83 Ry as opposed to -0.18 Ry for the phenyl group. The phenoxy group thus provides the most robust system.

We computed the change in Löwdin charges (projecting the final wavefunctions on the atomic wavefunctions used for pseudopotential generation) of each atom of the system during grafting. The results, presented in figure 4, illustrate how there is indeed a partial reduction of Fe^{3+} atoms, the d orbitals being reduced, showing a marked increase in charge, especially around the linking oxygen atoms in the case of the phenoxy group. In the case of the phenyl ligand, a small change in the s orbitals is noticed, and the reduction of Fe^{3+} atoms is not as important.

We also computed the reduced gradient of the electronic density according to the method described in ref [21], plotting the isosurface at a value of 0.5. At this value, this method also called Electron Pair Localization Function (EPLF) allows to characterize whether chemical bonds are ionic or covalent. One can check in figure 4 that the bonding of the atoms in the ligand is, as expected, covalent (no isosurface is present except at the center of the aromatic ring), and the bonding in iron oxide is strongly ionic (high presence of the isosurface). The welcome result is then that the bonding of phenoxy group to the iron oxide surface is covalent, a little less so in the case of the phenyl group, which is also a strong requirement for pharmaceutical applications of the considered nanohybrids.

Conclusion

In this paper, using a combination of *ab initio* modelling and Mössbauer spectrometry, we could demonstrate the nature of bonding of aryl groups on iron oxide nanoparticles. The covalent and robust nature of the bonding offers interesting perspectives for applications of those nanoparticles.

Corresponding author

Florent Calvayrac, *Fax: +33 2 43833518; Tel: +33 243832626; mail: florent.calvayrac@univ-lemans.fr.*

Notes and references

[a]*ITODYS UMR CNRS 7086, Université Paris Diderot, Rue Jean-Antoine de Baïf 75205, Paris, France.*

[b]*LUNAM Université du Maine, IMMM UMR CNRS 6283, Avenue Olivier Messiaen, 72085 Le Mans, France.*

(1) J. H. Gao, H. W. Gu, B. Xu, *Acc. Chem. Res.*, 2009, **42**, 1097 ; S. Mornet, S. Vasseur, F. Grasset, E. Duguet, *J. Mater. Chem.*, 2004, **14**, 2161 ; C. Corot, P. Robert, J. M. Idee, M. Port, *Adv. Drug Delivery Rev.*, 2006, **58**, 1471 ; S. Laurent, S. Dutz, U. O. Häfeli, M. Mahmoudi, *Adv. Colloid Interface Sci.*, 2011, **166**, 8.

(2) R. Valenzuela, *Magnetic Ceramics*, Cambridge University Press (UK) 1994.

(3) B. D. Cullity, *Introduction to magnetic materials*, Addison-Wesley Publishing Company (Philippines) 1972.

(4) R. Tadmor, R. E. Rosensweig, J. Frey, J. Klein, *Langmuir*, 2000, **16**, 9117 ; R. E. Rosensweig, R. Kaiser, G. Miskolczy, *J. Colloid Interface Sci.,* 1969, **29**, 680.

(5) J. Rockenberger, E. C. Scher, A. P. Alivisatos, *J. Am. Chem. Soc.*, 1999, **121**, 11595.

(6) C. Yee, G. Kataby, A. Ulman, T. Prozorov, H. White, A. King, M. Rafailovich, J. Sokolov, A. Gedanken, *Langmuir*, 1999, **15**, 7111.

(7) J. Lu, J. Fan, R. Xu, S. Roy, N. Ali, Y. Gao, *J. Colloid Interface Sci*., 2003, **258**, 427 ; G. Kataby, A. Ulman, R. Prozorov, A. Gedanken, *Langmuir*, 1998, **14**, 1512.

(8) S. Mahouche-Chergui , S. Gam-Derouich , C. Mangeney, M. M. Chehimi, *Chem. Soc. Rev*., 2011, **40**, 4143.

(9) N. Griffete, F. Herbst, J. Pinson, S. Ammar, C. Mangeney, *J. Am. Chem. Soc*., 2011, **133**, 1646.

(10) T. Risse, A. Carlsson, M. Baümer, T. Klüner, H. J. Freund, Surface Sci., 2003, **546**, L829 ; M. Borasio, O. Rodrıguez de la Fuente, G. Rupprechter, H. J. Freund, *J. Phys. Chem. B*, 2005, **109**, 17791.

(11) A. Nilsson, L. Gunnar, M. Pettersson*, Surface Sci. Rep.,* 2004, **55**, 49 ; C. Vericat, M. E. Vela, G. A. Benitez, J. A. M. Gago, X. Torrelles, R. C. Salvarezza, *J. Phys.: Condens. Matter*., 2006, **18**, R867 ; S. Chen, W. Li, *Mater. Chem. Phys*., 2006, **98**, 183.

(12) Y. Fleger, Y. Mastai, M. Rosenbluh, D. H. Dressler, *J. Raman Spectrosc.*, 2009, **40**, 1572 ; L. Laurentius, S. R. Stoyanov, S. Gusarov, A. Kovalenko, R. Du, G. P. Lopinski, M. T. McDermott, *ACS Nano*, 2011, **5**, 4219.

(13) J. Fouineau, K. Brymora, L. Ourry, N. Yaacoub, F. Calvayrac, S. Ammar, J. M. Grenèche, 'Synthesis, Mössbauer characterization, and *ab initio* modelling of iron oxide nanoparticles of medical interest functionalized by dopamine', *J. Phys. Chem. C*, 2013 under revision.

(14) H. Basi, L. Ben Tahar, L. S. Smiri, F. Herbst, M. J. Vaulay, F. Chau, S. Ammar, S. Benderbous, *J. Colloid Interface Sci.,* 2010, **341**, 248 ; A. Hanini, A. Schmitt, K. Kacem, F. Chau, S. Ammar, J. Gavard, *J. Int. J. Nanomedecine*, 2011, **6**, 787.

(15) S. Mahouche, N. Mekni, L. Abbassi, P. Lang, C. Perruchot, M. Jouini, F. Mammeri, M. Turmine, H. Ben Romdhane, M. M. Chehimi, *Surf. Sci*., 2009, **603**, 3205.

(16) M.A. Ashwell, W.R. Solvibile Jr, S. Han, E. Largis, R. Mulvey, J. Tillet, *Bioorg. Med. Chem. Lett*., 2001, **11**, 3123.

(17) W. B. White, B.A. De Angelis, *Spectrochim. Acta A*, 1967, **23**, 985; L.M. Salah, *Phys. Status Solidi A*, 2006, **203**, 271.

(18) R. D. Waldron, *Phys. Rev*., 1955, **99**, 1727

(19) P. Giannozzi, S. Baroni, N. Bonini, M. Calandra, R. Car, C. Cavazzoni, D. Ceresoli, G. L. Chiarotti, M. Cococcioni, I. Dabo, A. Dal Corso, S. de Gironcoli, S. Fabris, G. Fratesi, R. Gebauer, U. Gerstmann, C. Gougoussis, A. Kokalj, M. Lazzeri, L. Martin-Samos, N. Marzari, F. Mauri, R. Mazzarello, S. Paolini, A. Pasquarello, L. Paulatto, C. Sbraccia, S. Scandolo, G. Sclauzero, A. P. Seitsonen, A. Smogunov, P. Umari, R. M. Wentzcovitch, *J. Phys.: Condens. Matter*., **21**, 395502 (2009)

(20) J. P. Perdew, A. Zunger, *Phys. Rev. B*, **23**, 5048– 5079 (1981)

(21) A. Scemama, M. Caffarel, R. Chaudret, J. P. Piquemal, *J. Chem. Theory Comput.,* **7**, 618 (2011)

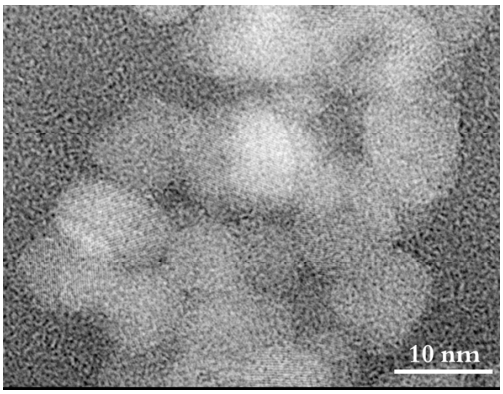

Figure 1. TEM image of the polyol-made γ-Fe_2O_3 NPs.

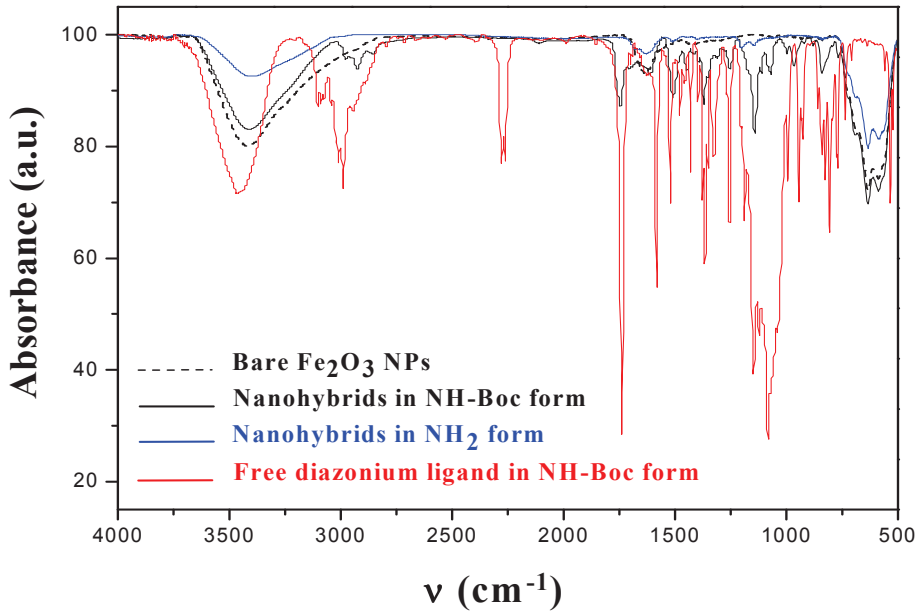

Figure 2. FTIR spectrum of NP-C_6H_4-C_2H_4-NH_2 compared to those of bare NPs and free diazonium salts, namely [BF_4^-,$^+N_2$-C_6H_4-C_2H_4-NH-Boc] and [BF_4^-,$^+N_2$-C_6H_4-C_2H_4-NH_2].

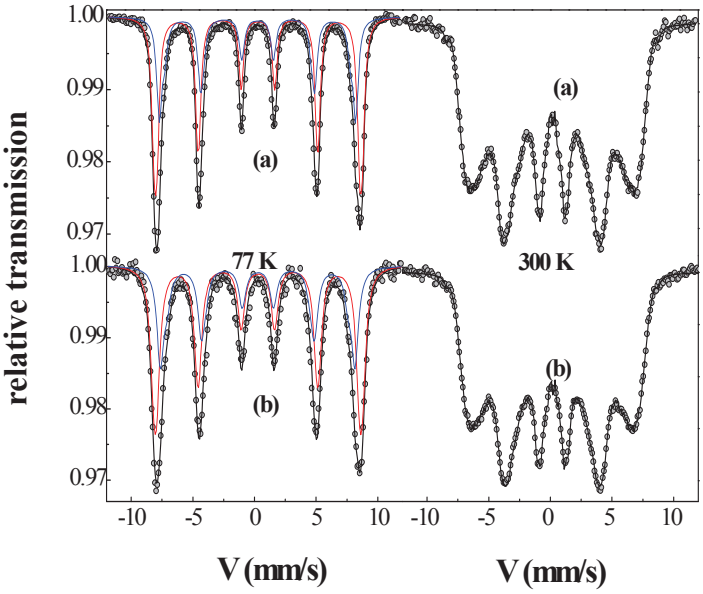

Figure 3. ^{57}Fe Mössbauer spectra recorded on bare (a) and hybrid (b) particles at 77 (left side) and at 300 K (right side)

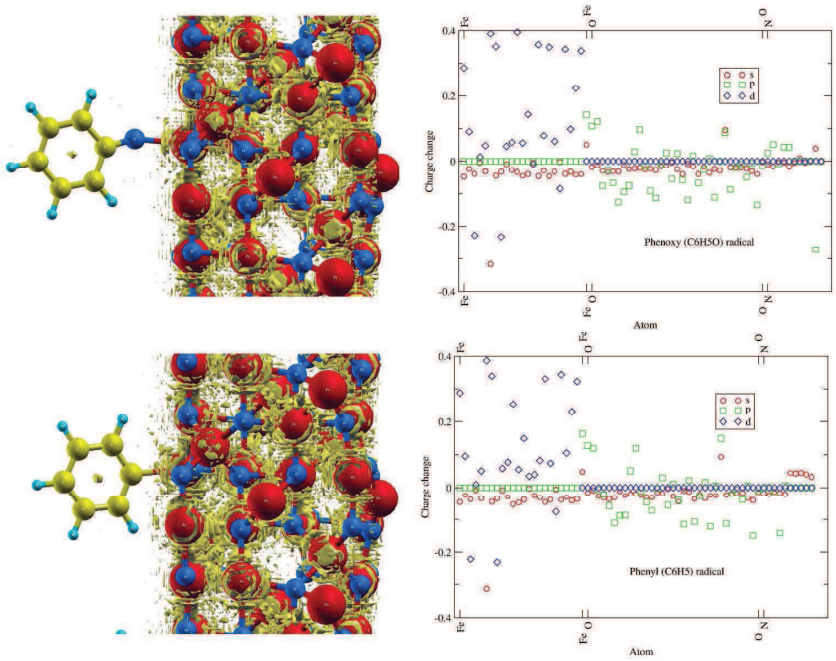

Figure 4 : Optimized structures of phenyl (a) and phenoxy (b) bonded to maghemite surface as well as reduced electronic density gradient isosurfaces at a value of 0.5. The right panel shows the change in Löwdin charges after bonding

	Site	δ (mm/s)	ε (mm/s)	B_{hyp} (T)	Ratio (%)
Bare	Fe^{3+}(A)	0.40	0.02	49.4	39
NPs	Fe^{3+}(B)	0.44	-0.01	51.7	61
	average	**0.43**		**50.3**	
Hybrid	Fe^{3+}(A)	0.42	-0.02	49.0	39
NPs	Fe^{3+}(B)	0.44	0.02	51.7	61
	average	**0.43**		**50.1**	

Table 1. Main refined values of 77 K Mössbauer parameters on both bare and related hybrids Fe_2O_3 NPs

Appendix C - Density Functional Theory

DFT as we know it today was born in 1964 when a landmark paper by Hohenberg and Kohn appeared in the Physical Review. DFT is based on the Hohenberg and Kohn theorem and on a computational scheme proposed by Kohn and Sham (1965).

1. The electronic structure of the ground state of a system is uniquely determined by the ground state electronic density, $\rho_0(\mathbf{r})$

2. A variational criterion for the determination of ρ_0 and E_0 starting from an arbitraty function ρ_r constrained by the normalization condition:

$$\int d\boldsymbol{r}\rho(\boldsymbol{r}) = N \tag{1}$$

$$E[\rho] \geqslant E[\rho_0], E[\rho_0] = E_0 \tag{2}$$

Where N is the total number of the electrons of the system. E_0 can be therefore be found by minimizing with the method of Lagrange multipliers the functional

$$E[\rho] = V_{en} + J + E_{kxc} + V_{nn} \tag{3}$$

A set of those two theorems is now called DFT. The name highlights the fact that for the calculating the properties of interacting electrons we do not need to know a priori the wave function [Magnasco 2006].

Density functional methods are generally considered as a valuable alternative to the traditional *ab initio* quantum chemical model. Indeed, they are in principle also based on a parameter free theory, i.e. they attempt to find solutions "from first principles" to the SCF mean-field model of electronic structure, while treating the electron correlation problem differently from the post-Hartree-Fock. Together with an approximate (local) expression of the exchange operator, this leads to a new set of one-electron equations, the solution of which involves a substantial reduction of computational effort as compared to Hartree-Fock method. Consequently, density functional methods can be advantageously

applied to large systems, such as clusters of transition metals or organometallic complexes [Weber *et al.* 1996].

Electrons are quantum mechanical spin particles. Density functional theory allows to compute all properties of systems by the electron density ρ_r which is a function of three variables: $\rho(r) = f(x, y, z)$. As density is the function of the wavefunction, it is referred to as functional. It is a formulation of N-particle quantum mechanics with conceptual simplicity and computational efficiency.
The major development in this field are as follows:

- The introduction of the Thomas-Fermi model (1920)
- Hohenberg-Kohn proving the existence of DFT (1964)
- The introduction of the Kohn-Sham (KS) scheme (1965)
- DFT in molecular dynamics (Car-Parrinello, 1985)
- Becke and LYP functionals (1988)
- Walter Kohn receives the Nobel prize for developing a complete DFT (1998) [Ramachandran *et al.*

In the DFT all properties of the ground state of an interacting electron gas may be described by introducing certain functionals of the electron density ρ_r. The standard Hamiltonian of the system is replaced by

$$E[\rho] = \int dr\rho(\boldsymbol{r})\, v_{ext}(r) + \iint dr dr' \frac{\rho(r)\,\rho(r')}{|r - r'|} + G(\rho) \tag{4}$$

where $v_{ext}(r)$ is the external field incorporating the field of the nuclei; the functional $G[\rho]$ includes the kinetic and exchange correlation energy of the interacting electrons. The total energy of the system is given by the extremum of the functional $\delta E[\rho]_{\rho=\rho_{0(r)}} = 0$, where ρ_0 is the distribution of the ground state electron charge. Thus, to determine the total energy E of the system it is not necessary to know the wave function of all the electrons, it suffices to determine a certain functional $E[\rho]$ and to obtain its minimum. $G[\rho]$ is universal and does not depend on any external fields.
This concept was further developed by Sham and Kohn who suggested a form for $G[\rho]$

$$G[\rho] = T[\rho] + E_{XC}[\rho] \tag{5}$$

Here $T[\rho]$ is the kinetic energy of the system of noninteracting electrons with density $\rho(r)$; functional $E_{XC}[\rho]$ contains the many - electron effects of the exchange and the correlation. The electron density may be written as

$$\rho(r) = \sum_{N}^{i=1} |\varphi_i(r)|^2 \tag{6}$$

where N is the number of electrons. In new variables φ_i

$$\left[-\nabla^2 \sum_I \frac{2Z_I}{|r-R_I|} + \int 2\frac{\rho(r')}{|r-r'|}dr' + V_{XC}(r)\right]\varphi_i = \varepsilon_i\varphi_i \tag{7}$$

Here, R_I is the position of the nucleus I of charge Z_I ; ε_i are the Lagrange factors forming the energy spectrum of single - particles states. The exchange - correlation potential V_{XC} is a functional derivative

$$V_{XC(r)} = \frac{\delta E_{XC}[\rho]}{\delta\rho(r)} \tag{8}$$

From (7) is possible to find the electron density $\rho(r)$ and the total energy of the ground state of the system.

Although the DFT is rigorously applicable only for the ground state, and the exchange - correlation energy functional at present is only known approximately, the importance of this theory to practical applications can hardly be overestimated. It reduces the many electron problem to an essentially single-particle problem with the effective local potential

$$V(r) = -\sum_I \frac{2Z_I}{|r-R_I|} + \int 2\frac{\rho(r')}{|r-r'|}dr' + V_{XC}(r) \tag{9}$$

Obviously, (7) should be solved self - consistently, since $V(r)$ depends on the orbitals $\varphi_i(r)$ that what are seeking.

Equations (4 - 7) are exact in so far as they define exactly the electron density and the total energy when an exact value of $E_{XC}[\rho]$ functional is given. Thus, the central issue in applying DFT is the way in which the functional $E_{XC}[\rho]$ is defined. It is convenient to introduce more general properties for the charge density correlation determining E_{XC}. The exact expression of $E_{XC}[\rho]$ for an inhomogeneous electron gas may be written as a Coulomb interaction between the electron with its surrounding exchange -correlation hole and the charge density $\rho_{XC} = (r, r'-r)$:

$$E_{XC}[\rho] = \frac{1}{2}\int dr\rho(r)\int dr'\frac{\rho_{XC}(r, r'-r)}{|r-r'|} \tag{10}$$

In (10) ρ_{XC} is defined as

$$\rho_{XC}(r, r'-r) = \rho(r')\int_0^2 d\lambda\left[g(r, r';\lambda) - 1\right] \tag{11}$$

where $g(r, r';\lambda)$ is the pair correlation function; is the coupling constant.

$E_{XC}[\rho]$ is independent of the actual shape of the exchange - correlation hole. Making the substitution $R = r - r'$ is can be shown that

$$E_{XC}[r] = 4\pi\int dr\rho(r)\int RdR\bar{\rho}_{XC}(r, R) \tag{12}$$

And depends only on the spherical average of $\bar{\rho}_{XC}$,

$$\bar{\rho}_{XC}(r,R) = \frac{1}{4\pi}\int d\Omega \rho_{XC}(r,R) \tag{13}$$

This means that the Coulomb energy depends only on the distance, not on the direction. Moreover, the hole charge density satisfies the sum rule

$$4\pi \int R^2 dR \bar{\rho}_{XC}(r,R) = -2 \tag{14}$$

This implies that the exchange - correlation hole corresponds to a net charge around the electron of one [Antonov *et al.* 2004].

DFT would yield the exact ground state energy and electron density if the exchange correlation functional was known. In practice, the exact functional is unknown but one may try some approximate form. This has led to an extensive search for functional with new variations being published on a regular basis. Because the quality of the results depends critically on the functional, selecting a suitable form will be a vital factor in using the method. DFT methods are broadly classified into two methods: pure DFT and hybrid DFT. They are designated on the basis of type of correlation energy functional, the exchange energy functional, and the potential.

Applications of modern DFT calculations have been extended from small molecules for testing the accuracy to transition metal complexes. For complex molecules, DFT appears to be the method of choice at present. In the last few years, people have begun to apply DFT methods to a variety of systems such as biomolecules, polymers, macromolecules, and so on. Recently, researchers started examining spin densities in bio-inorganic complexes. These are very challenging calculations, involving up to hundreds of electrons. In about 1985, Car and Parrinello introduced a new method whereby one can solve for the electron density for a configuration of nuclei, and then move the nuclei based on the resulting forces, resolve the electronic structure problem, and so on. This means one can do real-time simulations without using any made up force fields. This technique has been applied to many problems in chemistry and materials science [Ramachandran *et al.* 2008].

Appendix D - Monte-Carlo / Metropolis fitting program

```
cp begins.scf.in begin.scf.in

for i in  1 2 3 4 5
  do
for j in   1 2 3 4 5
  do
for k in  37 38 39 40 41
  do
echo "fixed_magnetization(1)=" $i "," > middle.scf.in
echo "fixed_magnetization(2)=" $j "," >> middle.scf.in
echo "fixed_magnetization(3)=" $k "," >> middle.scf.in
       echo -n >> middle.scf.in
        cat begin.scf.in middle.scf.in end.scf.in > job.scf.in
/opt/openmpi_intel/bin/mpiexec -np 2 /opt/espresso-5.0.1-GPU/bin/pw.x  < job.scf.in > result$i$j$
k
cp beginr.scf.in begin.scf.in
#cp -R * $PBS_O_WORKDIR
done
done
done




rm totmag2 ; rm pas; rm pas2; rm magnet2; rm absol2; rm field2; rm totenergy2; rm polar; rm energ
y; rm magnetization; rm absolute; rm magnetic; rm field


for f in result*
 do
         rm energy
 cat $f | grep polar  > polar
 cat $f | grep "!    total energy"  >  energy
 if test -s energy  ; then
 cat $f | grep "total magnetization"  > magnetization
 cat $f | grep "absolute "  > absolute
 cat $f | grep "External magnetic"  > magnetic
 g="$(basename $f .scf.out | cut -b 7-11)"
 tail -21 polar   | cut -b 41-78 | head -13 > field
tail -1 energy | cut -b 35-48 > en2
tail -1 magnetization | cut -b 33-60 > totmag
tail -1 absolute | cut -b 33-42 > absol
tail -1 magnetic | cut -b 31-70 > magnet



 nl -s "  ""$g""   "  totmag  >>  totmag2
 nl -s "  ""$g""   "  magnet  >>  magnet2
 nl -s "  ""$g""   "  absol  >>  absol2
 nl -s "  ""$g""   "  field  >>  field2
 nl -s "  ""$g""   "  en2  >>  totenergy2
 nl -s "  ""$g""   "  totmag  >  totmag3
 nl -s "  ""$g""   "  magnet  >  magnet3
 nl -s "  ""$g""   "  absol  >  absol3
 nl -s "  ""$g""   "  en2  >  totenergy3

paste totmag3 magnet3 absol3 totenergy3 >> pas
paste magnet3 totenergy3 >> pas2
fi
done
mv field2 fort.12
mv pas2 fort.11
```

```
program heisfit
  integer,parameter :: n=13,nb=103
  ! n = number of Fe atoms
  ! nb : number of different values of hz

  integer::neigh(n,n),nneigh(n)
  real,dimension(n) :: x,y,z
  real::jc(n,n),ks(n),kv,g

  real :: en(nb),bz(3,nb),sx(n,nb),sy(n,nb),sz(n,nb)



  call init(n,neigh,nneigh,x,y,z)
  call initb(n,nb,en,bz,sx,sy,sz)

  jc=0
  do i=1,n
     nneigh(i)=13
     do j=1,nneigh(i)
        neigh(i,j)=j
        !     nneigh(i)=j
        jc(i,neigh(i,j))=0.0001/13.6*(ran1(idum)-0.5)
        jc(i,j)=0.0001/13.6*(ran1(idum)-0.5)
        jc(j,i)=jc(i,j)
     enddo
     jc(i,i)=0.0
     ks(i)=2/13.6*(ran1(idum)-0.5)
  enddo
  kv=2e-6/13.6
  e0=en(1)
  g=0.0



  call fit(n,nb,en,bz,sx,sy,sz,jc,neigh,nneigh,ks,kv,x,y,z,e0,g)


  j=0
  do i=1,n
     write(6,*) (jc(i,j)*13.6*1000,j=1,n)
     write(6,*) ks(i)*13.6
  enddo

  write(6,*) kv*13.6,e0,g
  do ib=1,nb
     write(6,10) en(ib),energy(n,nb,ib,bz,sx,sy,sz,jc,neigh,nneigh,ks,kv,x,y,z,e0,g)
     write(76,10) en(ib),energy(n,nb,ib,bz,sx,sy,sz,jc,neigh,nneigh,ks,kv,x,y,z,e0,g)
  enddo
10 format(f15.8,f15.8)

end program heisfit


!************************************8

subroutine init(n,neigh,nneigh,x,y,z)

  !*********************************


  integer,intent(in)::n
  integer,intent(out)::neigh(n,n),nneigh(n)
  real,dimension(n),intent(out) :: x,y,z
  real,parameter :: cutoff=3.23
  integer,parameter::no=8
  real,dimension(no) :: xo,yo,zo
  real ::  aneigho(n,n)

  character *2 name
  i=1
```

```
10 continue
  read(10,*,end=999) name,x(i),y(i),z(i)
  i=i+1
  if(i.gt.n) goto 999
  goto 10
999 continue


  i=1
20 continue
  read(20,*,end=1999) name,xo(i),yo(i),zo(i)
  i=i+1
  if(i.gt.no) goto 1999
  goto 20
1999 continue



  aneigho=0.0


  do i=1,n
     nneigh(i)=0
     do j=1,no
        dist=(x(i)-xo(j))*(x(i)-xo(j))
        dist=dist+(y(i)-yo(j))*(y(i)-yo(j))
        dist=dist+(z(i)-zo(j))*(z(i)-zo(j))
        if(dist.lt.cutoff*cutoff) then
           if(i.ne.j) then

              cstheta=2.0
              do k=1,n
                 dist=(x(k)-xo(j))*(x(k)-xo(j))
                 dist=dist+(y(k)-yo(j))*(y(k)-yo(j))
                 dist=dist+(z(k)-zo(j))*(z(k)-zo(j))
                 if(dist.lt.cutoff*cutoff) then

                    if(i.ne.k) then
                       if(j.ne.k) then
                          nneigh(i)=nneigh(i)+1
                          neigh(i,nneigh(i))=k

                          v1x=x(i)-xo(j)
                          v1y=y(i)-yo(j)
                          v1z=z(i)-zo(j)
                          v2x=x(k)-xo(j)
                          v2y=y(k)-yo(j)
                          v2z=z(k)-zo(j)
                          sca=v1x*v2x
                          sca=sca+v1y*v2y
                          sca=sca+v1z*v2z
                          an1=v1x*v1x
                          an1=an1+v1y*v1y
                          an1=an1+v1z*v1z
                          an1=sqrt(an1)
                          an2=v2x*v2x
                          an2=an2+v2y*v2y
                          an2=an2+v2z*v2z
                          an2=sqrt(an2)
                          cstheta=sca/an1/an2
                          aneigho(i,k)=cstheta
                       endif
                    endif

                 endif

              enddo
           endif
        endif
     end do
  enddo
```

```
  do i=1,n
     write(69,'(13(g18.7))') (aneigho(i,j),j=1,n)
  enddo


end subroutine init


!**********************************

subroutine initb(n,nb,en,bz,sx,sy,sz)

  !**********************************
  integer,intent(in) :: n,nb

  real,intent(out) :: en(nb),bz(3,nb),sx(n,nb),sy(n,nb),sz(n,nb)

  i=1
10 continue
  read(11,*,end=999) jid,id,bz(1,nb),bz(2,nb),bz(3,nb),jid,id,en(i)
  i=i+1
  if(i.gt.nb) goto 999
  goto 10
999 continue

  i=1
20 continue
  do j=1,n
     read(12,*,end=1999) id,jid,r,th,phi
     if(id.ne.j) stop 'error id diff j'

     sx(j,i)=r*sin(th)*cos(phi)
     sy(j,i)=r*sin(th)*sin(phi)
     sz(j,i)=r*cos(th)
  enddo
  i=i+1
  if(i.gt.nb) goto 1999
  goto 20
1999 continue

end subroutine initb


!************************************************

function energy(n,nb,ib,bz,sx,sy,sz,jc,neigh,nneigh,ks,kv,x,y,z,e0,g)

  !************************************************

  integer,intent(in) :: n,ib,nb
  real,intent(in) :: bz(3,nb),sx(n,nb),sy(n,nb),sz(n,nb)
  integer,intent(in)::neigh(n,n),nneigh(n)
  real,intent(in) :: ks(n),kv,e0,g
  real,intent(in)::jc(n,n)
  real,dimension(n),intent(in) :: x,y,z
  ene=e0
  do i=1,n
     do j=1,nneigh(i)
        k=neigh(i,j)
        sca=0.0
        sca=sca+sx(i,ib)*sx(k,ib)
        sca=sca+sy(i,ib)*sy(k,ib)
        sca=sca+sz(i,ib)*sz(k,ib)
        ene=ene-2*jc(i,k)*sca
     enddo
  enddo

  sca=0.0
  do i=1,n
     sca=sca+sx(i,ib)*sx(i,ib)*sy(i,ib)*sy(i,ib)
```

```
      sca=sca+sy(i,ib)*sy(i,ib)*sz(i,ib)*sz(i,ib)
      sca=sca+sx(i,ib)*sx(i,ib)*sz(i,ib)*sz(i,ib)
   enddo
   ene=ene-kv*sca



   cx=0.0
   cy=0.0
   cz=0.0
   do i=1,n
      cx=cx+x(i)
      cy=cy+y(i)
      cz=cz+z(i)
   enddo
   cx=cx/n
   cy=cy/n
   cz=cz/n

   sca=0.0

   do k=1,n
      if(nneigh(k).lt.6) then ! warning
         do i=1,nneigh(k)
            j=neigh(k,i)
            if(nneigh(j).lt.6) then ! warning
               anx=x(k)-x(j)
               anny=y(i)-y(j)
               anz=z(i)-z(j)
            endif
         enddo
         an=sqrt(anx*anx+anny*anny+anz*anz)
         anx=anx/an
         anny=anny/an
         anz=anz/an
         sc=0.0
         sc=sc+sx(k,ib)*anx
         sc=sc+sy(k,ib)*anny
         sc=sc+sz(k,ib)*anz
         ene=ene-ks(k)*sc
      end if
   enddo


   do i=1,n
      ene=ene+g*bz(1,ib)*sx(i,ib)+g*bz(2,ib)*sy(i,ib)+g*bz(3,ib)*sz(i,ib)
   enddo

   energy=ene
   return
end function energy

!************************************************

function penalty(n,nb,en,bz,sx,sy,sz,jc,neigh,nneigh,ks,kv,x,y,z,e0,g)

   !************************************************

   integer,intent(in) :: n,nb
   real,intent(in) :: en(nb),bz(3,nb),sx(n,nb),sy(n,nb),sz(n,nb)
   integer,intent(in)::neigh(n,n),nneigh(n)
   real,intent(in) :: ks(n),kv,e0,g
   real,intent(in)::jc(n,n)
   real,dimension(n),intent(in) :: x,y,z
   pen=0.0
   pena=0.0
   penm=-1
   do ib=1,nb
      pen=pen+abs(en(ib)-energy(n,nb,ib,bz,sx,sy,sz,jc,neigh,nneigh,ks,kv,x,y,z,e0,g))
   enddo
   pen=pen/nb
```

```
  penalty=pen
end function penalty

!*************************************************

subroutine fit(n,nb,en,bz,sx,sy,sz,jc,neigh,nneigh,ks,kv,x,y,z,e0,g)

  !*************************************************

  integer,intent(in) :: n,nb
  real,intent(in) :: en(nb),bz(3,nb),sx(n,nb),sy(n,nb),sz(n,nb)
  integer,intent(in)::neigh(n,n),nneigh(n)
  real,intent(inout) :: ks(n),kv,e0,g
  real :: ksold(n),kvold,e0old,gold
  real,intent(inout)::jc(n,n)
  real :: jcold(n,n)
  real,dimension(n),intent(in) :: x,y,z

  integer,parameter::maxmloop=50,maxmc=150000,ipasinf=5000
  real::temp0=0.001,tper0=3.59
  real::bestp,jcbest(n,n),ksbest(n),kvbest,e0best,gbest

  nmc=0
  nyes=0
  nyesmc=0
  nref=0
  nbut=0



  bestp=1e12

  do mloop=1,maxmloop
     p=0.0
     pold=1e12
     temp1=temp0*(((mloop+1)*100.0)**(-0.4))  ! annealing law as a function of
     do k=1,maxmc ! succession of
        ! annealing steps
        !
1       continue
        i=(n+5)*ran1(idum)! random point to be changed
        if(i.eq.0) goto 1
        jcold=jc
        ksold=ks
        kvold=kv
        e0old=e0
        gold=g
        pold=penalty(n,nb,en,bz,sx,sy,sz,jc,neigh,nneigh,ks,kv,x,y,z,e0,g)
        if(pold.lt.bestp) then
           bestp=pold
           if(bestp.eq.0.0) goto 999
           jcbest=jc
           ksbest=ks
           kvbest=kv
           e0best=e0
           gbest=g
        endif


        nmc=nmc+1

        temp=temp1*(((k+1)*1.0)**(-0.3))  ! annealing law as a function of
        ! iteration number k
        facrer=(16./(1.-sqrt(temp)))**(1./6.)
        facrer=facrer-(16./(1.+sqrt(temp)))**(1./6.)

        tper=tper0*facrer

        if(i.le.n) then
2          continue
```

```
            !do j=1,n
            j=(n+1)*ran1(idum)
            if((j.eq.0).or.(j.gt.n)) goto 2
            if(jc(i,j).ne.0) then
               jc(i,j)=jc(i,j)+tper*0.01*(ran1(idum)-0.5)
               jc(j,i)=jc(i,j)
            endif
            !enddo
         endif

         if(i.eq.(n+1)) then
            !do j=1,n
3           continue
            j=(n+1)*ran1(idum)
            if((j.eq.0).or.(j.gt.n)) goto 3
            ks(j)=ks(j)+tper*0.1*(ran1(idum)-0.5)
            !enddo
         endif
         if(i.eq.(n+2)) then
            kv=kv+tper*0.0001*(ran1(idum)-0.5)
         endif
         if(i.eq.(n+3)) then
            e0=e0+tper*1.0*(ran1(idum)-0.5)
         endif
         if(i.eq.(n+4)) then
            g=g+tper*0.1*(ran1(idum)-0.5)
         endif

         p=penalty(n,nb,en,bz,sx,sy,sz,jc,neigh,nneigh,ks(i),kv,x,y,z,e0,g)
         w=min(1.,exp(-(p-pold)/(1.0*temp)))    ! temp is the fictious temperature

         nyesc=nyesc+1!moves satisfying constraints
         if (ran1(idum).gt.w) then ! Metropolis step refused
            nref=nref+1
            jc=jcold
            ks=ksold
            kv=kvold
            e0=e0old
            g=gold
         else
            if(p.gt.pold) then
               nbut=nbut+1
            else
               nyesmc=nyesmc+1
            endif
         ENDIF

         if(mod(nmc,ipasinf).eq.0) then
            write(6,*) '---------------------------------------'
            write(6,*) 'Annealing loop                        ',mloop
            write(6,*) 'iteration in loop                     ',k
            write(6,*) 'actual penalty               ',pold,bestp
            write(6,*) 'fictious temperature                  ',temp,tper
            write(6,*) 'number of mc steps                    ',nmc
            write(6,*) 'number of accepted steps              ',nyesmc
            write(6,*) 'number of accepted defavourable steps ',nbut
            write(6,*) 'number of refused steps               ',nref
            if(nref.ne.0) write(6,*) 'ratio of refused to accepted',nbut/(nref*1.0)
            write(6,*) kvbest,e0best,gbest
            do i=1,n
               ! write(6,*) (jcbest(i,j)*13.6*1000,j=1,n)
               write(6,'(13(g18.7))') (jcbest(i,j)*13.6*1000,j=1,n)
            enddo
            do i=1,n
               write(6,'(1(g18.7))') ksbest(i)
            enddo
         endif
      enddo
   enddo
999 continue
   jc=jcbest
   ks=ksbest
```

```
  kv=kvbest
  e0=e0best
  g=gbest
  write(6,*) 'best result',bestp
  write(6,*) kvbest,e0best,gbest
  do i=1,n
     write(6,*) (jcbest(i,j)*13.6*1000,j=1,n)
     write(6,'(1(g18.7))') ksbest(i)
  enddo
  write(66,*) 'best result',bestp
  write(66,*) kvbest,e0best,gbest
  do i=1,n
     write(66,*) (jcbest(i,j)*13.6*1000,j=1,n)
     write(67,'(13(g18.7))') (jcbest(i,j)*13.6*1000,j=1,n)
     write(68,'(1(g18.7))') (jcbest(i,j)*13.6*1000,j=1,n)
     write(69,'(1(g18.7))') ksbest(i)
     write(66,'(1(g18.7))') ksbest(i)
  enddo
end subroutine fit



function ran1(idum)
  idum=123456789*idum+987654321
  idum=mod(idum,2**30)
  ran1=idum/(2**30*1.0)
  if(ran1.lt.0.0) ran1=ran1+1.0
  return
end function ran1
```

Appendix E - Details of the atomic structures and pseudopotentials used in this work

Table 1: Comparision of the cell dimensions of structures used in this study with other works.

Structure	This work	Other theoretical work	Experiment
Maghemite	a = 8.33 $\mathring{A}$ (bulk) a = 8.329 $\mathring{A}$ c = 24.987 $\mathring{A}$ (supercell)	a = 8.359 $\mathring{A}$ c =24.854 $\mathring{A}$ [Grau-Crespo *et al.* 2010a]	a = 8.347 $\mathring{A}$ c = 25.042 $\mathring{A}$ [Shmakov *et al.* 1995]
Magnetite	a = 8.372 $\mathring{A}$ (bulk) a = 8.421 $\mathring{A}$ c = 27.8 $\mathring{A}$ (supercell)	a = 8.4 $\mathring{A}$ [Frik *et al.* 2007]	a = 8.396 $\mathring{A}$ [Cornell *et al.* 1996]

Table 2: Comparision of the bond in different sites (octahedral and tetrahedral) of structures used in this study with other works.

Bond	This work	Other theoretical work	Experiment
Magnetite:			
Fe_{tetra} - O	1.87 $\mathring{A}$	1.889 $\mathring{A}$	1.889 $\mathring{A}$
Fe_{octa} - O	2.08 $\mathring{A}$	2.07 $\mathring{A}$ [Yang *et al.* 2009]	2.047 $\mathring{A}$ [Wright *et al.* 2002]
Maghemite:			
Fe_{tetra} - O	1.8 $\mathring{A}$	1.85 $\mathring{A}$	1.84 $\mathring{A}$
Fe_{octa} - O	2.02 $\mathring{A}$	2.06 $\mathring{A}$ [Bennyt 2010]	2.09 $\mathring{A}$ [Jrgensen *et al.* 2007]

Table 3: Comparision of the structural properties of $Fe_{13}O_8$ (Fig. 1) used in this study with other theoretical work.

Properties	**This work**	**Other theoretical work** [Sun *et al.* 2000]
Angle:		
O - Fe2 - O	170.5539^o	170.4^o
O - Fe3 - O	170.5527^o	159.1^o
Bond distance:		
O - Fe1	$3.1493\mathring{A}$	$3.141\mathring{A}$
O - Fe2	$1.8243\mathring{A}$	$1.848\mathring{A}$
O - Fe3	$1.8245\mathring{A}$	$1.807\mathring{A}$

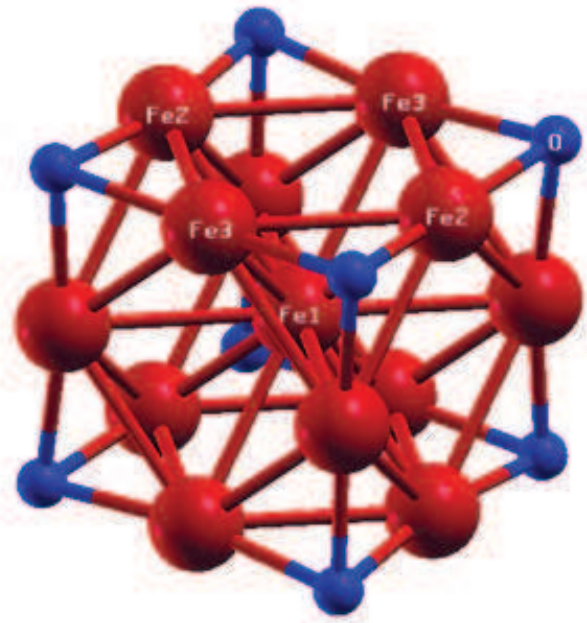

Figure 1: Optimized structure of $Fe_{13}O_8$.

Table 4: Summary of the details concerning pseudopotentials used in this work for iron atoms.

Calculations	**Pseudopotential**	**Exchange - correlation potential**	**Electronic states**
GGA	Fe.pbe-nd-rrkjus.UPF scalar relativistic	Perdew - Burke - Ernzerhof (PBE)	4s1 4s 4p 4p 3d7 3d
LDA+U	Fe.pz-sp-van-ak.UPF scalar relativistic	Perdew - Zunger (PZ)	3s2 3p6 3d6.5 4s1 4p
magnetic modeling in Chapter 4	generated using code by A. Del Corso	PBE	valence configuration: 3s2 4s2 3p2 3p4 4p 4p 3d4 3d2 generation configuration: 3s2 4s2 3p2 3p4 4p 4p 3d4 3d2 3d 3d

Table 5: Summary of the details concerning pseudopotentials used in this work for oxygen atoms.

Calculations	**Pseudopotential**	**Exchange - correlation potential**	**Electronic states**
GGA	O.pbe-van-ak.UPF scalar relativistic	Perdew - Burke - Ernzerhof (PBE)	2s2 2p4
LDA+U	O.pz-van-ak.UPF scalar relativistic	Perdew - Zunger (PZ)	2s2 2p4
magnetic modeling in Chapter 4	generated using code by A. Del Corso	PBE	valence configuration: 2s2 2p2 2p2 generation configuration: 2s2 2s 2p2 2p 2p2 2p 3d-2 3d-2

Table 6: Summary of the details concerning pseudopotentials used in this work for carbon atoms.

Calculations	**Pseudopotential**	**Exchange - correlation potential**	**Electronic states**
GGA	C.pbe-van-bm.UPF scalar relativistic	Perdew - Burke - Ernzerhof (PBE)	2s2 2p2
LDA+U	C.pz-van-ak.UPF scalar relativistic	Perdew - Zunger (PZ)	2s2 2p2
magnetic modeling in Chapter 4	generated using code by A. Del Corso	PBE	valence configuration: 2s2 2p2 2p generation configuration: 2s2 2s 2p2 2p 2p 2p 3d-2 3d-2

Table 7: Summary of the details concerning pseudopotentials used in this work for hydrogen atoms.

Calculations	**Pseudopotential**	**Exchange - correlation potential**	**Electronic states**
GGA	H.pbe-van-bm.UPF scalar relativistic	Perdew - Burke - Ernzerhof (PBE)	1s1
LDA+U	H.pz-van-ak.UPF scalar relativistic	Perdew - Zunger (PZ)	1s1
magnetic modeling in Chapter 4	generated using code by A. Del Corso	PBE	valence configuration: 1s1 generation configuration: 1s1 1s 2p 2p

Table 8: Summary of the details concerning pseudopotentials used in this work for nitrogen atoms.

Calculations	**Pseudopotential**	**Exchange - correlation potential**	**Electronic states**
GGA	N.pbe-van-bm.UPF scalar relativistic	Perdew - Burke - Ernzerhof (PBE)	2s2 2p3
LDA+U	N.pz-van-ak.UPF scalar relativistic	Perdew - Zunger (PZ)	2s2 2p3
magnetic modeling in Chapter 4	generated using code by A. Del Corso	PBE	valence configuration: 2s2 2p2 2p1 generation configuration: 2s2 2s 2p2 2p 2p1 2p 3d-2 3d-2

Table 9: Summary of the details concerning pseudopotentials used in this work for phosphorus atoms.

Calculations	**Pseudopotential**	**Exchange - correlation potential**	**Electronic states**
GGA	P.pbe-n-van.UPF scalar relativistic	Perdew - Burke - Ernzerhof (PBE)	3s2 3p3
LDA+U	P.pz-van-ak.UPF scalar relativistic	Perdew - Zunger (PZ)	3s2 3p3

Table 10: Summary of the details concerning pseudopotentials used in this work for silicon atoms.

Calculations	**Pseudopotential**	**Exchange - correlation potential**	**Electronic states**
GGA	Si.pbe-n.van.UPF scalar relativistic	Perdew - Burke - Ernzerhof (PBE)	3s2 3p2
LDA+U	Si.pz-vbc.UPF scalar relativistic	Perdew - Zunger (PZ)	3s2 3p2

Table 11: Summary of the details concerning pseudopotentials used in this work for gold atoms.

Calculations	**Pseudopotential**	**Exchange - correlation potential**	**Electronic states**
LDA	Au.pz-va-ak.UPF scalar relativistic	Perdew - Zunger (PZ)	6s1 6p0.5 5d9.5

Appendix F - Non-collinear Magnetism

Many of compounds exhibit magnetic behavior. This can be such phenomena as:

1. ferromagnetism - where spins are aligned in parallel directions
2. anti-ferromagnetism - where the spins are anti-parallel
3. non-collinear magnetism - where the spins are not parallel and may be disordered

Non-collinear magnetism can arise naturally due to geometric frustration of anti-ferromagnetic interactions. Other effects giving rise to non-collinear magnetism include magnetic anisotropy, which arises due to a preferred direction of magnetization [Hobbs & Hafner 2006]. There are several different types of anisotropy:

1. Magneto-crystalline - results from interactions of the spin magnetic moments with the crystal lattice. This relativistic effect enters via spin-orbit coupling and is strongly dependent on the crystal symmetry.
2. Surface due to broken symmetry at the surface.
3. Stress which is induced on the crystal structure due to magnetization, and vice versa.
4. Shape due to the shape of individual mineral grains.

Magnetic anisotropy strongly affects the shape of the materials hysteresis loop and is also of practical importance because it is exploited in the design of most magnetic materials of commercial importance. Finally, competition between exchange interactions and magnetic anisotropy also contribute to non-collinear magnetism.

A generalization of von Barth and Hedins LSDF theory to non-collinear magnetism [Barth & Hedin 1972] was first proposed by [Kubler *et al.* 1988] within the framework of the ASW method and the atomic-sphere approximation. The predicted well-defined sets

of directions for the spins, which are uncoupled from the crystal lattice unless spin-orbit coupling effects are small in comparison to the spin-spin interactions. The spin-polarized density functional theory is expressed in terms of a 2x2 density matrix with elements $n^{\alpha\beta}(\vec{r})$. The electron density is then:

$$Tr\left[n^{\alpha\beta}(\vec{r})\right] \equiv n_{Tr}(\vec{r}) = \sum_{\alpha} n^{\alpha\alpha}(\vec{r}) \tag{15}$$

The total-density matrix may then be defined as:

$$n^{\alpha\beta}(\vec{r}) = (n_{Tr}(\vec{r})\delta_{\alpha\beta} + \vec{m}(\vec{r}) \cdot \vec{\sigma}^{\alpha\beta})/2 \tag{16}$$

In addition, for the density matrix, we can make a transformation to the equivalent magnetization density using the following formula:

$$\vec{m}(\vec{r}) = \frac{e\hbar}{mc} \sum_{\alpha\beta} n^{\alpha\beta}(\vec{r}) \cdot \vec{\sigma}^{\alpha\beta} \tag{17}$$

Where

$$\vec{\sigma} = (\sigma_x, \sigma_y, \sigma_z)$$

are the Pauli spin matrices. As the electron density becomes a 2x2 density matrix in the noncollinear spin-polarized theory this leads to a significant increase in the computational effort [Hobbs & Hafner 2006].

In non-collinear system density matrix has a form:

$$\underline{\rho} = \frac{1}{2} n \mathbf{I_2} + \sigma \cdot \mathbf{m} = \frac{1}{2} \begin{pmatrix} n + m_z & m_x - i m_y \\ m_x + i m_y & n - m_z \end{pmatrix} \tag{18}$$

where, σ is the is the Pauli spin space matrix. The potential matrix can be defined in the same way by the following equation:

$$\underline{V} = V \mathbf{I_2} + \mu_B \sigma \cdot B = \begin{pmatrix} V + \mu_B B_z & \mu_B (B_x - i B_y) \\ \mu_B (B_z + i B_y) & V - \mu_B B_z \end{pmatrix} \tag{19}$$

The components of the density matrix are given in terms of the solutions of the Kohn-Sham equation:

$$\rho_{\alpha\beta} = \sum_{i=1}^{N} \psi^*_{i,\alpha} \psi_{i,\beta} \tag{20}$$

where, $\psi_{i,\alpha\equiv} \begin{pmatrix} \phi_i^{\uparrow}\mathbf{r} \\ \phi_i^{\downarrow}\mathbf{r} \end{pmatrix}$

are Pauli wave functions that reproduce the electron and the magnetization density.

Using the potential matrix , he Kohn-Sham equation becomes

$$\{-\frac{\hbar^2}{2m} \bigtriangledown^2 \mathbf{I_2} + \underline{\mathbf{V}}\}\psi_i = \epsilon_i \psi_i \tag{21}$$

The kinetic energy part of the Hamiltonian is diagonal in the two spin directions. If the magnetic field is collinear, (B_x and iB_y are zero and thus $\underline{V}$ is diagonal. The notation $V_\uparrow = V + \mu_B B_z, V_\downarrow = V$ is commonly used for the diagonal elements of $\underline{V}$ in the collinear case. Since the two spin directions become completely independent, the spin-up and down problem can be solved separately in two steps. Each step can be treated like the non-magnetic problem with the appropriate potential $V_\uparrow$ and $V_\downarrow$ [Al-Zubi 2010].

Bibliography

[Anisimov *et al.* 1997] V. Anisimov, F. Aryasetiawan and A. Lichtenstein. *First-principles calculations of the electronic structure and spectra of strongly correlated systems: the LDA+U method*. J. Phys.: Condens. Matter, vol. 26, no. 4, 1997.

[Antonov *et al.* 2004] V. Antonov, B. Harmon and A. Yaresko. Electronic structure and magneto-optical properties of solids. Springer, February 29, 2004.

[Bachelet & Christensen 1985] Giovanni B. Bachelet and Niels E. Christensen. *Relativistic and core-relaxation effects on the energy bands of gallium arsenide and germanium*. Phys. Rev. B, vol. 31, pages 879–887, Jan 1985.

[Bachelet *et al.* 1982] G. B. Bachelet, D. R. Hamann and M. Schluter. *Pseudopotentials that work: From H to Pu*. Physical Review B, vol. 26, 1982.

[Bahn & Jacobsen 2002] S. R. Bahn and K. W. Jacobsen. *An object-oriented scripting interface to a legacy electronic structure code*. Comput. Sci. Eng., vol. 4, no. 3, pages 56–66, MAY-JUN 2002.

[Bambini *et al.* 2006] F. Bambini, L. Greci, L. Meme, A. Santarelli, F. Carinci, F. Pezzetti, M. Procaccini and L. L. Muzio. *Raloxifene covalently bonded to titanium implants by interfacing with (3-aminopropyl)-triethoxysilane affects osteoblast-like cell gene expression.* Int J Immunopathol Pharmacol., vol. 19, no. 4, pages 905–14, 2006.

[Barth & Hedin 1972] U. von Barth and L. Hedin. *A local exchange-correlation potential for the spin polarized case : I.* Solid State Phys, vol. 5, page 1629, 1972.

[Bennyt 2010] Sreelekha Bennyt. *High Temperature Water Gas Shift Catalysts: A Computer Modelling Study* . PhD thesis, Department of Chemistry University College London, 2010.

[Berkowitz *et al.* 1975] A. E. Berkowitz, J. A. Lahut, I. S. Jacobs, Lionel M. Levinson and D. W. Forester. *Spin Pinning at Ferrite-Organic Interfaces*. Phys. Rev. Lett., vol. 34, no. 10, page 594597, March 1975.

[Berry & Curtis 2003] Catherine C Berry and Adam S G Curtis. *Functionalisation of magnetic nanoparticles for applications in biomedicine.* Journal of Physics D: Applied Physics, vol. 36, no. 13, page R198, 2003.

[Brazdova & Bowler 2013] V. Brazdova and D. R. Bowler. Atomistic computer simulations. Wiley-Vch, 2013.

[Calvayrac *et al.* 2000] F Calvayrac, P-G Reinhard, E Suraud and CA Ullrich. *Nonlinear electron dynamics in metal clusters.* Physics Reports, vol. 337, no. 6, page 493578, 2000.

[Chan & Ceder 2010] M. K. Y. Chan and G. Ceder. *Efficient Band Gap Prediction for Solids.* Phys. Rev. Lett., vol. 105, 2010.

[Cheang *et al.* 2012] T.Y. Cheang, B. Tang, AW Xu, GQ Chang, ZJ Hu, WL He, ZH Xing, JB Xu, M. Wang and SM Wang. *Promising plasmid DNA vector based on APTES-modified silica nanoparticles.* Int J Nanomedicine, pages 1061–7, 2012.

[Chen *et al.* 2008] X. Chen, H. Y. Zhu, J. C. Zhao, Z. F. Zheng and X. P. Gao. *Visible - Light - Driven Oxidation of Organic Contaminants in Air with Gold Nanoparticle Catalysts on Oxide Supports.* Angewandte Chemie, vol. 120, no. 29, 2008.

[Chen *et al.* 2009] T. J. Chen, T. H. Cheng, C. Y. Chen, S. C. N. Hsu, T. L. Cheng, G. C. Liu and Y. M. Wang. *Targeted Herceptindextran iron oxide nanoparticles for noninvasive imaging of HER2/neu receptors using MRI.* Journal of Biological Inorganic Chemistry, vol. 14, pages 253–260, 2009.

[Cococcioni & de Gironcoli 2005] Matteo Cococcioni and Stefano de Gironcoli. *Linear response approach to the calculation of the effective interaction parameters in the* LDA + U *method.* Phys. Rev. B, vol. 71, page 035105, Jan 2005.

[Cornell *et al.* 1996] R. M. Cornell, U. Schwertmann and U. Schertmann. The iron oxides: Structure, properties, reakctions, occurence and uses. John Wiley and Son Ltd, 1996.

[Dobson 2006] J. Dobson. *Magnetic Nanoparticles for Drug Delivery.* Drug Development Research, vol. 67, pages 55 – 60, 2006.

[Figuerola *et al.* 2010] Albert Figuerola, Riccardo Di Corato, Liberato Manna and Teresa Pellegrino. *From iron oxide nanoparticles towards advanced iron-based inorganic materials designed for biomedical applications.* Pharmacological Research, vol. 62, no. 2, pages 126 – 143, 2010. ¡ce:title¿Towards clinical applications of nanoscale medicines¡/ce:title¿.

[Fouineau *et al.* 2013] J. Fouineau, K. Brymora, L. Ourry, F. Mammeri, N. Yaacoub, F. Calvayrac, S. Ammar and J.-M. Greneche. *Synthesis, Mőssbauer characterization, and ab initio modelling of iron oxide nanoparticles of medical interest functionalized by dopamine.* The Journal of Physical Chemistry C, vol. 117, no. 27, pages 14295 – 14302, 2013.

[Frik *et al.* 2007] Martin Frik, Arno Schindlmayr and Matthias Scheffler. *Ab initio study of the half-metal to metal transition in strained magnetite.* New Journal of Physics, vol. 9, no. 1, page 5, 2007.

[Frisch *et al.*] M. J. Frisch, G. W. Trucks, H. B. Schlegel, G. E. Scuseria, M. A. Robb, J. R. Cheeseman, G. Scalmani, V. Barone, B. Mennucci, G. A. Petersson, H. Nakatsuji, M. Caricato, X. Li, H. P. Hratchian, A. F. Izmaylov, J. Bloino, G. Zheng, J. L. Sonnenberg, M. Hada, M. Ehara, K. Toyota, R. Fukuda, J. Hasegawa, M. Ishida, T. Nakajima, Y. Honda, O. Kitao, H. Nakai, T. Vreven, J. A. Montgomery Jr., J. E. Peralta, F. Ogliaro, M. Bearpark, J. J. Heyd, E. Brothers, K. N. Kudin, V. N. Staroverov, R. Kobayashi, J. Normand, K. Raghavachari, A. Rendell, J. C. Burant, S. S. Iyengar, J. Tomasi, M. Cossi, N. Rega, J. M. Millam, M. Klene, J. E. Knox, J. B. Cross, V. Bakken, C. Adamo, J. Jaramillo, R. Gomperts, R. E. Stratmann, O. Yazyev, A. J. Austin, R. Cammi, C. Pomelli, J. W. Ochterski, R. L. Martin, K. Morokuma, V. G. Zakrzewski, G. A. Voth, P. Salvador, J. J. Dannenberg, S. Dapprich, A. D. Daniels, . Farkas, J. B. Foresman, J. V. Ortiz, J. Cioslowski and D. J. Fox. *Gaussian 09 Revision A.1.* Gaussian Inc. Wallingford CT 2009.

[Gao *et al.* 2010] F. Gao, Y. Cai, J. Zhou, X. Xie, W. Ouyang, Y. Zhang, X. Wang, X. Zhang, X. Wang, L. Zhao and J. Tang. *Pullan Acetate Coated Magnetite Nanoparticles for Hyperthermia: Preparation, Characterization and In Vitro Experiments.* Nano. Res., vol. 3, pages 23–31, 2010.

[Gautier *et al.* 2013] J. Gautier, E. Allard Vannier, E. Munnier, M. Souce and I. Chourpa. *Recent advances in theranostic nanocarriers of doxorubicin based on iron oxide and gold nanoparticles.* Journal of Controlled Release, vol. 169, no. 12, pages 48 – 61, 2013.

[Giannozzi *et al.* 2009] Paolo Giannozzi, Stefano Baroni, Nicola Bonini, Matteo Calandra, Roberto Car, Carlo Cavazzoni, Davide Ceresoli, Guido L Chiarotti, Matteo Cococcioni, Ismaila Dabo, Andrea Dal Corso, Stefano de Gironcoli, Stefano Fabris, Guido Fratesi, Ralph Gebauer, Uwe Gerstmann, Christos Gougoussis, Anton Kokalj, Michele Lazzeri, Layla Martin-Samos, Nicola Marzari, Francesco Mauri,

Riccardo Mazzarello, Stefano Paolini, Alfredo Pasquarello, Lorenzo Paulatto, Carlo Sbraccia, Sandro Scandolo, Gabriele Sclauzero, Ari P Seitsonen, Alexander Smogunov, Paolo Umari and Renata M Wentzcovitch. *QUANTUM ESPRESSO: a modular and open-source software project for quantum simulations of materials.* Journal of Physics: Condensed Matter, vol. 21, no. 39, page 395502 (19pp), 2009.

[Globocan 2013] Globocan. *Section of cancer information*, June 2013.

[Grau-Crespo *et al.* 2010a] R. Grau-Crespo, A. Y. Al-Baitai, I. Saadoune and N. H. De Leeuw. *Vacancy ordering and electronic structure of - Fe 2 O 3 (maghemite): a theoretical investigation.* Journal of Physics: Condensed Matter, vol. 22, no. 25, page 255401, 2010.

[Grau-Crespo *et al.* 2010b] Ricardo Grau-Crespo, Asmaa Y Al-Baitai, Iman Saadoune and Nora H De Leeuw. *Vacancy ordering and electronic structure of - Fe $_2$ O $_3$ (maghemite): a theoretical investigation.* Journal of Physics: Condensed Matter, vol. 22, no. 25, page 255401, June 2010.

[Grazulis *et al.* 2012] S. Grazulis, A. Daskevc, A. Merkys, D. Chateigner, L. Lutterotti, M. Quiros, N. R. Serebryanaya, P. Moeck, R. T. Downs and A. Le Bail. *Crystallography Open Database (COD): an open-access collection of crystal structures and platform for world-wide collaboration.* Nucleic Acids Research, vol. 40, no. D1, pages D420–D427, 2012.

[Gross & Kohn 1985] E. K. U. Gross and Walter Kohn. *Local density-functional theory of frequency-dependent linear response.* Phys. Rev. Lett., vol. 55, pages 2850–2852, Dec 1985.

[Gunnarsson *et al.* 1974] O. Gunnarsson, B. I. Lundqvist and J. W. Wilkins. *Contribution to the cohesive energy of simple metals: Spin-dependence effect.* Physical Review B, vol. 10, 1974.

[Hajra *et al.* 2012] Partha Hajra, Pradip Brahma, Saurav Dutta, Sourish Banerjee and Dipankar Chakravorty. *Enhancement of magnetic anisotropy in mechanically attrited Cr2O3 nanoparticles.* Journal of Magnetism and Magnetic Materials, vol. 324, no. 7, pages 1425–1430, April 2012.

[Hedin 1965] L. Hedin. *New Method for Calculating the One-Particle Green's Function with Application to the Electron-Gas Problem.* Physical Review, vol. 139, 1965.

[Hiergeist *et al.* 1999] R Hiergeist, W Andr, N Buske, R Hergt, I Hilger, U Richter and W Kaiser. *Application of magnetite ferrofluids for hyperthermia.* Journal of Magnetism and Magnetic Materials, vol. 201, no. 13, pages 420 – 422, 1999.

[Hobbs & Hafner 2006] D. Hobbs and J. Hafner. *Nonollinear Magnetism*, June 2006.

[Hofer 2002] K. G. Hofer. *Hyperthermia and cancer.* European Cells and Materials, 2002.

[Hohenberg & Kohn 1964] P. Hohenberg and W. Kohn. *Inhomogeneous Electron Gas.* Phys. Rev., vol. 136, pages B864–B871, Nov 1964.

[Howarter & Youngblood 2006] J. A. Howarter and J. P. Youngblood. *Optimization of Silica Silanization by 3-Aminopropyltriethoxysilane.* Langmuir, vol. 22, no. 26, pages 11142–11147, 2006.

[Huang & El-Sayed 2010] Xiaohua Huang and Mostafa A. El-Sayed. *Gold nanoparticles: Optical properties and implementations in cancer diagnosis and photothermal therapy.* Journal of Advanced Research, vol. 1, no. 1, pages 13 – 28, 2010.

[Huang *et al.* 2006] D.J. Huang, H.J. Lin, J. Okamoto, K. Chao, H.T. Jeng, G. Guo, C.H. Hsu, C.M. Huang, D.C. Ling, W.B. Wu, C.S. Yang and C.T. Chen. *Charge-Orbital Ordering and Verwey Transition in Magnetite Measured by Resonant Soft X-Ray Scattering.* Phys. Rev. Lett., vol. 96, pages 487–97, 2006.

[Huang *et al.* 2011] C. Huang, J. Jiang, C. Muangphat, X. Sun and Y. Hao. *Trapping Iron Oxide into Hollow Gold Nanoparticles.* Nanoscale Research Letters, vol. 6, 2011.

[Ito *et al.* 2005] A. Ito, M . Shinkai, H. Honda and T. Kobayashi. *Medical application of functionalized magnetic nanoparticles.* Journal of Bioscience and Bioengineering, vol. 100, no. 1, 2005.

[Jones & Gunnarsson 1989] R. O. Jones and O. Gunnarsson. *The density functional formalism, its applications and prospects.* Rev. Mod. Phys., vol. 61, pages 689–746, Jul 1989.

[Jordan *et al.* 1993] A. Jordan, P. Wust, H. Fahling, W. John, A. Hinz and R. Felix. *Inductive heating of ferrimagnetic particles and magnetic fluids: physical evaluation of their potential for hyperthermia.* International Journal of Hyperthermia, vol. 9, no. 1, pages 51–68, 1993.

[Jordan *et al.* 1997] A. Jordan, P. Wust, R. Scholz, H. Faehling, J. Krause and R. Felix. *Magnetic Fluid Hyperthermia (MFH).* Scientific and Clinical Applications of Magnetic Carriers Scientific and Clinical Applications of Magnetic Carriers, 1997.

[Jrgensen *et al.* 2007] Jens-Erik Jrgensen, Lene Mosegaard, Line E. Thomsen, Torben R. Jensen and Jonathan C. Hanson. *Formation of -Fe2O3 nanoparticles and vacancy ordering: An in situ X-ray powder diffraction study.* Journal of Solid State Chemistry, vol. 180, no. 1, pages 180 – 185, 2007.

[Karra & Benita 2012] P. Karra and S. Benita. *The ligand nanoparticle conjugation approach for targeted cancer therapy.* Current Drug Metabolism, vol. 13, pages 22–41, 2012.

[Kaupp *et al.* 2004] M. Kaupp, M. Buhl and V. G. Malkin. Calculations of nmr and epr parameters. Wiley-Vch, 2004.

[Kayal & Ramanujan 2010] S. Kayal and R. V. Ramanujan. *Anti-Cancer Drug Loaded Iron-Gold Core-Shell Nanoparticles (Fe@Au) for Magnetic Drug Targeting.* Journal of Nanoscience and Nanotechnology, vol. 10, pages 1–13, 2010.

[Kihal *et al.* 2012] A. Kihal, G. Fillion, B. Bouzabata and B. Barbara. *High field surface magnetic study of Fe3O4 nanoparticles.* physica status solidi (b), vol. 249, no. 3, pages 604–614, March 2012.

[Kim *et al.* 2010] S. C. Kim, W. Ju and A. Szasz. *Hystory of hyperthermia and electromedicine.* Oncothermia Journal, 2010.

[Kodama 1999] R. H. Kodama. *Magnetic nanoparticles.* Journal of Magnetism and Magnetic Materials, vol. 200, no. 13, pages 359 – 372, 1999.

[Kokalj 1999] A. Kokalj. *XCrySDen - a new program for displaying crystalline structures and electron densities.* Jornal of Molecular Graphics and Modelling, vol. 17, pages 176–179, Jun 1999.

[Korobchevskaya *et al.* 2011] Kseniya Korobchevskaya, Chandramohan George, Alberto Diaspro, Liberato Manna, Roberto Cingolani and Alberto Comin. *Ultrafast carrier dynamics in gold/iron-oxide nanocrystal heterodimers.* Applied Physics Letters, vol. 99, no. 1, page 011907, 2011.

[Kreibig & Vollmer 1995] U. Kreibig and M. Vollmer. Optical properties of metal clusters. Springer, 1995.

[Kseolu 2006] Yksel Kseolu. *Effect of surfactant coating on magnetic properties of Fe3O4 nanoparticles: {ESR} study.* Journal of Magnetism and Magnetic Materials, vol. 300, no. 1, pages e327 – e330, 2006.

[Kubler *et al.* 1988] J. Kubler, K. H. Hock, J. Sticht and A. R. Williams. *Local spin-density functional theory of noncollinear magnetism.* Journal of Applied Physics, vol. 63, 1988.

[Lacroix *et al.* 2008] L. M. Lacroix, J. Carrey and M. Respaud. *A frequency-adjustable electromagnet for hyperthermia measurements on magnetic nanoparticles.* Rev Sci Instrum., vol. 79, 2008.

[Lesar 2013] R. Lesar. Computational materials science. fundamentals to applications. Cambridge University Press, 2013.

[Levy & Perdew 1985] Mel Levy and John P. Perdew. *Hellmann-Feynman, virial, and scaling requisites for the exact universal density functionals. Shape of the correlation potential and diamagnetic susceptibility for atoms.* Phys. Rev. A, vol. 32, pages 2010–2021, Oct 1985.

[Levy 1979] Mel Levy. *Universal variational functionals of electron densities, first-order density matrices, and natural spin-orbitals and solution of the v-representability problem.* Proceedings of the National Academy of Sciences, vol. 76, no. 12, pages 6062–6065, 1979.

[Li *et al.* 2009] Hongyan Li, Michael T. Klem, Karl B. Sebby, David J. Singel, Mark Young, Trevor Douglas and Yves U. Idzerda. *Determination of anisotropy constants of protein encapsulated iron oxide nanoparticles by electron magnetic resonance.* J. Magn. Magn. Mater., vol. 321, no. 3, page 175, FEB 2009.

[Lin *et al.* 2010] M. Z. Lin, M. R. McKeown, H. L.Ng, T. A. Aguilera, N. C. Shaner, R. E. Campbell, S. R. Adams, L. A. Gross, W. Ma, T. Alber and R. Y. Tsien. *Autofluorescent proteins with excitation in the optical window for intravital imaging in mammals.* Chem. Biol., vol. 16, no. 11, 2010.

[Liong *et al.* 2008] M. Liong, J. Lu, M. Kovochich, T. Xia, S. G. Ruehm, A. E. Nel, F. Tamanoi and J. I. Zink. *Multifunctional Inorganic Nanoparticles for Imaging, Targeting, and Drug Delivery.* ACS Nano, vol. 2, no. 5, 2008.

[Liu 2012] S. Liu. *Epigenetics advancing personalized nanomedicine in cancer therapy.* Advanced Drug Delivery Reviews, vol. 64, no. 13, pages 1532 – 1543, 2012.

[Lodziana 2007] Zbigniew Lodziana. *Surface Verwey Transition in Magnetite*. Phys. Rev. Lett., vol. 99, page 206402, Nov 2007.

[Luis *et al.* 2002] F. Luis, J. Torres, L. Garca, J. Bartolom, J. Stankiewicz, F. Petroff, F. Fettar, J.-L. Maurice and A. Vaurs. *Enhancement of the magnetic anisotropy of nanometer-sized Co clusters: Influence of the surface and of interparticle interactions*. Physical Review B, vol. 65, no. 9, February 2002.

[Madsen & Novak 2005] G. K. H. Madsen and P. Novak. *Charge order in magnetite. An LDA+U study*. Europhysics Letters, vol. 69, 2005.

[Magnasco 2006] Valerio Magnasco. Elementary methods of molecular quantum mechanics. Elsevier Science, December 29, 2006.

[Makov & Payne 1995] G. Makov and M. C. Payne. *Periodic boundary conditions in ab initio calculations*. Phys. Rev. B, vol. 51, pages 4014–4022, Feb 1995.

[Malcolu *et al.* 2011] O. B. Malcolu, R. Gebauer, D. Rocca and S. Baroni. *turboTDDFT A code for the simulation of molecular spectra using the LiouvilleLanczos approach to time-dependent density-functional perturbation theory*. Computer Physics Communications, vol. 182, no. 8, pages 1744 – 1754, 2011.

[Marini *et al.* 2009] A. Marini, C. Hogan, M. Gruning and D. Varsano. *Yambo: an ab initio tool for excited state calculations*. Computer Physics Communications, vol. 180, 2009.

[Markides *et al.* 2012] H. Markides, M. Rotherham and A. J. El Haj. *Biocompatibility and Toxicity of Magnetic Nanoparticles in Regenerative Medicine*. Journal of Nanomaterials, vol. 2012, 2012.

[Martyna & Tuckerman 1999] G. J. Martyna and M. E. Tuckerman. *A reciprocal space based method for treating long range interactions in ab-initio and force-field-based calculation in clusters*. Journal of Chemical Physics, vol. 110, 1999.

[Mazo-Zuluaga *et al.* 2009] J. Mazo-Zuluaga, J. Restrepo, F. Munoz and J. Mejia-Lopez. *Surface anisotropy, hysteretic, and magnetic properties of magnetite nanoparticles: A simulation study*. Journal of Applied Physics, vol. 105, no. 12, page 123907, 2009.

[Metropolis *et al.* 1953] N. Metropolis, A. W. Rosenbluth, M. N. Rosenbluth, A. H. Teller and E. Teller. *Equation of State Calculations by Fast Computing Machines*. Journal of Chemical Physics, vol. 21, no. 6, 1953.

[Mitchell 1999] M. Mitchell. An introduction to genetic algorithms (complex adaptive systems). Massachusetts Institute of Technology, 1999.

[Mohanraj & Chen 2006] V. J. Mohanraj and Y. Chen. *Nanoparticles - A Review*. Tropical Journal of Pharmaceutical Research, vol. 5, no. 1, 2006.

[Mornet *et al.* 2004] S. Mornet, S. Vasseur, F. Grasset and E. Duguet. *Magnetic nanoparticles design for medical diagnosis and therapy*. Journal of Materials Chemistry, no. 14, pages 2161 – 2175, 2004.

[Nadeem *et al.* 2012] K. Nadeem, H. Krenn, T. Traussnig, R. Wurschum, D. V. Szabo and I. Letofsky-Papst. *Spin-glass freezing of maghemite nanoparticles prepared by microwave plasma synthesis*. Journal of Applied Physics, vol. 111, no. 11, page 113911, 2012.

[Natarajan *et al.* 2008] A. Natarajan, C. Chun, JJ Hickman and P. Molnar. *Growth and electrophysiological properties of rat embryonic cardiomyocytes on hydroxyl- and carboxyl-modified surfaces*. J Biomater Sci Polym Ed, vol. 19, no. 10, pages 1319–31, 2008.

[Neuberger *et al.* 2005] T. Neuberger, B. Schopf, H. Hofmann, M. Hofmann and B. von Rechnberg. *Superparamagnetic nanoparticles for biomedical applications: Possibilities and limitations of a new drug delivery system*. Journal of Magnetism and Magnetic Materials, vol. 293, no. 1, pages 483 – 496, 2005.

[Nitta & Numata 2013] S. K. Nitta and K. Numata. *Biopolymer-Based Nanoparticles for Drug/Gene Delivery and Tissue Engineering*. International Journal of Molecular Sciences, vol. 14, no. 1, 2013.

[Nohyun & Taeghwan 2012] L. Nohyun and H. Taeghwan. *Designed synthesis of uniformly sized iron oxide nanoparticles for efficient magnetic resonance imaging contrast agents*. Chem. Soc. Rev., vol. 41, pages 2575–2589, 2012.

[Panaa *et al.* 2007] O. Panaa, C.M. Teodorescub, O. Chauvetc, C. Payenc, D. Macoveib, R. Turcua, M.L. Sorana, N. Aldeaa and L. Barbud. *Structure, morphology and magnetic properties of FeAu core-shell nanoparticles*. Surface Science, vol. 601, pages 4352–4357, 2007.

[Pankhurst *et al.* 2003] Q. A. Pankhurst, J. Conolly, S. K. Jones and J. Dobson. *Applications of magnetic nanoparticles in medicine*. Journal of Physics D, vol. 36, 2003.

[Parkinson *et al.* 2010] Gareth S. Parkinson, Narasimham Mulakaluri, Yaroslav Losovyj, Peter Jacobson, Rossitza Pentcheva and Ulrike Diebold. *Semiconductor-half metal transition at the Fe3O4(001) surface upon hydrogen adsorption.* Phys. Rev. B, vol. 82, no. 12, SEP 9 2010.

[Perdew & Zunger 1981] J. P. Perdew and Alex Zunger. *Self-interaction correction to density-functional approximations for many-electron systems.* Phys. Rev. B, vol. 23, pages 5048–5079, May 1981.

[Perdew *et al.* 1996a] J. P. Perdew, K. Burke and M. Ernzerhof. *Generalized Gradient Approximation Made Simple.* Physical Review Letters, vol. 77, no. 18, 1996.

[Perdew *et al.* 1996b] John P. Perdew, Kieron Burke and Matthias Ernzerhof. *Generalized Gradient Approximation Made Simple.* Phys. Rev. Lett., vol. 77, pages 3865–3868, Oct 1996.

[Persson & Mirbt 2006] C. Persson and S. Mirbt. *Improved Electronic Structure and Optical Properties of sp-Hybridized Semiconductors Using LDA+U.* Brazilian Journal of Physics, vol. 36, 2006.

[Pinto & Elliott 2006] H P Pinto and S D Elliott. *Mechanism of the Verwey transition in magnetite: JahnTeller distortion and charge ordering patterns.* Journal of Physics: Condensed Matter, vol. 18, no. 46, page 10427, 2006.

[Pissuwan *et al.* 2006] D. Pissuwan, S. M. Valenzuela and M. B. Cortie. *Therapeutic possibilities of plasmonically heated gold nanoparticles.* Trend in Biotechnology, vol. 24, pages 62–67, 2006.

[Porsch *et al.* 2013] C. Porsch, Y. Zhang, A. Ostlund, P. Damberg, C. Ducani, E. Malmstrom and A. Nystrom. *Drug Delivery: In Vitro Evaluation of Non-Protein Adsorbing Breast Cancer Theranostics Based on 19F-Polymer Containing Nanoparticles.* Particle and Particle Systems Characterization, vol. 30, no. 4, pages 380 – 390, 2013.

[Press *et al.* 1992] W. H. Press, B. P. Flannery, S. A. Teukolsky and W. T. Vetterling. Numerical recipes in fortran 77: The art of scientific computing. Cambridge University Press, NY, 1992.

[Prijic & Sersa 2011] S. Prijic and G. Sersa. *Magnetic Nanoparticles as targeted delivery systems in oncology.* Radiology and Oncology, vol. 45, no. 1, 2011.

[Rajh *et al.* 2002] T. Rajh, L. X. Chen, K. Lukas, T. Liu, M. C. Thurnauer and D. M. Tiede. *Surface Restructuring of Nanoparticles: An Efficient Route for Ligand-Metal Oxide Crosstalk*. The Journal of Physical Chemistry B, vol. 106, no. 41, pages 10543–10552, 2002.

[Ramachandran *et al.* 2008] K. I. Ramachandran, G. Deepa and K. Nambarii. Computational chemistry and molecular modeling. Springer, July 24, 2008.

[Rocca *et al.* 2008] Dario Rocca, Ralph Gebauer, Yousef Saad and Stefano Baroni. *Turbo charging time-dependent density-functional theory with Lanczos chains*. The Journal of Chemical Physics, vol. 128, no. 15, page 154105, 2008.

[Runge & Gross 1984] E. Runge and E. K. U. Gross. *Density-Functional Theory for Time-Dependent Systems*. Phys. Rev. Lett., vol. 52, pages 997–1000, Mar 1984.

[Sattler 2011] Klaus D. Sattler. Handbook of nanophysics. nanomedicine and nanorobotics. CRC Press, Taylor and Francis Group, 2011.

[Scarberry *et al.* 2010] K. E. Scarberry, E. B. Dickerson, Z. J. Zhang, B. B. Benigno and J. F. McDonald. *Selective removal of ovarian cancer cells from human ascites fluid using magnetic nanoparticles*. Nanomedicine: Nanotechnology, Biology and Medicine, vol. 6, 2010.

[Scemama *et al.* 2011] Anthony Scemama, Michel Caffarel, Robin Chaudret and Jean-Philip Piquemal. *Electron Pair Localization Function (EPLF) for Density Functional Theory and ab Initio Wave Function-Based Methods: A New Tool for Chemical Interpretation*. Journal of Chemical Theory and Computation, vol. 7, no. 3, pages 618–624, 2011.

[Sham & Schlüter 1985] L. J. Sham and M. Schlüter. *Density-functional theory of the band gap*. Phys. Rev. B, vol. 32, pages 3883–3889, Sep 1985.

[Shevchenko *et al.* 2008] E. V. Shevchenko, M. I. Bodnarchuk, M. V. Kovalenko, D. V. Talapin, R. K. Smith, S. Alonie, W. Heiss and A. P. Alivaistos. *Gold/Iron Oxide Core/Hollow-Shell Nanoparticles*. Advanced Materials, vol. 20, pages 4323–4329, 2008.

[Shmakov *et al.* 1995] A. N. Shmakov, G. N. Kryukova, S. V. Tsybulya, A. L. Chuvilin and L. P. Solovyeva. *Vacancy ordering in -Fe2O3: Synchrotron X-ray Powder Diffraction and High-Resolution Electron Microscopy Studies*. Journal of Applied Crystallography, vol. 28, pages 141–145, 1995.

[Singh & Papaconstantopoulos 2003] D. J. Singh and D. A. Papaconstantopoulos. Electronic structure and magnetism of complex materials. Springer, 2003.

[Stegh 2013] A. H. Stegh. *Toward personalized cancer nanomedicine - past, present, and future.* Integr. Biol., vol. 5, pages 48–65, 2013.

[Steinhauser *et al.* 2006] Isabel Steinhauser, Birgit Spnkuch, Klaus Strebhardt and Klaus Langer. *Trastuzumab-modified nanoparticles: Optimisation of preparation and uptake in cancer cells.* Biomaterials, vol. 27, no. 28, pages 4975 – 4983, 2006.

[Sun *et al.* 2000] Q. Sun, Q. Wang, K. Parlinski, J. Z. Yu, Y. Hashi, X. G. Gong and Y. Kawazoe. *First-principles studies on the intrinsic stability of the magic $Fe_{13}O_8$ cluster.* Physical Review B, vol. 6, no. 8, 2000.

[Sun *et al.* 2006] Q. Sun, A. K. Kandalam, . Wang, P. Jena, Y. Kawazoe and M .Marquez. *Effect of Au coating on the magnetic and structural properties of Fe nanoclusters for use in biomedical applications: A density-functional theory study.* Phys. Rev. B, vol. 73, page 134409, Apr 2006.

[Sun *et al.* 2007] Q. Sun, B. V., M. Marquez, P. Jena, C. Gonzalez and Q. Wang. *Theoretical Study on Gold-Coated Iron Oxide Nanostructure: Magnetism and Bioselectivity for Amino Acids.* The Journal of Physical Chemistry C, vol. 111, pages 4159–4163, 2007.

[Tamer *et al.* 2013] U. Tamer, D. Cetin, Z. Suludere, I. H. Boyaci, H. T. Temiz, H. Yegenoglu, P. Daniel, I. Dincer and Y. Elermans. *Gold-Coated Iron Composite Nanospheres Targeted the Detection of Escherichia coli.* International Journal of Molecular Sciences, vol. 14, pages 6223–6240, 2013.

[Tartaj *et al.* 2003] P. Tartaj, M. del Puerto Morales, S. Veintemillas Verdaugers, T. Gonzalez Carreno and C. J. Serna. *The preparation of magnetic nanoparticles for applications in biomedicine.* Journal of Physics D, vol. 36, no. 13, 2003.

[Tronc *et al.* 2000] E. Tronc, A. Ezzir, R. Cherkaoui, C. Chanac, M. Nogues, H. Kachkachi, D. Fiorani, A. M. Testa, J. M. Greneche and J. P. Jolivet. *Surface-related properties of -Fe< sub> 2</sub> O< sub> 3</sub> nanoparticles.* Journal of Magnetism and Magnetic Materials, vol. 221, no. 1, page 6379, 2000.

[Tronc *et al.* 2003] E Tronc, D Fiorani, M Nogus, A.M Testa, F Lucari, F DOrazio, J.M Grenche, W Wernsdorfer, N Galvez, C Chanac, D Mailly and J.P Jolivet. *Surface effects in noninteracting and interacting -Fe2O3 nanoparticles.* Journal of Magnetism and Magnetic Materials, vol. 262, no. 1, pages 6 – 14, 2003.

¡ce:title¿Proceedings of the International Workshop on Electronics Transport in Magnetic Nanogranular Systems¡/ce:title¿.

[Tsai *et al.* 2001] C. L. Tsai, J. C. Chen and W. J. Wang. *Near-infrared Absorption Property of Biological Soft Tissue Constituents*. Journal of Medical and Biological Engineering, vol. 21, no. 1, 2001.

[Uhl & Siberchicot 1995] M. Uhl and B. Siberchicot. *A first-principles study of exchange integrals in magnetite*. Journal of Physics: Condensed Matter, vol. 7, no. 22, page 4227, 1995.

[Valko *et al.* 2007] M. Valko, D. Leibfritz, J. Moncol, M. T. D. Cronin, M. Mazur and J. Telser. *Free radicals and antioxidants in normal physiological functions and human disease*. The International Journal of Biochemistry and Cell Biology, vol. 39, pages 44–84, 2007.

[van Leeuwen *et al.* 1994] David A. van Leeuwen, J. M. Van Ruitenbeek, L. J. De Jongh, A. Ceriotti, G. Pacchioni, O. D. Hberlen and N. Rsch. *Quenching of magnetic moments by ligand-metal interactions in nanosized magnetic metal clusters*. Physical review letters, vol. 73, no. 10, page 14321435, 1994.

[Wang *et al.* 1999] Q. Wang, Q. Sun, B. L. Gu, K. Sumiyama and Y. Kawazoe. *Geometry and electronic structure of magic iron oxide clusters*. Physical Review B, vol. 59, no. 19, 1999.

[Ward *et al.* 2005] J. Ward, PJ. Robinson, JA. Guthrie, S. Downing, D. Wilson, JP. Lodge, KR. Prasad, GJ. Toogood and JI. Wyatt. *Liver Metastases in Candidates for Hepatic Resection: Comparison of Helical CT and Gadolinium- and SPIO-enhanced MR Imaging*. Radiology, vol. 237, no. 1, 2005.

[Weber *et al.* 1996] J. Weber, J. P. Doucet and Jean-Pierre Doucet. Computer-aided molecular design: Theory and applications. Academic Pr Inc, April 1, 1996.

[Weinstein *et al.* 2010] J. S. Weinstein, C. G. Varllyay, E. Dosa, S. Gahramanov, B. Hamilton, W. D. Rooney, L. L. Muldoon and E. A. Neuwelt. *Superparamagnetic iron oxide nanoparticles: diagnostic magnetic resonance imaging and potential therapeutic applications in neurooncology and central nervous system inflammatory pathologies, a review*. Journal of Cerebral Blood Flow and Metabolism, vol. 30, no. 1, 2010.

[Widder *et al.* 1779] K. J. Widder, A. E. Senyei and D. F. Ranney. *Magnetically Responsive Microspheres and Other Carriers for the Biophysical Targeting of Antitumor Agents*. Advances in Pharmocology and Chemotherapy, vol. 16, 1779.

[Wright *et al.* 2002] Jon P. Wright, J. Paul Attfield and Paolo G. Radaelli. *Charge ordered structure of magnetite* Fe_3O_4 *below the Verwey transition*. Phys. Rev. B, vol. 66, page 214422, Dec 2002.

[Wu *et al.* 2008] W. Wu, Q. He and C. Jiang. *Magnetic Iron Oxide Nanoparticles: Synthesis and Surface Functionalization Strategies.* Nanoscale Res. Lett., vol. 3, pages 397–415, 2008.

[Wust *et al.* 2002] P Wust, B Hildebrandt, G Sreenivasa, B Rau, J Gellermann, H Riess, R Felix and PM Schlag. *Hyperthermia in combined treatment of cancer*. The Lancet Oncology, vol. 3, no. 8, pages 487 – 497, 2002.

[Xiang & Wang 2011] Y. Xiang and J. Wang. *Superparamagnetic iron oxide based MRI contrast agents: Current status of clinical application*. Quant Imaging Med Surg, vol. 1, no. 1, 2011.

[Yang *et al.* 2009] T. Yang, X. D. Wen, Y. W. Li, J. Wang and H Jiao. *Interaction of alkali metals with the Fe3O4(1 1 1) Surface*, 2009.

[Zeng *et al.* 2007] Q. Zeng, I. Baker, J. A. Loudis, Y. F. Liao and P. J. Hoopes. *Synthesis and heating effect of iron/iron oxide composite and iron oxide nanoparticles*, 2007.

[Zhang & Noguez 2008] J. Z. Zhang and C. Noguez. *Plasmonic Optical Properties and Applications of Metal Nanostructures*. Plasmonic, vol. 3, pages 127–150, 2008.

[Zhou *et al.* 2001] W.L. Zhou, E.E. Carpenter, J. Lin, A. Kumbhar, J. Sims and C.J. O'Connor. *Nanostructures of gold coated iron core-shell nanoparticles and the nanobands assembled under magnetic field*. The European Physical Journal D, vol. 16, pages 289–292, 2001.

l'université nantes angers le mans
PÔLE DE RECHERCHE ET D'ENSEIGNEMENT SUPÉRIEUR

Université du Maine

Thèse de Doctorat

Katarzyna BRYMORA

Modélisation des propriétés magnétiques et optiques de nanoparticules d'intérêt médical

Modeling of magnetic and optical properties of nanoparticles in medical interest

Résumé
Cette thèse porte sur la modélisation ab initio des ligands et des nanoparticules magnétiques utilisés en médecine (hyperthermie magnétique, imagerie médicale ...). Les calculs sont effectués par le logiciel Quantum Espresso basé sur théorie de la fonctionnelle de la densité et LDA + U. L'objectif est d'abord de comprendre la liaison des ligands sur des nanoparticules magnétiques, la nature de l'ionicité dans les particules, puis de décrire le changement d'anisotropie magnétique due aux liaisons chimiques sur la surface, et enfin de décrire la modification des propriétés optiques due également à la liaison de différents ligands sur la surface de nanoparticules hybrides d'or et d'oxyde de fer.

Abstract
This thesis concerns the ab initio modeling of ligands and magnetic nanoparticles used in medicine (magnetic hyperthermia, medical imaging). Calculations are performed by the Quantum Espresso software based on density functional theory and LDA+U. The goal is first to understand the binding of ligands on magnetic nanoparticles, the nature of ionicity in the particles, then to describe the change in magnetic anisotropy due to the chemical bondings on surface, and finally to describe the change in optical properties due also to the bonding of various ligands or clusters on the surface of hybrid gold and iron oxide nanoparticles.

Mots clés
nanoparticules magnétiques, ab initio, DFT, fonctionnalisation.

Key Words
magnetic nanoparticles, ab initio, DFT, functionalization.